JAERI-M
87-002

EVALUATION REPORT ON CCTF CORE-II REFLOOD TEST C2-9 (Run 68) — EFFECT OF LPCI FLOW RATE —

February 1987

Hajime AKIMOTO, Tadashi IGUCHI, Kazuharu OKABE*
Jun SUGIMOTO**, Tsutomu OKUBO and Yoshio MURAO

日本原子力研究所
Japan Atomic Energy Research Institute

JAERI-Mレポートは，日本原子力研究所が不定期に公刊している研究報告書です。
入手の問合わせは，日本原子力研究所技術情報部情報資料課（〒319-11茨城県那珂郡東海村）あて，お申しこしください。なお，このほかに財団法人原子力弘済会資料センター（〒319-11茨城県那珂郡東海村日本原子力研究所内）で複写による実費頒布をおこなっております。

JAERI-M reports are issued irregularly.
Inquiries about availability of the reports should be addressed to Information Division Department of Technical Information, Japan Atomic Energy Research Institute, Tokai-mura, Naka-gun, Ibaraki-ken 319-11, Japan.

編集兼発行　日本原子力研究所
印　　刷　㈱高野高速印刷

Evaluation Report on CCTF Core-II Reflood Test C2-9 (Run 68) - Effect of LPCI flow rate -

Hajime AKIMOTO, Tadashi IGUCHI, Kazuharu OKABE*
Jun SUGIMOTO**, Tsutomu OKUBO and Yoshio MURAO

Department of Reactor Safety Research,
Tokai Research Establishment
Japan Atomic Energy Research Institute
Tokai-mura, Naka-gun, Ibaraki-ken

(Received January 8, 1987)

In order to study the LPCI flow rate effect on the core cooling and system behavior, a test was performed with the LPCI flow rate of 0.025 m^3/s, which corresponds to the flow rate in case of no pump failure in a PWR system. Through the comparisons of test results with those from the reference test with the LPCI flow rate of 0.011 m^3/s, the following conclusions were obtained:

(1) The higher LPCI flow rate resulted in the worse core-cooling in these two tests. The test results show that the lower LPCI flow rate is not necessarily a conservative assumption for the evaluation of the core cooling during the reflood phase of a PWR LOCA.

(2) The worse core-cooling in the high LPCI flow rate test is attributed to the lower core-pressure than in the reference test. It is found that the lower core-pressure results from the lower pressure drop through the broken cold leg.

(3) It is expected that the current evaluation model(EM) code is still conservative because it usually predicts the low pressure drop through the broken cold leg.

(4) The flow oscillation in the cold leg was not significant even in the high LPCI flow rate test before the whole core quench.

Keywords: Reactor Safety, Loss-of-coolant, PWR Reflood, LPCI Flow Rate Effect, CCTF, Heat Transfer, Two-phase Flow

---

The work was performed under the contract with the Atomic Energy Bureau of Science and Technology Agency of Japan.

* Mitsubishi Atomic Power Industry
** Science and Technology Agency of Japan

大型再冠水円筒第２次炉心試験Ｃ２－９（Run68）評価報告書
―― ＬＰＣＩ注入流量の影響 ――

日本原子力研究所東海研究所原子炉安全工学部
秋本　　肇・井口　　正・岡部　一治*
杉本　純**・大久保　努・村尾　良夫

（１９８７年１月８日受理）

ＬＰＣＩ流量が炉心冷却とシステム挙動に与える影響を調べるために，ＬＰＣＩ流量条件を0.025 m^3／ｓとした試験を実施した。上記の流量条件は，加圧水型原子炉システムでＬＰＣＩポンプ電源の故障がない時に相当する。ＬＰＣＩ流量条件を0.011m^3／ｓとした参照試験結果との比較検討から，以下の結論が得られた。

(1) 高ＬＰＣＩ流量試験（ＬＰＣＩ流量0.025m^3／ｓ）での炉心冷却は低ＬＰＣＩ流量試験（ＬＰＣＩ流量0.011m^3／ｓ）での炉心冷却に比べて悪かった。この結果は，加圧水型原子炉冷却材喪失事故再冠水時の炉心冷却を評価する上で，低めにＬＰＣＩ流量を評価することが必ずしも保守的な仮定ではないことを示す。

(2) 高ＬＰＣＩ流量試験での炉心冷却の悪化は，炉心内圧力が低かったことに起因する。また，炉心内圧力の低下が破断コールドレグでの圧力損失が低かったことにより生じたことがわかった。

(3) 現在の評価コードでは通常破断コールドレグでの圧力損失を低く評価することから，評価コードは依然として保守的であると考えられる。

(4) 高ＬＰＣＩ流量試験においても，炉心全クエンチ終了までの期間においては，顕著なコールドレグ振動は観察されなかった。

東海研究所：〒３１９－１１　茨城県那珂郡東海村白方字白根２－４

本報告書は，電源開発促進特別会計法に基づき，科学技術庁からの受託によって行った研究の成果である。

＊　三菱原子力工業
＊＊　科学技術庁

Contents

1. Introduction ····· 1
2. Test description ····· 2
2.1 Test facility ····· 2
2.1.1 Pressure vessel and internals ····· 2
2.1.2 Heater rod assembly ····· 3
2.1.3 Primary loops and ECCS ····· 3
2.1.4 Instrumentation ····· 4
2.2 Planned test procedure ····· 4
3. Measured test conditions and data presentation ····· 24
3.1 Measured test conditions ····· 24
3.2 Data presentation ····· 25
3.3 Comparison of test conditions between high and low LPCI flow rate tests ····· 25
4. Results and discussion ····· 31
4.1 LPCI flow rate effect on flow behavior in primary system ····· 31
4.2 LPCI flow rate effect on thermal hydraulic behavior in core ····· 34
5. Conclusions ····· 47
Acknowledgement ····· 48
References ····· 48

Appendix
Appendix A Definitions of Tag IDs for data in Appendix B ····· 49
Appendix B Selected data of CCTF Test C2-9(Run 68) ····· 61

目　　次

1. 序…… 1
2. 試験…… 2
2.1 試験装置…… 2
2.1.1 圧力容器および内部構造物…… 2
2.1.2 発熱棒集合体…… 3
2.1.3 一次系ループおよびＥＣＣＳ…… 3
2.1.4 計測器…… 4
2.2 試験手順の設定…… 4
3. 試験条件測定値と試験結果…… 24
3.1 試験条件測定値…… 24
3.2 試験結果…… 25
3.3 高ＬＰＣＩ流量試験と低ＬＰＣＩ流量試験の試験条件比較…… 25
4. 考察…… 31
4.1 一次系内の水力挙動に対するＬＰＣＩ流量の影響…… 31
4.2 炉心内熱水力挙動に対するＬＰＣＩ流量の影響…… 34
5. 結論…… 47
謝辞…… 48
参考文献…… 48
付録
付録Ａ 付録Ｂのデータに対するTag－ＩＤの定義…… 49
付録Ｂ 円筒第２次炉心試験Ｃ２－９（Run６８）データ捗…… 61

List of tables

Table 2.1 CCTF component scaled dimensions
Table 2.2 Component elevations of CCTF
Table 2.3 Instruments provided by USNRC
Table 3.1 Initial conditions for high LPCI flow rate test
Table 3.2 Chronology of events for high LPCI flow rate test
Table 3.3 Comparison of test conditions between high and low LPCI flow rate tests

List of figures

Fig. 2.1 Bird°s-eye view of CCTF
Fig. 2.2 Schematic diagram of CCTF
Fig. 2.3 CCTF core-II pressure vessel
Fig. 2.4 Cross section of CCTF-II
Fig. 2.5 Dimension of CCTF core-II pressure vessel
Fig. 2.6 Arrangement of upper plenum internals
Fig. 2.7 Upper plenum internals
Fig. 2.8 Buffle plates in control rod guide tube
Fig. 2.9 Dimensions of holes of end box tie plate
Fig. 2.10 Dimensions of plugging device
Fig. 2.11 Arrangement of non-heated rods and bundle direction
Fig. 2.12 Heater rod
Fig. 2.13 Axial power profile of CCTF core-II heater rod
Fig. 2.14 Top view of primary loop piping
Fig. 2.15 Dimensions of primary loop
Fig. 2.16 Steam generator simulator
Fig. 2.17 Pump simulator
Fig. 2.18 Configuration of upper plenum injection pipe
Fig. 2.19 Arrangement and location of upper plenum injection pipe
Fig. 3.1 Total power supplied to heater rods in core in CCTF test C2-9
Fig. 3.2 Pressure in containment tank 2 in CCTF test C2-9
Fig. 3.3 ECC water injection rates into lower plenum and three intact cold legs in CCTF test C2-9
Fig. 3.4 Fluid temperatures at ECC water injection nozzles in CCTF test C2-9
Fig. 4.1 LPCI flow rate effect on water head in upper plenum,core and downcomer
Fig. 4.2 LPCI flow rate effect on mass flow rate and differential pressure through primary loops in CCTF
Fig. 4.3 Comparison of the flow resistance coefficient through the intact loop between the high and low LPCI flow rate tests
Fig. 4.4 Comparison of the flow resistance coefficient through the broken loop between the high and low LPCI flow rate tests
Fig. 4.5 Comparison of flow resistance coefficients along the intact loop between the high and low LPCI flow rate tests
Fig. 4.6 Comparison of the steam mass flow rate with the condensability of the ECC water in the high LPCI flow rate test
Fig. 4.7 Fluid temperature along the cold leg in the high LPCI flow rate test
Fig. 4.8 Fluid density at the downstream of the ECC water injection port

in the high LPCI flow rate test

Fig. 4.9 Fluid density at the downstream of the ECC water injection port in the low LPCI flow rate test

Fig. 4.10 LPCI flow rate effect on water and steam mass flow rates through the broken cold leg

Fig. 4.11 LPCI flow rate effect on the clad surface temperature at the midplane of the peak power rod

Fig. 4.12 LPCI flow rate effect on flow parameters at the core inlet

Fig. 4.13 Comparison of containment pressure, differential pressure through the broken cold leg and downcomer water head between the high and low LPCI flow rate tests

1.Introduction

A reflood test program using large scale test facilities has been conducted at Japan Atomic Energy Research Institute(JAERI).[1]-[4] The facilities are the Cylindrical Core Test Facility(CCTF) and the Slab Core Test Facility(SCTF). This report presents an evaluation for the CCTF test C2-9(Run 68) which was performed using CCTF with LPCI(low pressure coolant injection) flow rate of 0.025 m^3/s on July 13,1983.

The CCTF is an experimental facility designed to model a full-height core section and four primary loops and their components of a pressurized water reactor(PWR). This facility is used to provide information of thermal-hydraulic behavior in pressure vessel (core, downcomer and upper and lower plenums) and in primary loops (including steam generator and pump simulator) during the refill and reflood phases of a hypothetical loss-of-coolant accident(LOCA) of a PWR.

The objectives of the test program using the CCTF are:

a. Demonstration of capability of emergency core cooling system (ECCS) during refill and reflood phases.
b. Verification of reflood analysis codes.
c. Collection of information to improve the thermal-hydraulic models in the analysis codes.

As the first series of the CCTF test, the CCTF Core-I series was initiated in March 1979 and completed in April 1981. Subsequently, as the second series of the CCTF tests, the CCTF Core-II series was initiated in March 1982.

The main objectives of the CCTF test C2-9(Run 68) are (1) to study the LPCI flow rate effect on the system behavior and (2) to check the possibility of the cold leg flow oscillation due to the direct contact of flowing steam with the subcooled water in the cold legs.

For these purposes, the test was performed with the LPCI flow rate of 0.025 m^3/s instead of 0.011 m^3/s of the reference test. The LPCI flow rate of the high LPCI flow rate test corresponds to the flow rate without the pump unit failure in a PWR, while the LPCI flow rate of the reference test corresponds to the flow rate in case of the single failure of pump unit.

This report presents the results of the CCTF test C2-9 in comparison with the results from the reference test, or the CCTF test C2-SH2(Run 54)[5] for evaluation of the LPCI flow rate effect.

2. Test description

2.1 Test facility

A bird's-eye view and schematic diagram of the CCTF are shown in Figs. 2.1 and 2.2, respectively. The scaled dimensions of the components are given in Tables 2.1 and 2.2.

2.1.1 Pressure vessel and internals

The pressure vessel is of a cylindrical type as shown in Fig. 2.3. The height is the same as the reference reactor pressure vessel. The dimension in the radial direction is scaled down based on the core flow area scaling, that is, 1/21.44. The upper ring was newly attached for the installation of the upper plenum ECC water injection lines and the instruments. Four vent valves and two downcomer water injection nozzles, which are called Core Flooding Nozzle(CFN), are also newly installed in the CCTF Core-II facility as shown in Figs. 2.3 and 2.4. Vent valves and CFNs are forcedly closed in this test.

The cross section of the pressure vessel is shown in Fig. 2.5. The dimensions of the pressure vessel is shown in Fig. 2.5. The core consists of thirty-two 8x8 rod bundles arranged in a cylindrical configuration. The rod bundles simulate Westinghouse 15x15 type fuel assemblies.

The downcomer is an annulus of 61.5 mm gap. In determining the gap size, the flow area of the core baffle region was added to that of the downcomer region. Thus, the core baffle flow area is included in the downcomer simulation in the CCTF. The vessel wall is constructed of carbon steel cladded with stainless steel lining. The wall thickness is 90 mm.

The design of upper plenum internals is based on that of the Westinghouse PWR with 17x17 type fuel assembly. The internals cosists of ten control-rod guide tubes, ten support columns and twelve open holes as shown in Fig. 2.6. The configuration of each intenal is illustrated in Fig. 2.7. The radius of each internal is scaled down by factor of 8/15 from that of a PWR. Flow resistance baffle plates are inserted into the guide tubes. Figure 2.8 shows the configurations of the baffle plates.

The end box and the upper core support plate(UCSP) are installed above the core. Figure 2.9 shows the structure of the end box tie plate for one heater rod bundle. The tie plate is a perforated plate 10 mm thick. Plugging devices are installed in the CCTF-II facility in order to

simulate the flow resistance more correctly as shown in Figs. 2.9 and 2.10. The UCSP is a perforated plate 60 mm thick.

2.1.2 Heater rod assembly

Figure 2.11 shows arrangement of heater rods in a bundle. Each bundle consists of fifty-seven heater rods and seven non-heated rods. All heater rods in a bundle have the same power density in the CCTF-II facility. As shown in Fig. 2.5, the core is subdivided into three regions to achieve a desired radial power profile.

Figure 2.12 shows the configuration of a heater rod. A heater rod consists of nichrome heating element, magnesium oxide(MgO) and boron nitride(BN) insulators, and inconel-600 sheath. BN is used only for the central part of the heated part. The length of the core heated part is 3.66 m and the diameter of the heater rod is 10.7 mm. The thickness of the sheath wall is 1.0 mm. By changing the pitch of the helical coil of the heating element, a 17-step chopped-cosine axial-power profile is attained as shown in Fig. 2.13. The axial peaking factor is 1.40 in the CCTF-II, instead of 1.489 in the CCTF-I.

Non-heated rods are either stainless steel pipe or solid pipe of 13.8 mm O.D. All pipes are utilized for installation of instruments such as superheat steam probes and thermocouples. All bars are used to support the assembly loads.

The heater rods and non-heated rods are held in radial position by grid spacers which are located at six elevations along the axial length as shown in Fig. 2.13. A grid spacer is a lattice composed of stainless plates of 0.4 and 0.8 mm thick and 40 mm high. The top and bottom edges of the stainless steel plates are sharpened in the CCTF-II.

The heater rods penetrate through the bottom plate of the pressure vessel to facilitate the connection of the power cables. The outer diameter of the heater rods in the lower plenum is reduced to 8.6 mm.

2.1.3 Primary loops and ECCS

The CCTF has three intact and a broken loops. The facility simulates the double-ended cold-leg break. Figures 2.14 and 2.15 show the primary loop arrangement in the CCTF. The inside diameter of the pipings is scaled down in proportion to the core flow area scaling. The length of each piping section is almost the same as the corresponding sections of the reference PWR.

Figure 2.16 shows the steam generator(SG) simulator. The SG

simulator is of U-tube and shell type. The primary coolant passes through the tubes. The secondary side is filled with water. The SG simulators of two loops are housed in a single shell assembly. The wall thickness of the U-tube is 2.9 mm instead of 1.27 mm in the reference PWR system because of higher pressure difference between the primary and secondary sides.

The pump simulator consists of the casing and vane simulators and an orifice plate as shown in Fig. 2.17. The each loop flow resistance is simulated with the orifice plate.

ECC water can be injected into each cold leg, lower plenum, upper plenum, and downcomer as shown in Fig. 2.14.

Figure 2.18 shows the upper plenum injection device. The radial locations of the water injection pipes are shown in Fig. 2.19.

2.1.4 Instrumentation

The instrumentation is divided into two groups. One is JAERI-supplied instruments. The other is the USNRC supplied instruments.

JAERI instrumentation includes 1316 channels and is recorded on magnetic tapes. The measuring location of the selected data is summarized in Appendix A.

USNRC supplied instruments include the advanced instrumentation for the two-phase flow measurement. 536 channels are used to record data from these instruments. Table 2.3 show the names and quantities of these instruments.

2.2 Planned test procedure

In the preparation for the test, the Acc tank, the LPCI tank, the saturated water tank, and the secondary side of the steam generators were filled with water which was purified with ion exchange resin. After all the components and instruments were inspected for mechanical and electrical leakages, the instruments were checked for their zero points and sensitivities.

After these preparatory operations, the primary system was heated to the specified temperatures (downcomer wall:471 K, core internals: 393 K, and the primary piping wall: 393 K) and pressurized to a specified pressure (0.2 MPa) by introduing steam into the primary system. The water in the Acc and LPCI tanks was heated to the specified temperature(308 K). The water in the LPCI tank was circulated through the circulation line to preheat the line to the same temperature as the LPCI water. The water in

the saturated water tank was preheated to the saturation temperature(393 K) at the expected primary system pressure(0.2 MPa). The water in the secondary side of each steam generator was also heated and pressurized to the specified temperature(539 K) and pressure(5.2 MPa).

After establishing these initial conditions of the test, the lower plenum was filled with the saturated water to the specified level(0.90 m from the bottom of the pressure vessel). When all initial test conditions were stabilized at the allowable tolerance, electric power was supplied to the heater rods in the core and the data recording was started. The temperature rises of the rods were monitored by using a computer. When a specified clad surface temperature (995 K) was attained at more than 4 monitoring locations of the clad surface temperatures, Acc water injection into the lower plenum was initiated(injection rate: 0.105 m^3/s). The clad surface temperature (995 K) of the heater rods for the initiation of the Acc injection into the lower plenum was predetermined by the interpolation of the clad surface temperatures at the test initiation(393 K) and the reflood initiation (1073 K). The core power decay was programmed to begin when the water level in the pressure vessel was estimated to reach the bottom of the core heated part (2.1 m high from the bottom of the pressure vessel). The decay of core power followed the normarized decay curve of (ANS x 1.0 + Actinide x 1.1 (30 s after scram)).

When the water level in the pressure vessel was estimated to reach the specified level(0.5 m high from the bottom of the core heated part), the injection location of Acc water was changed from the lower plenum to the ECC ports in the intact cold legs. The Acc injection into the cold legs was planned to be 0.0892 m^3/s for 11 s. This is defined as the Acc mode in the CCTF tests. After a specified time(11 s), the valves in the Acc lines and the LPCI circulation line began to close. The valves in the LPCI injection lines started openning at the same time in order to switch the ECC water injection mode. The ECC water injection was planned to be 0.0250 m^3/s. This ECC water injection is defined as the LPCI mode in the CCTF tests.

The generated steam in core flowed with the entrained water via primary loops to the containment tanks. The steam was then exhausted to the atmosphere through the flow control valve. The pressure in the containment tank was maintained at the specified level(0.2 MPa). After all thermocouples on the surface of the heater rods were quenched, the power supply to the heater rods and the ECC water injection were terminated. Then, the data recording system was stopped.

Table 2.1 CCTF Component scaled dimensions

Component		PWR	CCTF	Ratio
Pressure vessel				
Vessel inside diameter	(mm)	4394 (173")	1084	
Vessel thickness	(mm)	216 (8 1/2")	90	
Core barrel outside diameter	(mm)	3874	961	
Core barrel inside diameter	(mm)	3760	929	
Thermal shield outside diameter	(mm)	4170		
Thermal shield inside diameter	(mm)	4030		
Downcomer length	(mm)	4849	4849	1/1
Downcomer gap	(mm)	114.3	61.5	
Downcomer flow area	(m^2)	4.23	0.197	1/21.44
Lower plenum volume	(m^3)	29.6	1.38	1/21.44
Upper plenum volume	(m^3)	43.6	2.76	1/15.8
Fuel (heater rod) assembly				
Number of bundles	(—)	193	32	
Rod array	(—)	15×15	8×8	
Rod heated length	(mm)	3660	3660	1/1
Rod pitch	(mm)	14.3	14.3	1/1
Fuel rod outside diameter	(mm)	10.72	10.7	1/1
Thimble tube diameter	(mm)	13.87	13.8	1/1
Instrument tube diameter	(mm)	13.87	13.8	1/1
Number of heater rods	(—)	39372	1824	1/21.58
Number of non-heated rods	(—)	4053	244	1/18.09
Core flow area	(m^2)	5.29	0.25	1/21.2
Core fluid volume	(m^3)	17.95	0.915	1/19.6
Primary loop				
Hot leg inside diameter	(mm)	736.6 (29")	155.2	1/4.75
Hot leg flow area	(m^2)	0.426	0.019	1/22.54
Hot leg length	(mm)	3940	3940	1/1
Pump suction inside diameter	(mm)	787.4 (31")	155.2	1/5.07
Pump suction flow area	(m^2)	0.487	0.019	1/25.77
Pump suction length	(mm)	9750	7950	1/1

Table 2.1 (cont'd)

Component		PWR	CCTF	Ratio
Cold leg inside diameter	(mm)	698.5 (27.5")	155.2	1/4.50
Cold leg flow area	(m^2)	0.383	0.019	1/20.26
Cold leg length	(mm)	5600	5600	1/1
Steam generator simulator				
Number of tubes/loop	(—)	3388	158	1/21.44
Tube length (average)	(m)	20.5	15.2	1/1.35
Tube outside diameter	(mm)	22.225 (0.875")	25.4	
Tube inside diameter	(mm)	19.7 (0.05")	19.6	1/1
Tube wall thickness	(mm)	1.27	2.9	
Heat transfer area/loop	(m^3)	4784 (51500 ft^2)	192	1/24.92
Tube flow area/loop	(m^2)	1.03	0.048	1/21.44
Inlet plenum volume/loop	(m^3)	4.25	0.198	1/21.44
Outlet plenum volume/loop	(m^3)	4.25	0.198	1/21.44
Primary side volume/loop	(m^3)	30.50 (1077 ft^3)	1.2	1/25.4
Secondary side volume/loop	(m^3)	157.33 (5556 ft^3)	2.5	1/62.9
Containment tank 1	(m^3)		30	
Containment tank 2	(m^3)		50	
Storage tank	(m^3)		25	
Acc. tank	(m^3)		5	
Saturated water tank	(m^3)		3.5	

Table 2.2 Component elevations of Cylindrical Core Test Facility

COMPONENT		PWR	CCTF	DISCREPANCY
BOTTOM OF HEATED REGION IN CORE	(mm)	0	0	0
TOP OF HEATED REGION IN CORE	(mm)	3660	3660	0
TOP OF DOWNCOMER	(mm)	4849	4849	0
BOTTOM OF DOWNCOMER	(mm)	0	0	0
CENTERLINE OF COLD LEG	(mm)	5198	4927	-271
BOTTOM OF COLD LEG (INSIDE)	(mm)	4849	4849	0
CENTERLINE OF LOOP SEAL LOWER END	(mm)	2056	2047	- 9
BOTTOM OF LOOP SEAL LOWER END	(mm)	1662	1959	+297
CENTER OF HOT LEG	(mm)	5198	4927	-271
BOTTOM OF HOT LEG (INSIDE)	(mm)	4830	4849	+ 19
BOTTOM OF UPPER CORE PLATE	(mm)	3957	3957	0
TOP OF LOWER CORE PLATE	(mm)	- 108	- 50	+ 58
BOTTOM OF TUBE SHEET OF STEAM GENERATOR SIMULATOR	(mm)	7308	7307	- 1
LOWER END OF STEAM GENERATOR SIMULATOR PLENUM	(mm)	5713	5712	- 1
TOP OF TUBES OF STEAM GENERATOR SIMULATOR (avg)	(mm)	17952.7	14820	

Table 2.3 Instruments provided by USNRC

Instrument	Number of sets	Number of sensors
DC FDG	18	162
DC VOP	1	1
DC drag disk	4	4
Core velocimeter	4	4
Core impedance probe	12	24
Core LLD	6	96
LP LLD	3	15
End box turbine meter	8	8
UP turbine meter	4	4
UP FDG	11	110
UP film probe	2	4
UP prong probe	2	4
UP VOP	1	1
VV turbine meter	2	2
VV string probe	2	2
HL film probe	2	4
HL VOP	1	1
Reference probe	1	1
Spool piece	8	89
Total	92	536

Note :

DC : Downcomer, FDG: Fluid distribution grid,
VOP: Video optical probe, LLD: Liquid level detector,
LP : Lower plenum, UP : Upper plenum,
VV : Vent valve

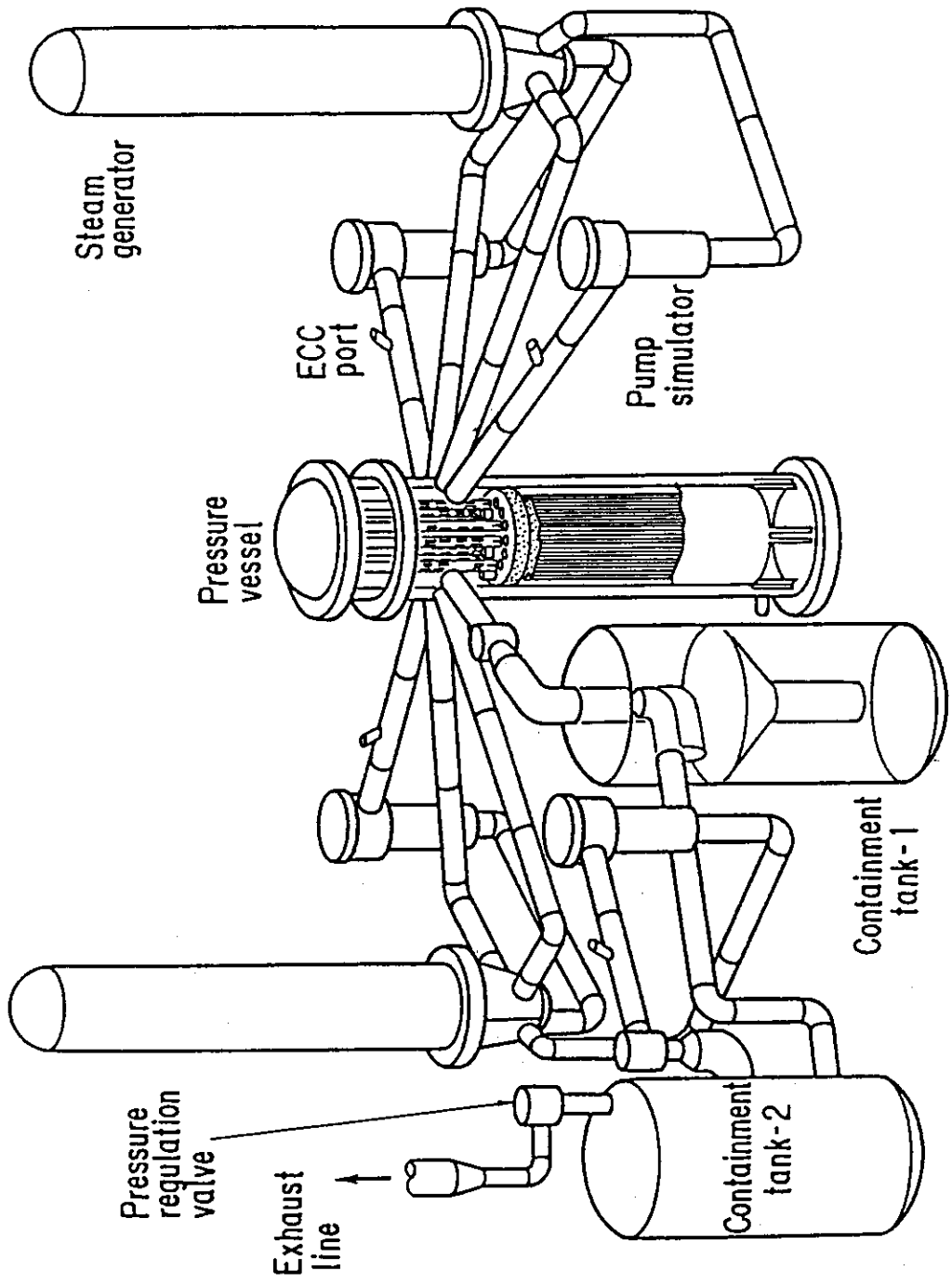

Fig. 2.1 Bird's-eye view of CCTF

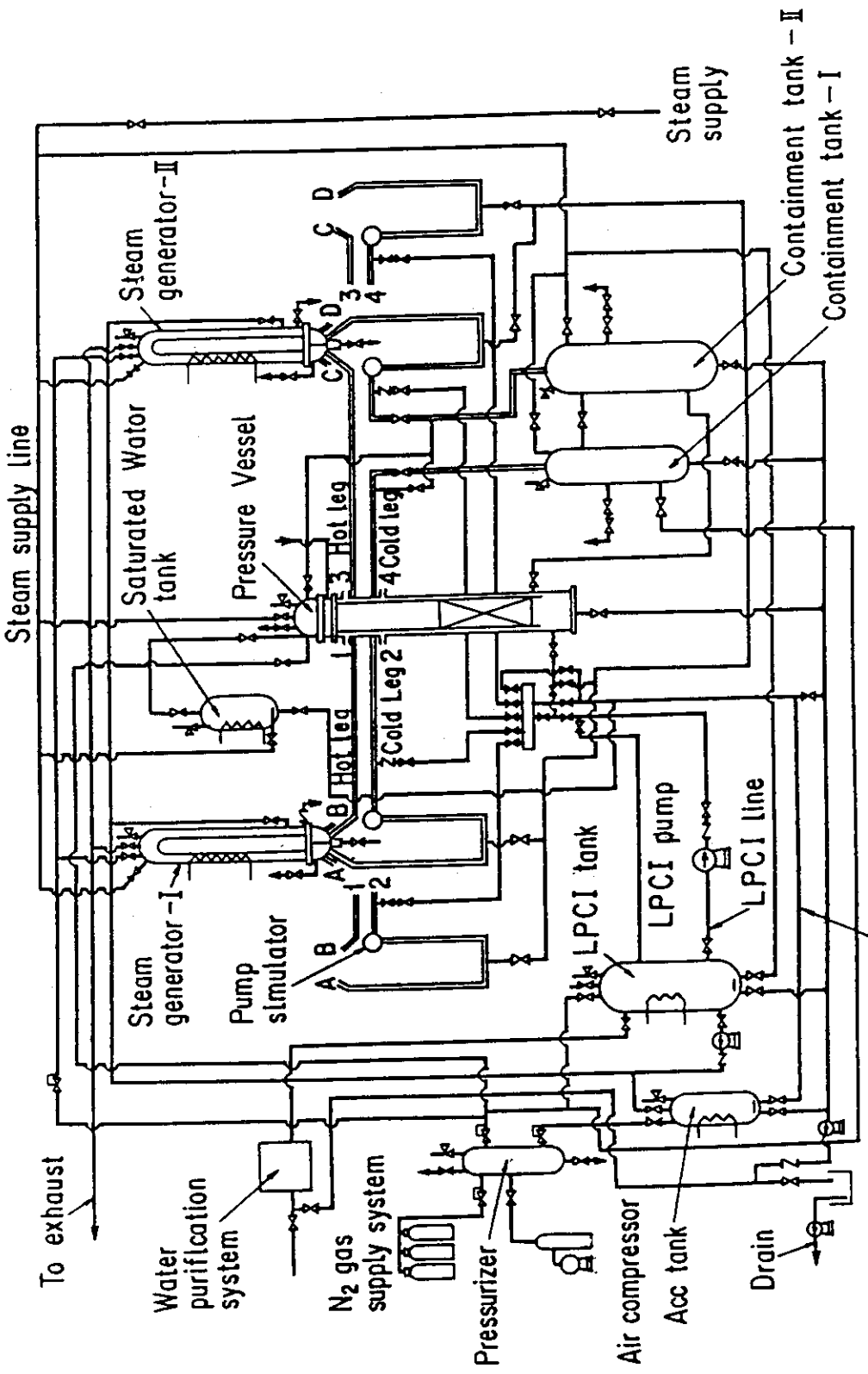

Fig. 2.2 Schematic diagram of CCTF

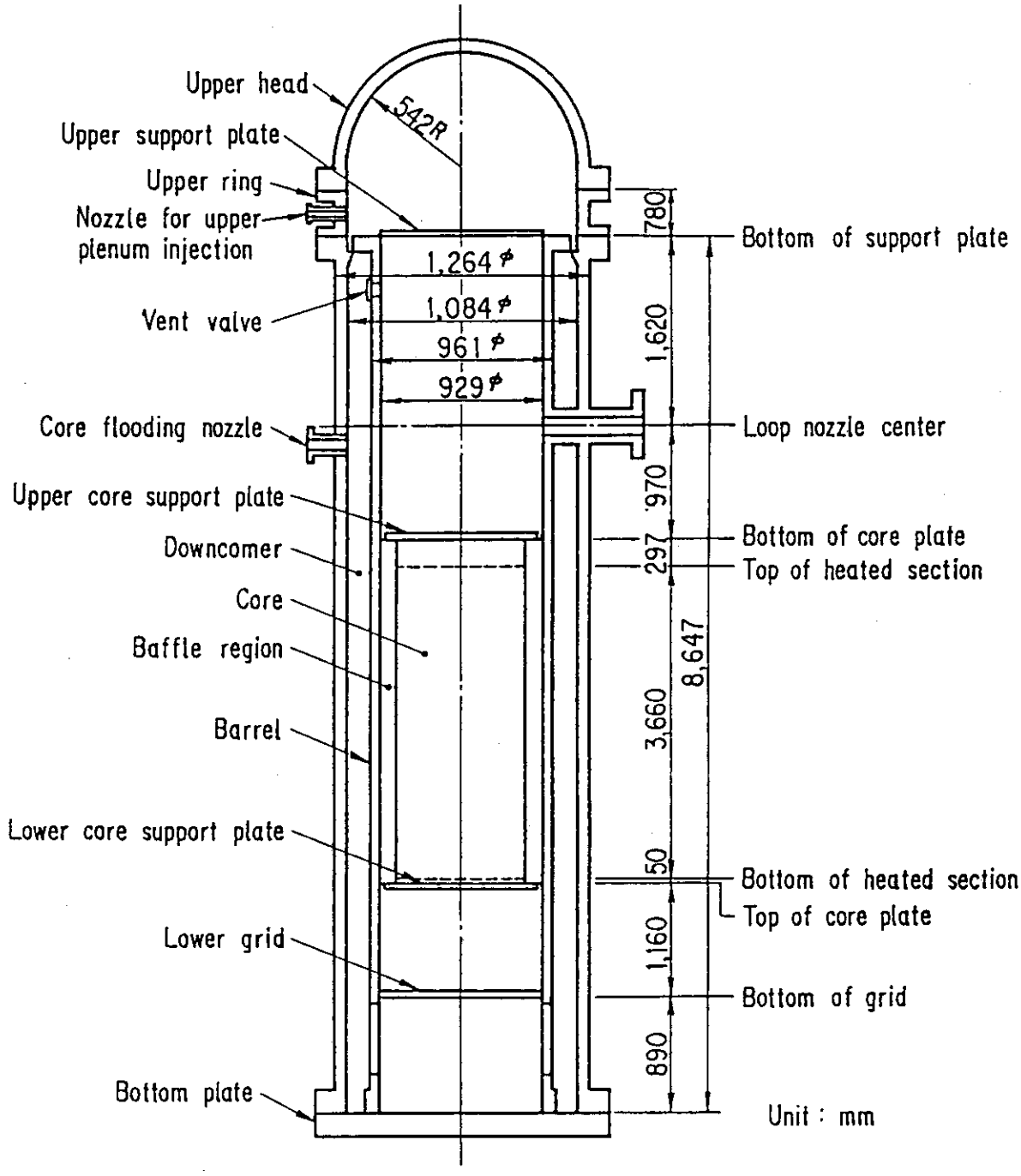

Fig. 2.3 CCTF Core-II pressure vessel

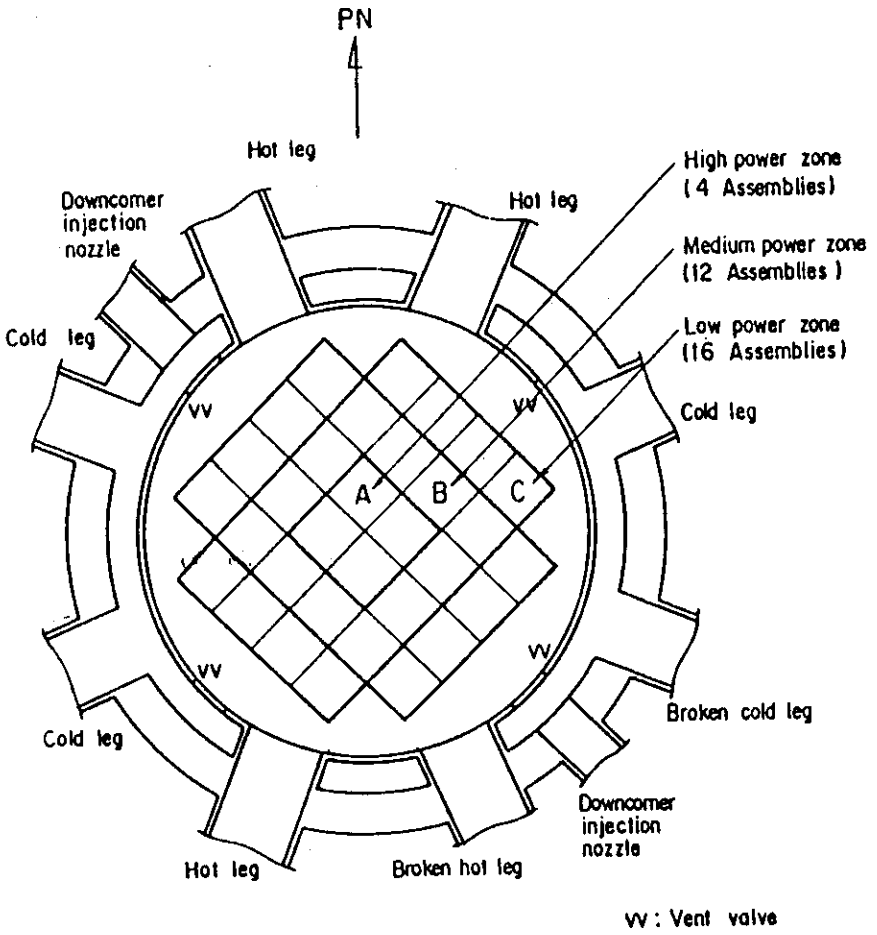

Fig. 2.4 Cross section of CCTF Core-II

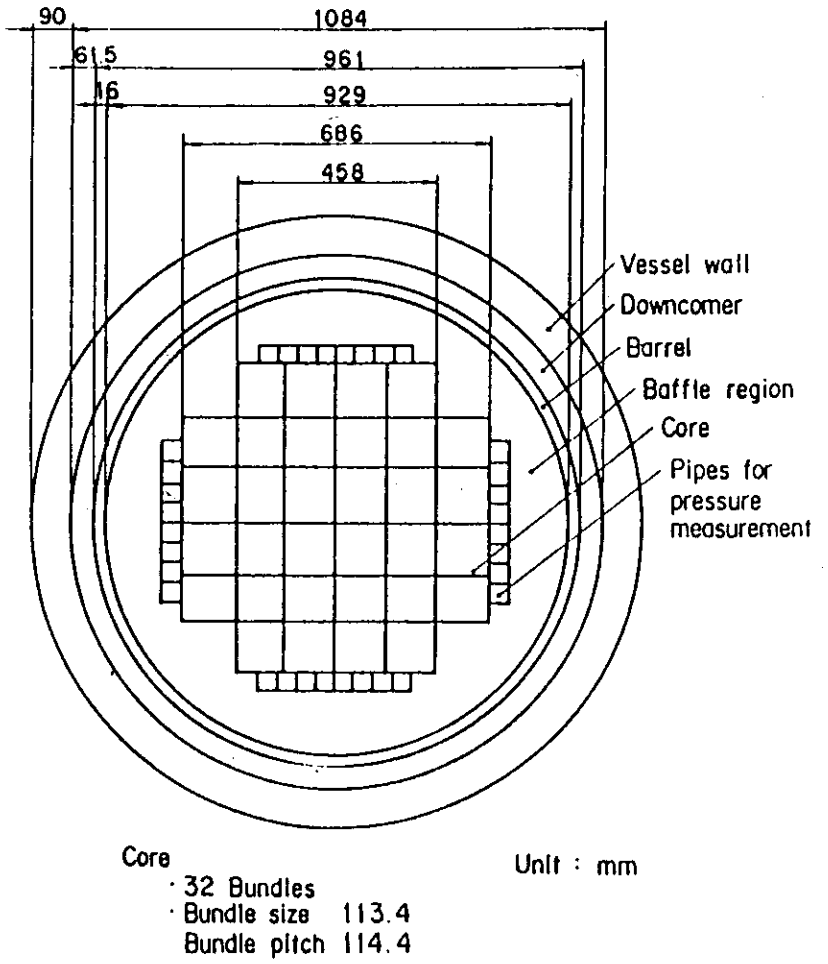

Fig. 2.5 Dimension of CCTF Core-II pressure vessel cross section

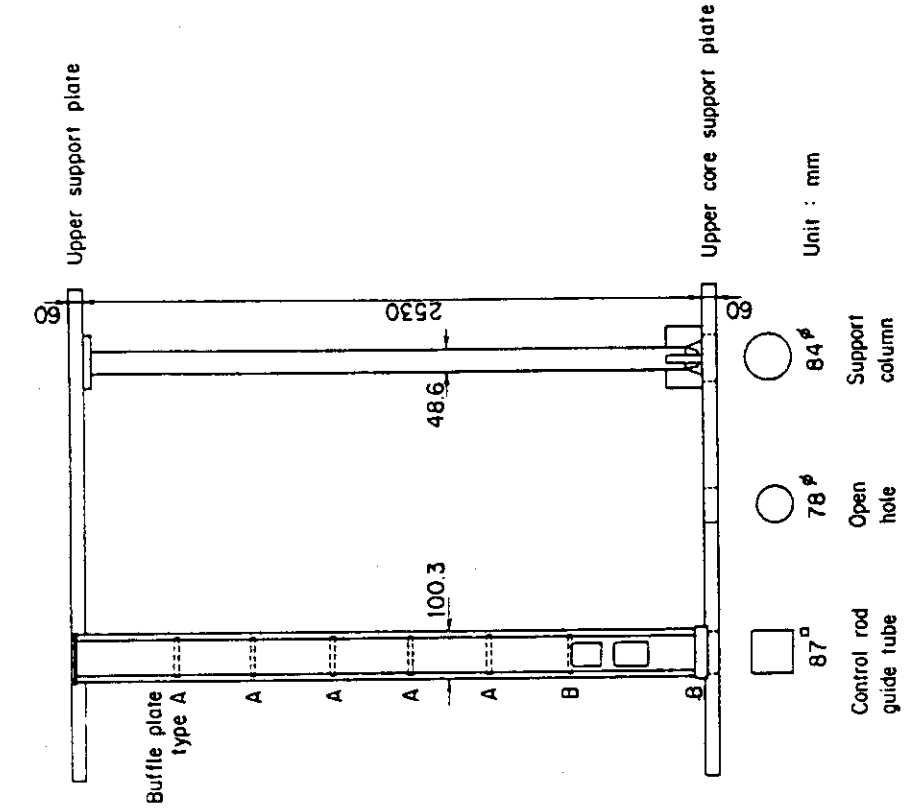

Fig. 2.7 Upper plenum internals

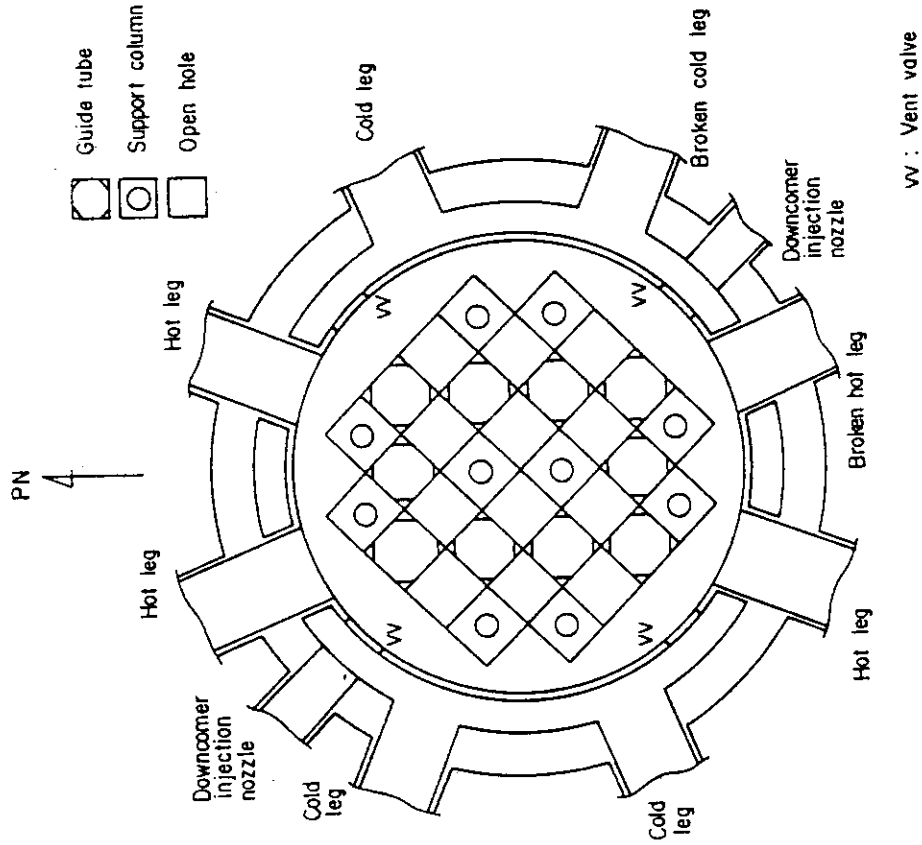

Fig. 2.6 Arrangement of upper plenum internals

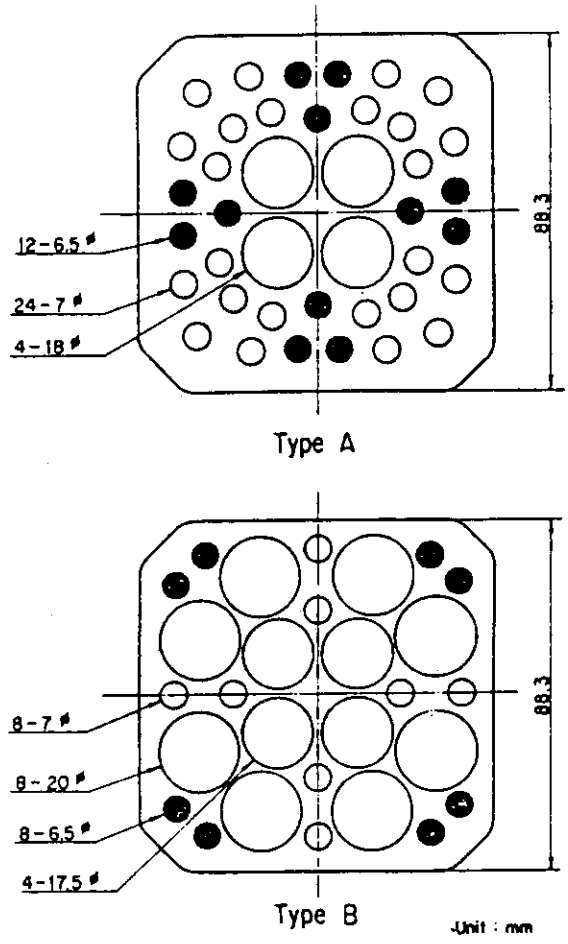

Fig. 2.8 Buffle plates in control rod guide tube

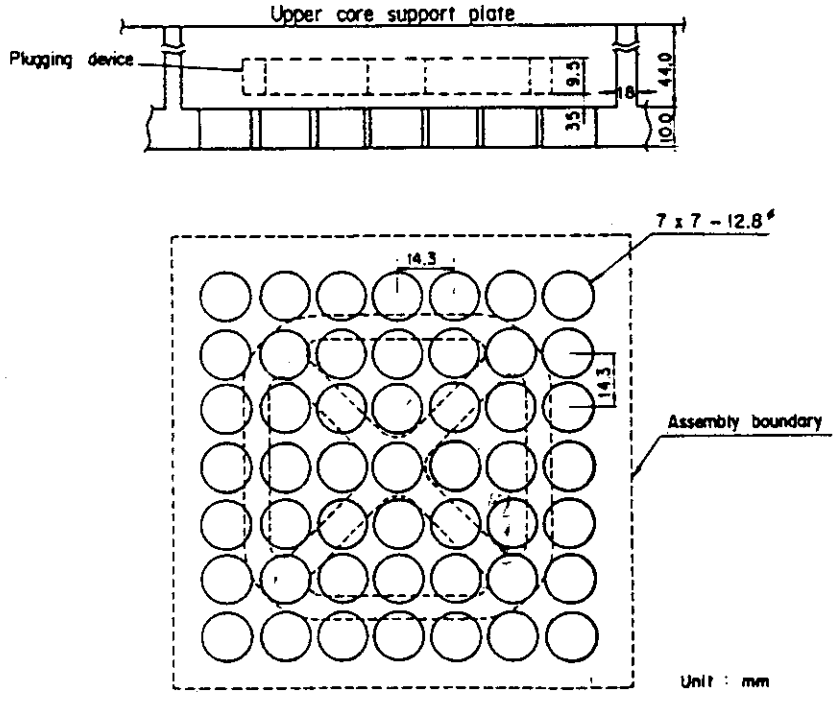

Fig. 2.9 Dimensions of holes of end box tie plate

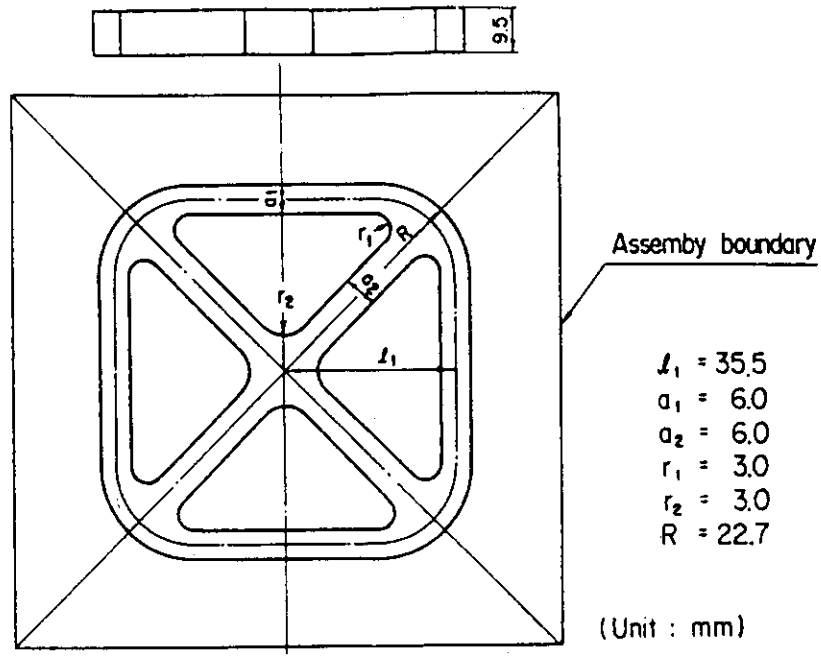

Fig. 2.10 Dimensions of plugging device

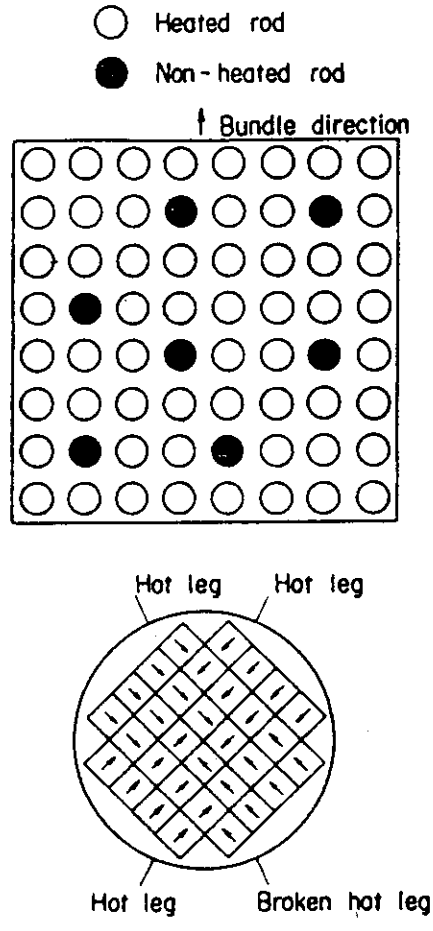

Fig. 2.11 Arrangement of non-heated rods bundle direction

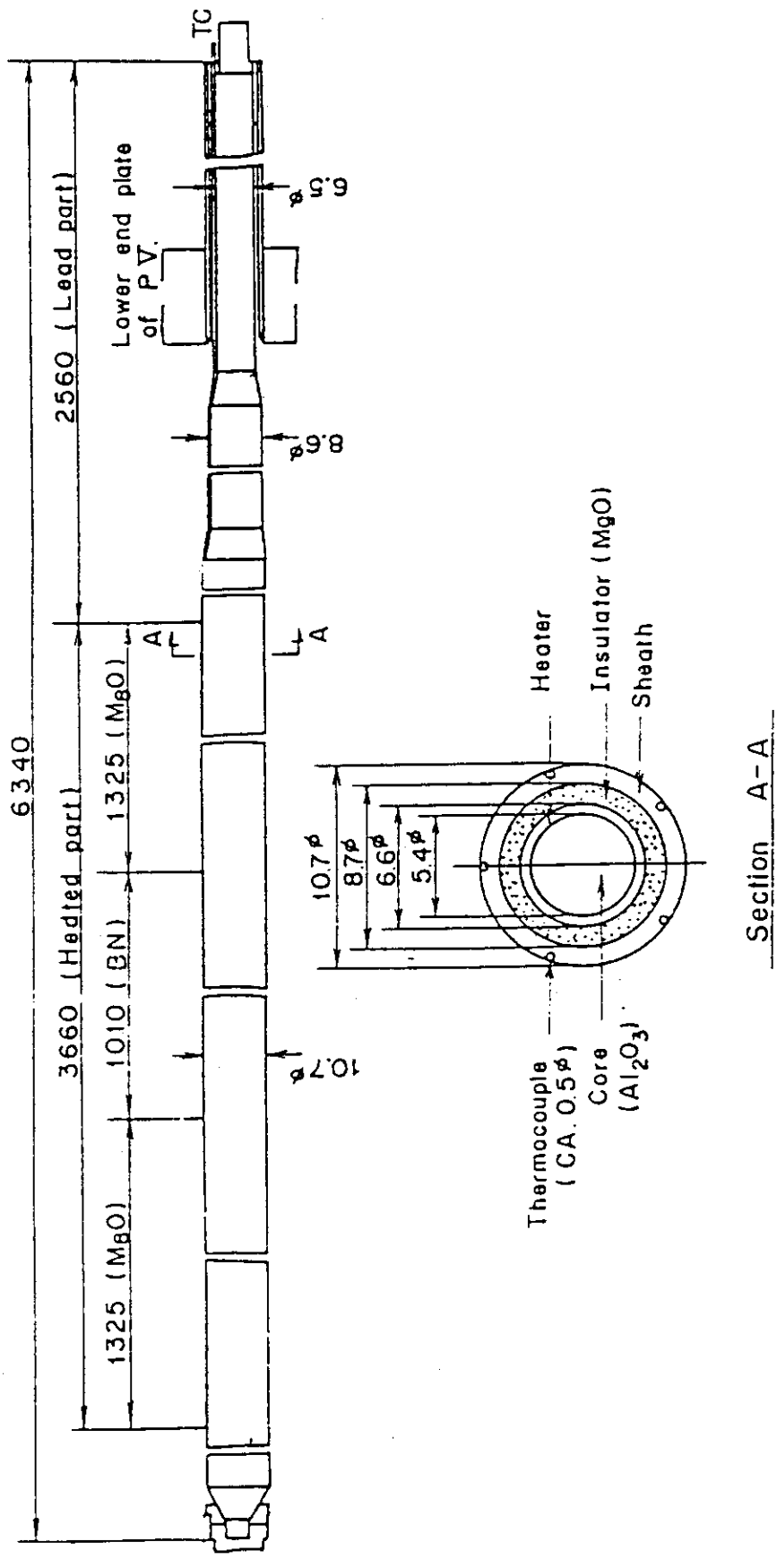

Fig. 2.12 Heater rod

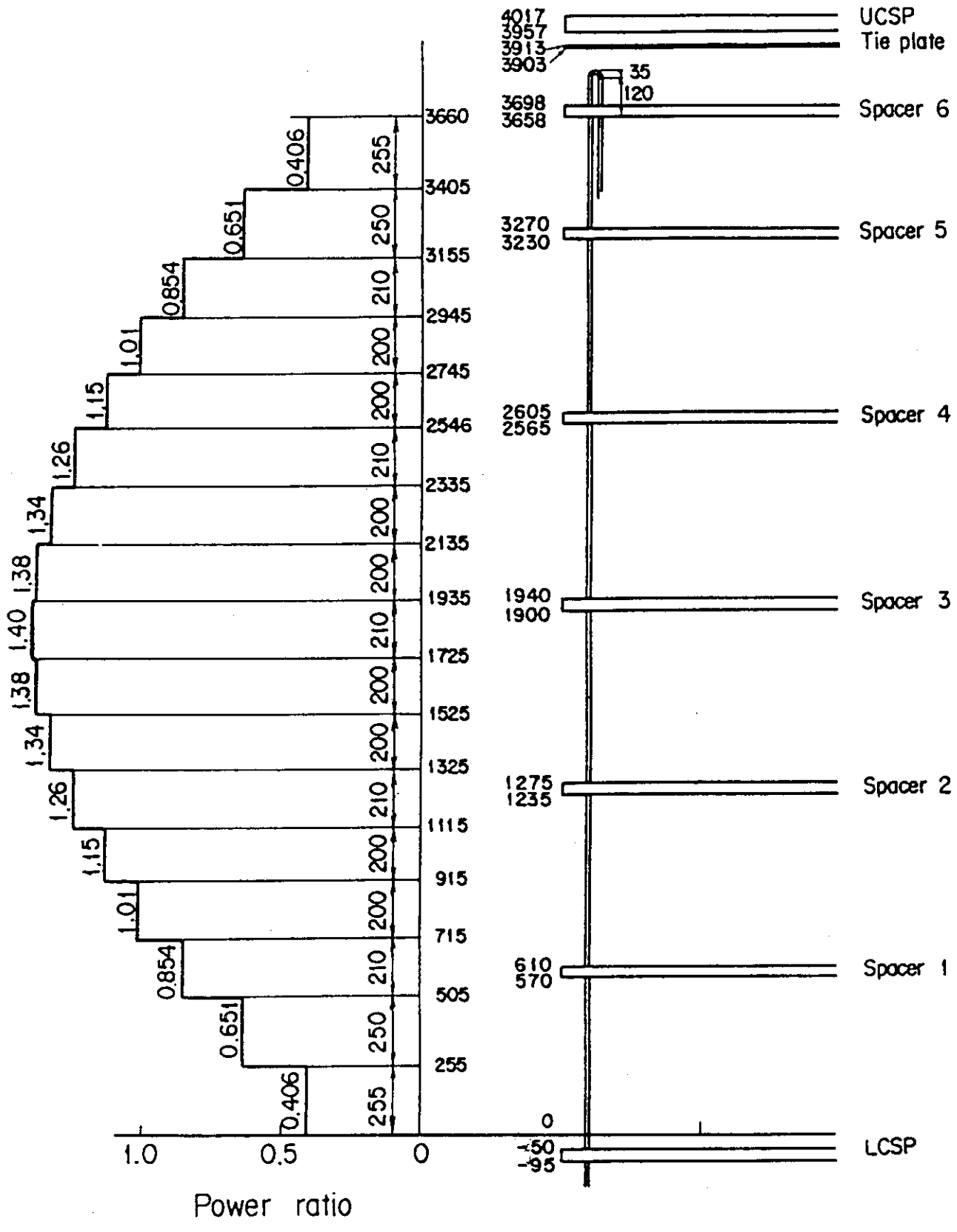

Fig. 2.13 Axial power profile of CCTF Core-II heater rod

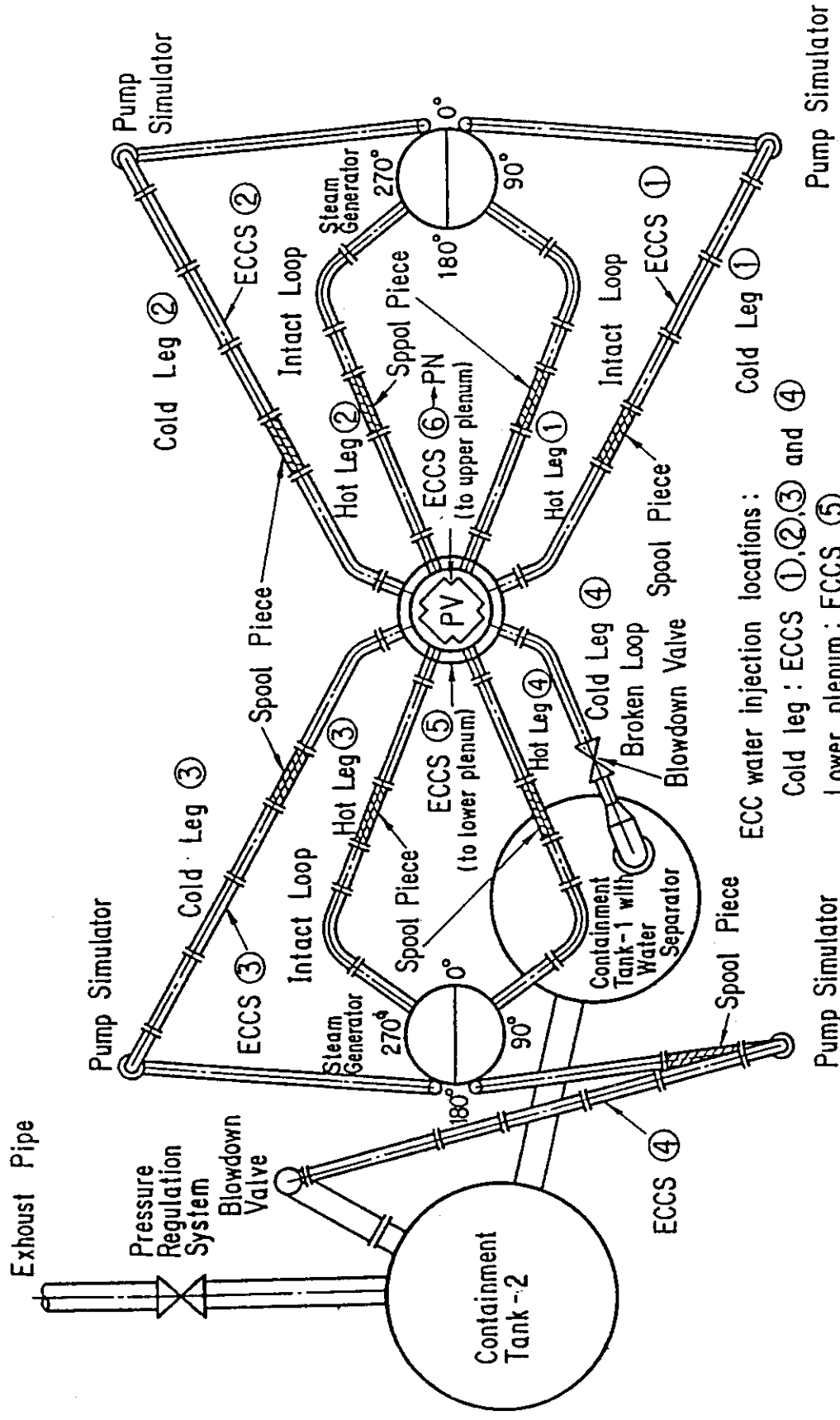

Fig. 2.14 Top view of primary loop pipings

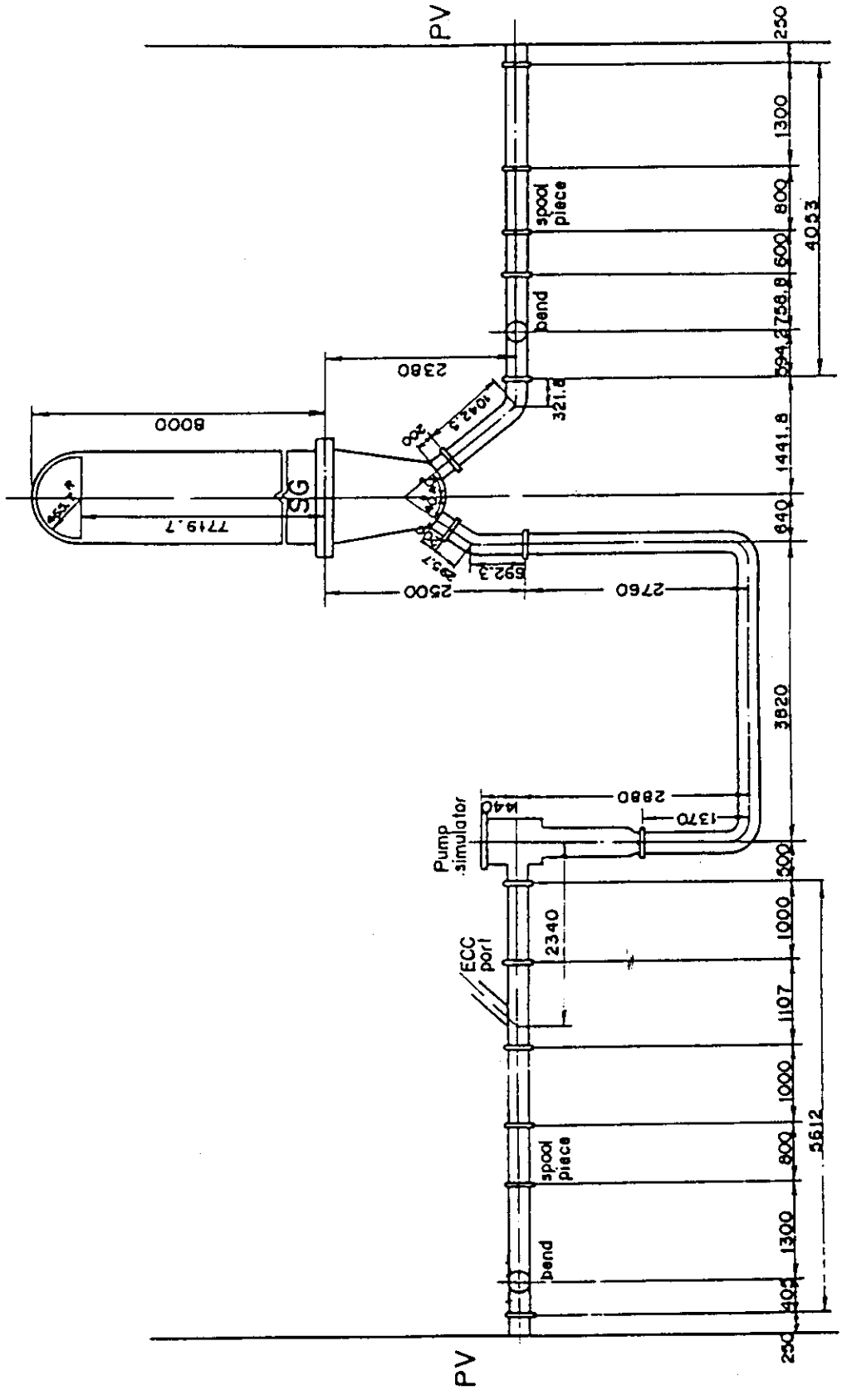

Fig. 2.15 Dimensions of primary loop

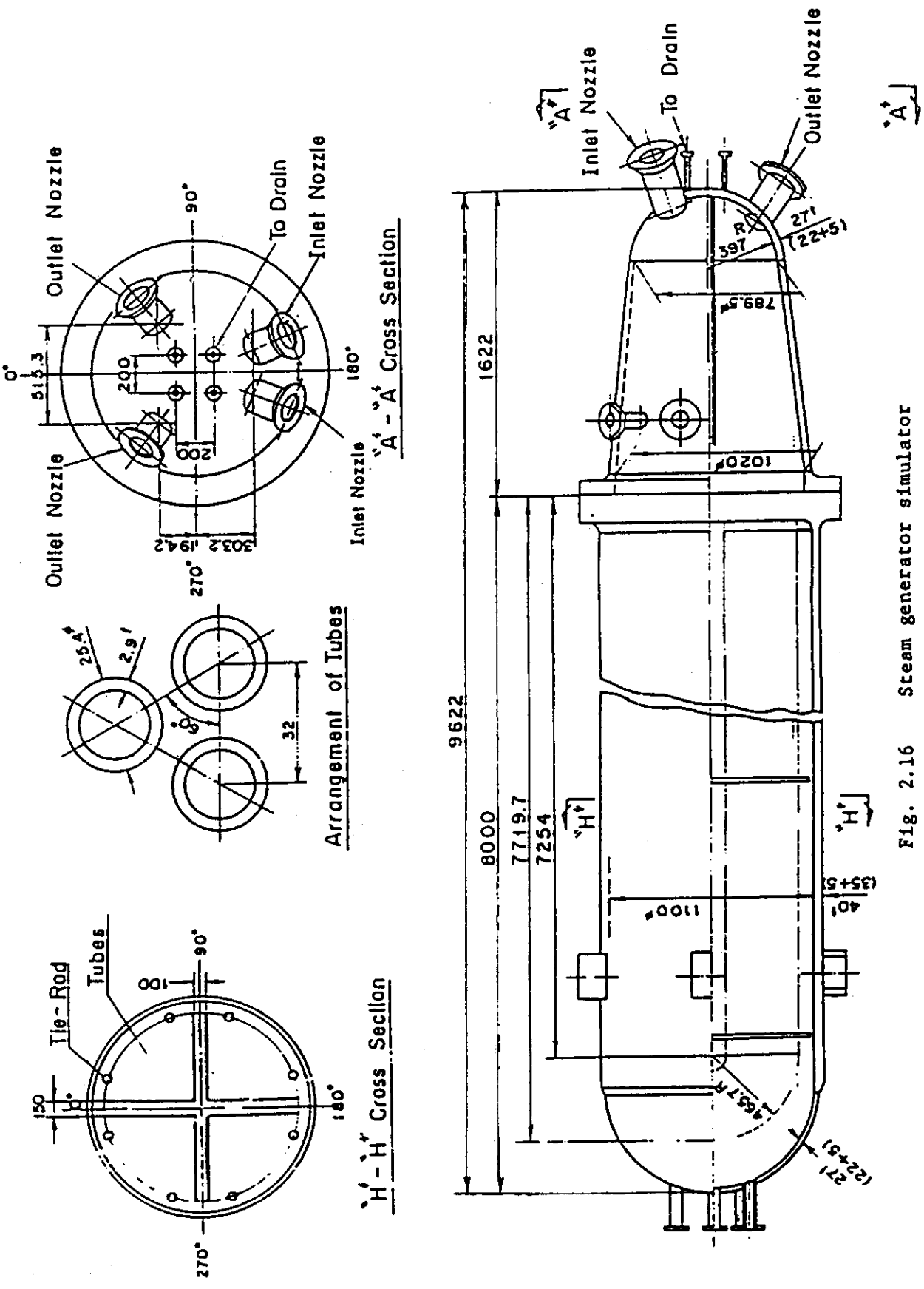

Fig. 2.16 Steam generator simulator

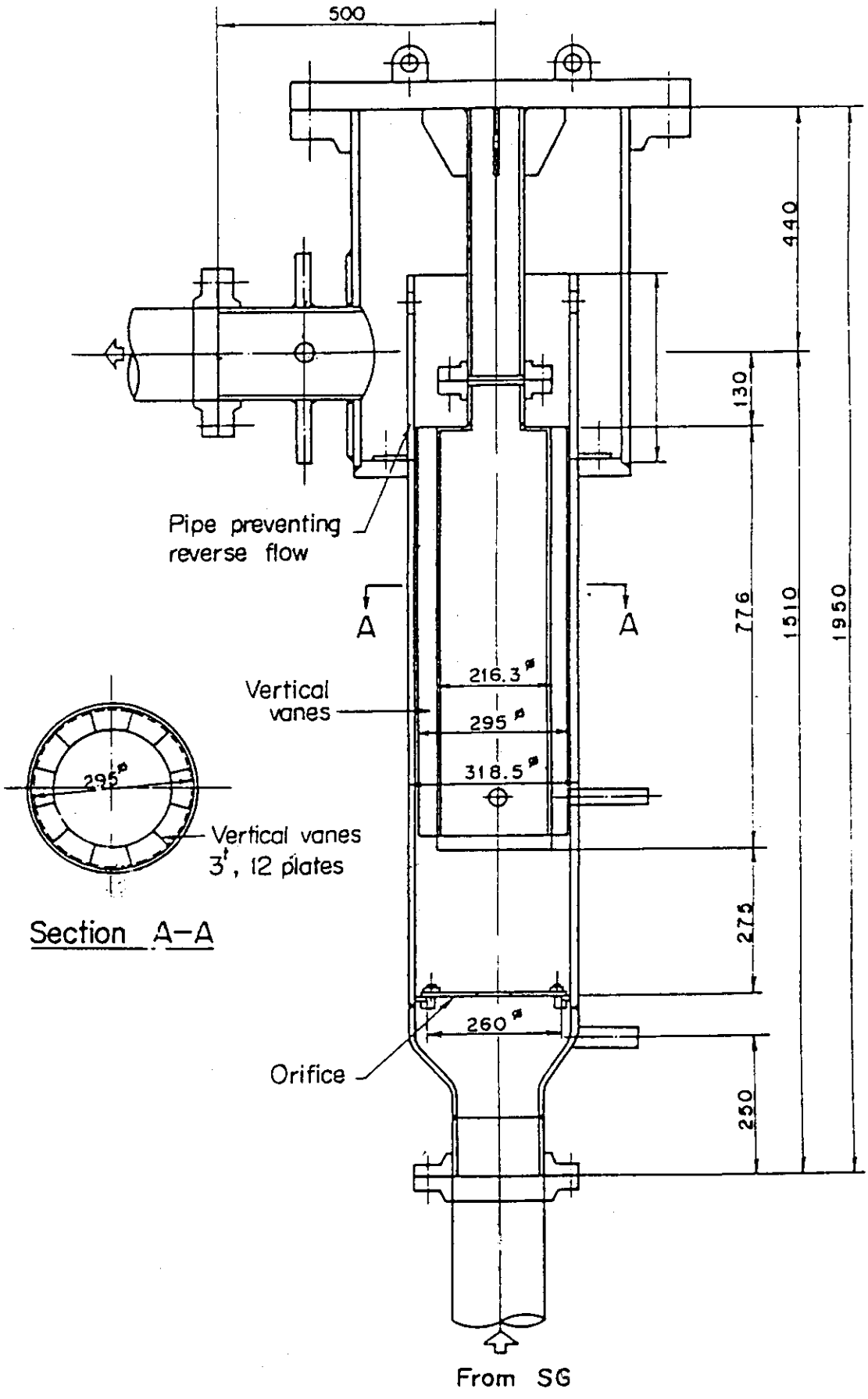

Fig. 2.17 Pump simulator

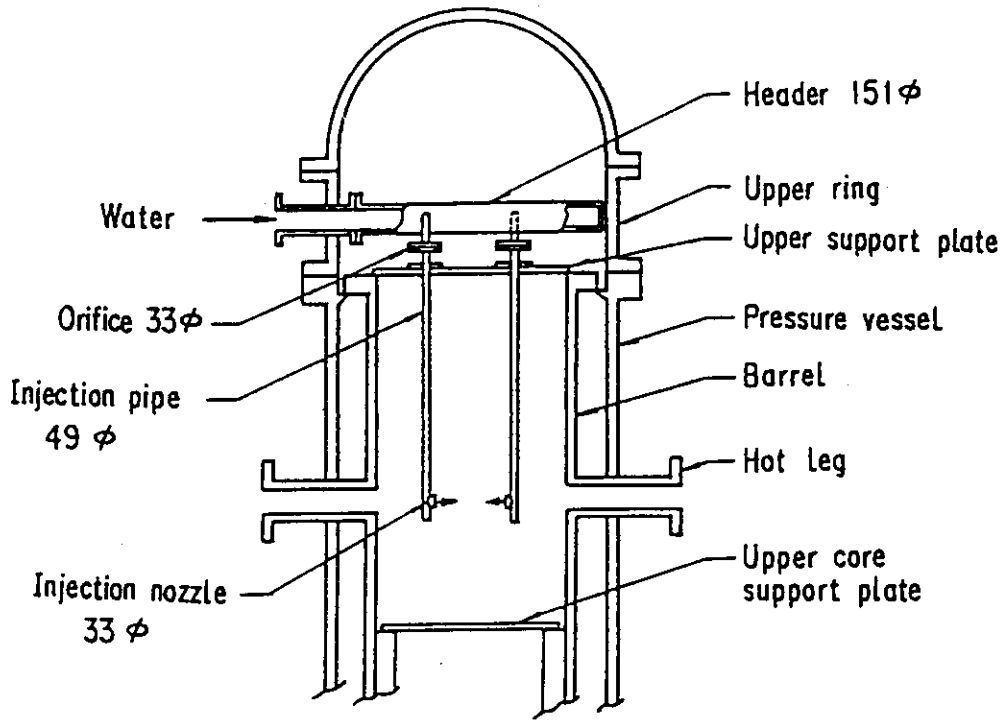

Fig. 2.18 Configuration of upper plenum injection pipe

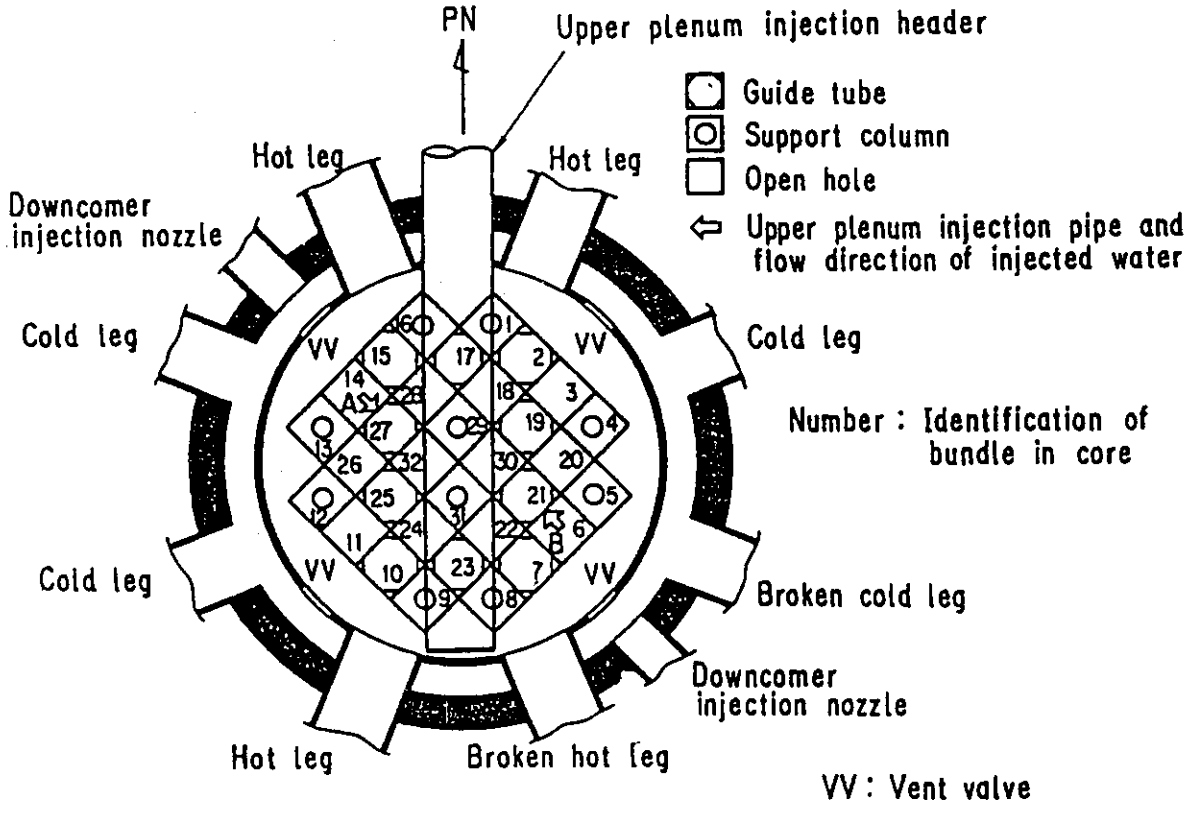

Fig. 2.19 Arrangement and location of upper plenum injection pipe

3. Measured test conditions and data presentation

3.1 Measured test conditions

When the CCTF test C2-9 was initiated(t= 0 s), the core was filled with the saturated steam at 0.2 MPa. The clad temperature of heater rods was about 393 K at t=0 s. The bottom of the pressure vessel was filled with saturated water to the level of 0.82 m from the bottom of the pressure vessel. The initial downcomer wall temperature was 468 K. The wall of the primary piping was preheated to the saturation temperature before the test initiation. The water level in the secondary side of the steam generator 1 and 2 were 7.40 and 7.40 m at the test initiation, respectively. The water temperature in the secondary side of the steam generator was about 540 K.

Figure 3.1 shows the transient of the total power supplied to heater rods in the core. At 0 s, the power is turned on. At 10 s,it reaches 9.34 MW. The decay of the power starts at 95.0 s. The power follows the decay curve type of (ANS x 1.0 + Actinide x 1.1 (30 s after scram)).

Figure 3.2 shows the pressure transient in the containment tank 2. The initial pressure is 0.2 MPa as planned. Figure 3.2 shows that the pressure control was performed successfully in the CCTF test C2-9.

Figure 3.3 shows the transients of the ECC water injection rates into the lower plenum and the three intact cold legs. Figure 3.4 shows the transients of the fluid temperatures at ECC water injection nozzles. The maximum clad surface temperature reached the specified level(995 K) at 86.0 s and the ECC water injection into the lower plenum was initiated. The injected water was accumulated in the lower plenum. At 96 s, the lower plenum was filled with water and the reflood of the heater rods started. At 98 s, the flow control valve in the lower plenum injection line began to close and the ECC water injection into lower plenum was terminated at 102.5 s. The flow control valves in the cold-leg accumulator injection line started openning at 98 s. The injection location of ECC water was switched from the lower plenum to the intact cold legs. The injection rate into cold legs increased with time and reached the setting rate(0.0910 m^3/s) at 102 s. The high injection rate simulates the accumulator injection in a PWR LOCA. At 110 s, the ECC water injection mode was switched to the LPCI mode. The ECC water injection from the accumulator tank was terminated at 113 s. The subcooled water(310 K) in the LPCI tank was pumped out to the intact cold legs by 1010 s.

Table 3.1 summarizes the measured test conditions with the planned ones. The chronology of events are summarized in Table 3.2.

3.2 Data presentation

The selected data from the CCTF test C2-9(Run 68) are presented in Figs. B-1 through B-28 in Appendix B. The Tag-ID of each measurement channel is shown in the upper part of each figure. Tag-IDs shown in each figure are listed in Appendix A with short descriptions of the data processing.

3.3 Comparison of test conditions between high and low LPCI flow rate tests

Table 3.3 summarizes the major test conditions of the tests C2-9 and C2-SH2. In this report the tests C2-9 and C2-SH2 will be called "high LPCI flow rate test" and "low LPCI flow rate test", respectively. The high LPCI flow rate test was planned to simulate the flow conditions of no failure of the LPCI pump unit in a PWR, while the low LPCI flow rate test simulates the flow conditions with the single failure of the pump unit. Except the LPCI flow rate, the other test conditions are almost the same between both the tests.

Table 3.1 Initial conditions for high LPCI flow rate test

	Planned	Measured
Power		
Total (KW) :	7.890	7.87
Linear (kW/m) :	1.182	1.179
Radial power distribution(kW/m) :	1.613:1.414:0.901	1.608:1.414:0.898
Decay type : ANS x 1.0 + Actinidex1.1 (40 s after scram)		
Pressure		
System (MPa) :	0.20	0.20
Steam generator secondary (MPa) :	5.20/5.20	5.18/5.22
Temperature		
Downcomer wall (K) :	471	468
Primary piping wall (K) :	393	395
Steam generator secondary (K) :	539/539	540/540
Peak clad at ECC initiation (K) :	995	995
Peak clad at reflood initiation (K) :	1073	1073
Lower plenum liquid (K) :	393	395
ECC liquid (K) :	308	310
Water level		
Lower plenum (m)	0.90	0.82
Steam generator secondary (m) :	7.4/7.4	7.40/7.40
ECC water injection rate		
Accumulator to lower plenum (m^3/s) :	0.1050	0.1067
Accumulator to cold legs (m^3/s) :	0.0892	0.0923
LPCI to cold legs (m^3/s) :	0.0250	0.0252

Table 3.2 Chronology of events for high LPCI flow rate test

Event	Time (s)
Test initiated (Heater power on) (Data recording initiated)	0.0
Accumulator injection to lower plenum initiated	86.0
Power decay initiated	95.0
Bottom of core recovery(BOCREC) (Reflood initiated)	96.0
Accumulator injection to cold legs initiated	98.0
Accumulator injection to lower plenum ended	102.0
LPCI injection to cold legs initiated	110.0
Accumulator injection to cold legs ended	113.0
All heater rods quenched	584.0
Power off	1010.0
LPCI injection to cold legs ended	1010.0
Test ended (Data recording ended)	1040.0

Table 3.3 Comparison of test conditions between high and low LPCI flow rate tests

Test name / Item	High LPCI flow rate test	Low LPCI flow rate test
Average linear power at reflood initiation (kW/m)	1.179	1.179
Decay curve type	ANSx1.0+actinidex1.1 (30 s after scram)	ANSx1.0+actinidex1.1 (30 s after scarm)
System pressure (MPa)	0.20	0.20
Peak clad temperature at reflood initiation (K)	1073	1073
ECC water temperature (K)	310	310
ECC water injection rate (m^3/s) (Injection time (s))		
Acc to lower plenum	0.107 (-10 s to 4 s)	0.104 (-10 s to 4 s)
Acc to cold legs	0.091 (4 s to 16 s)	0.088 (4 s to 16 s)
LPCI to cold legs	0.0252 (16 s to 914 s)	0.0111 (16 s to 889 s)

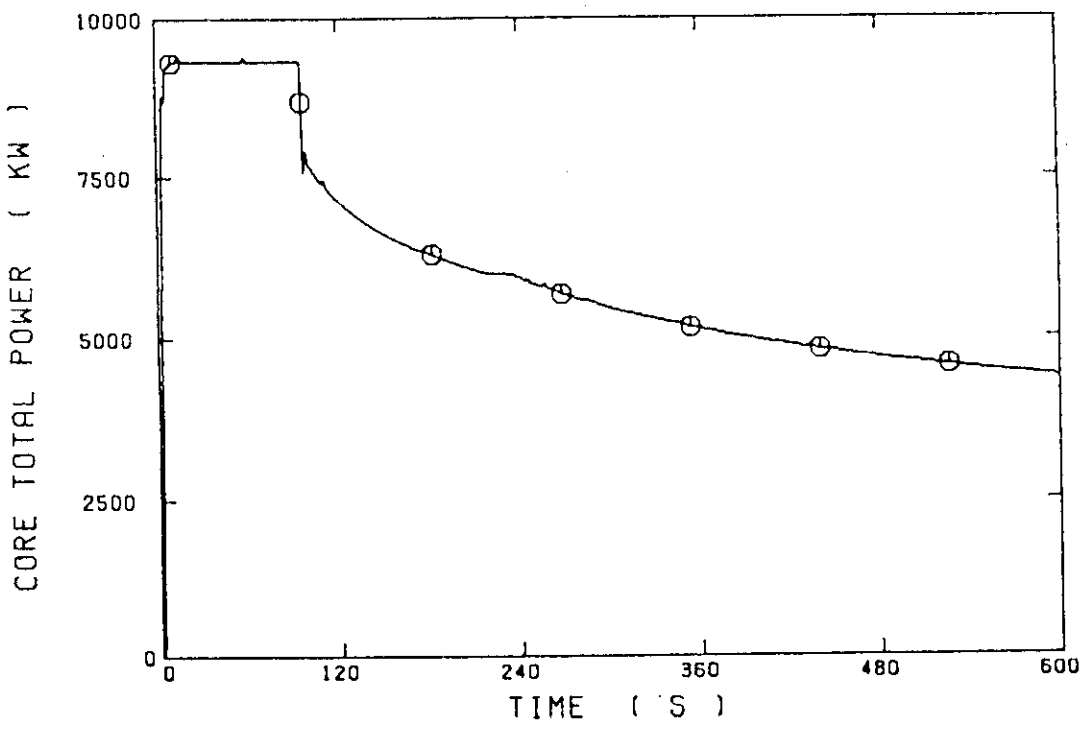

Fig.3.1 Total power supplied to heater rods in core in CCTF test C2-9

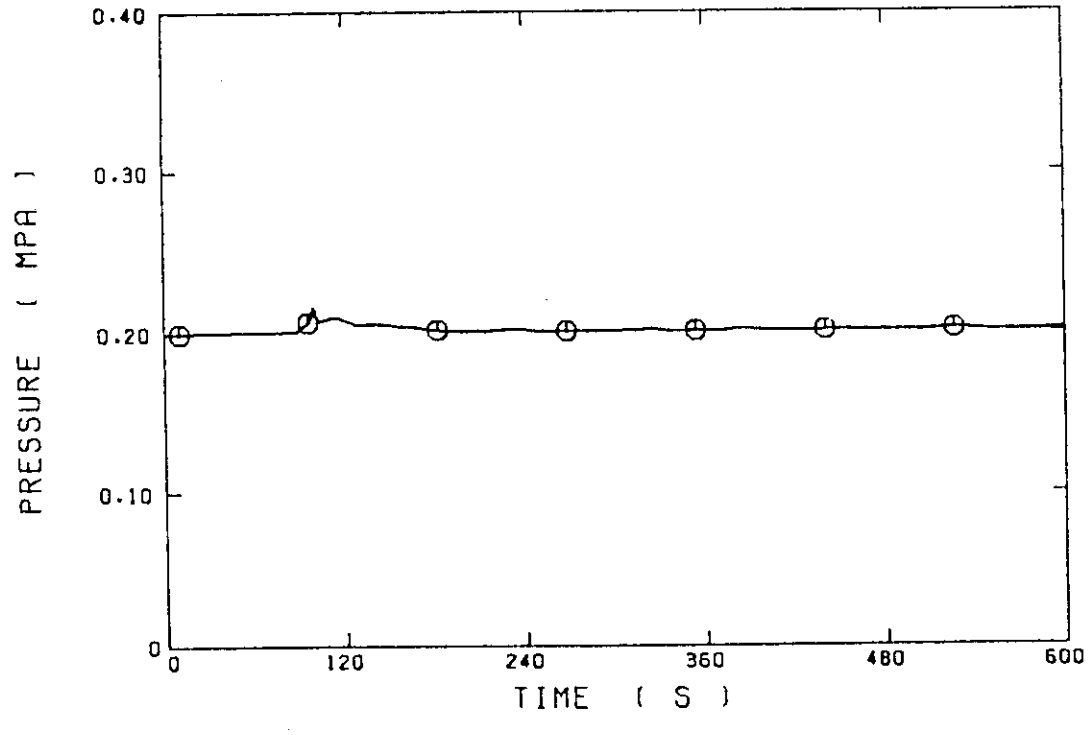

Fig.3.2 Pressure in containment tank 2 in CCTF test C2-9

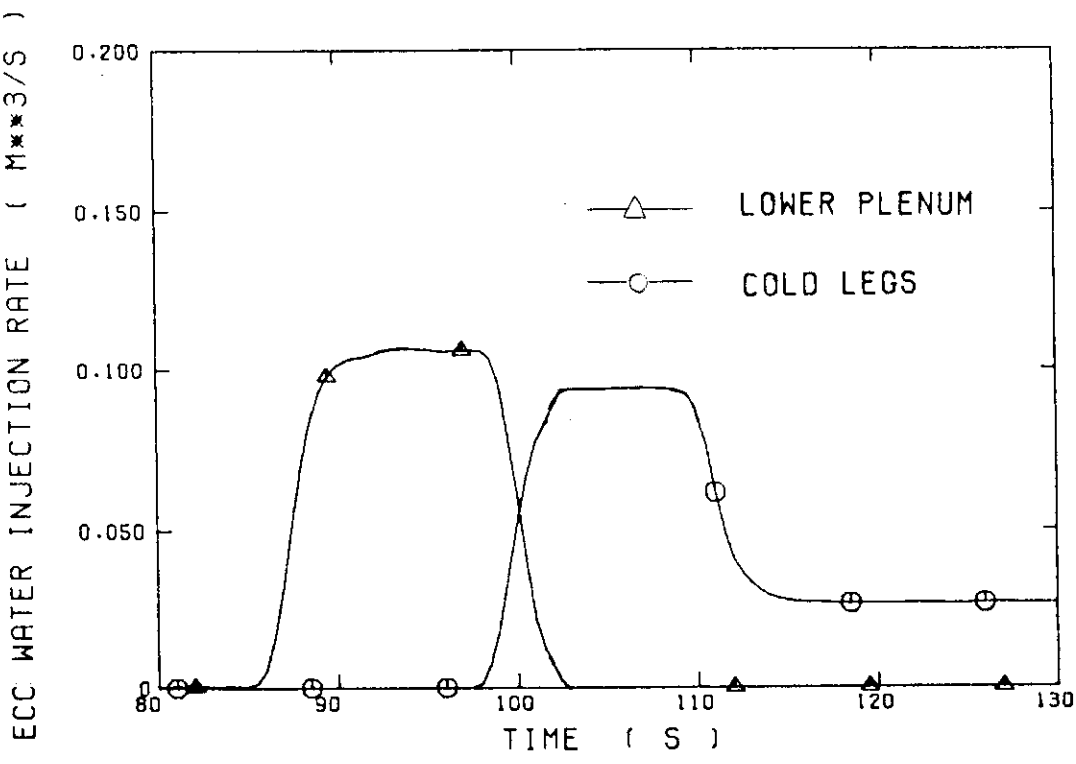

Fig.3.3 ECC water injection rates into lower plenum and three intact cold legs in CCTF test C2-9

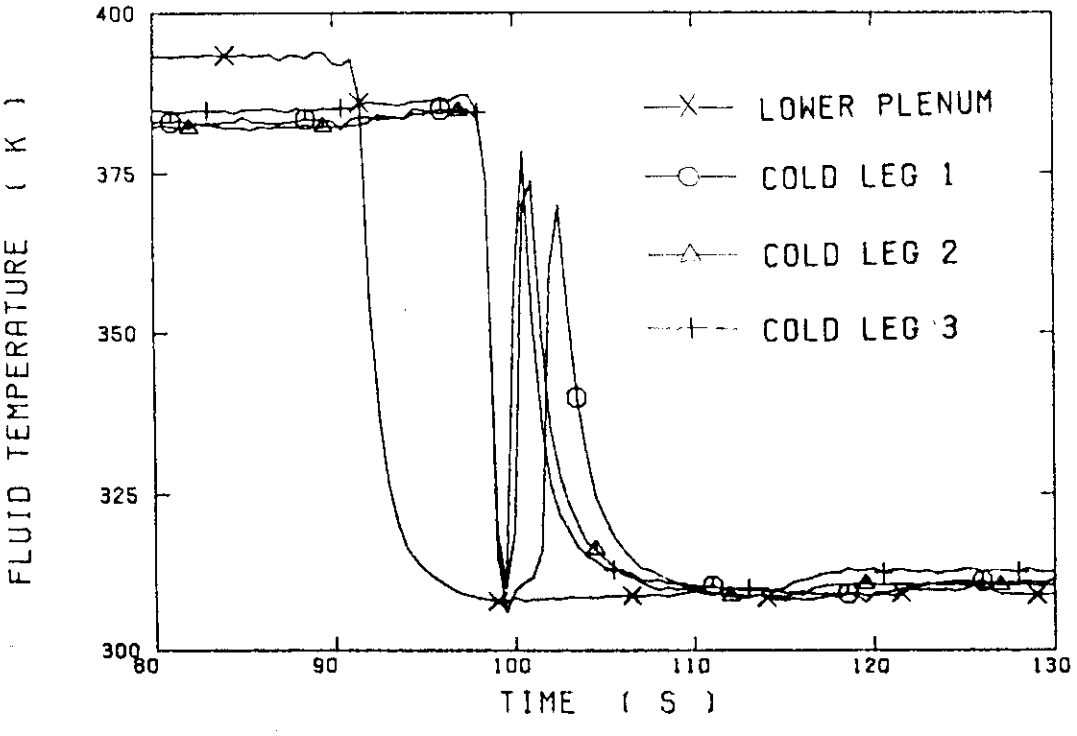

Fig.3.4 Fluid temperatures at ECC water injection nozzles in CCTF test C2-9

4. Results and discussion

4.1 LPCI flow rate effect on flow behavior in primary system

Figure 4.1 shows the comparison of the water head in upper plenum, core and downcomer between the high and low LPCI flow rate tests. Before 200 s, the water head in the upper plenum is almost the same between both tests. After 250 s, the water head in the low LPCI flow rate test is higher than that in the high LPCI flow rate test. The core water head increases rapidly just after the reflood initiation. Before 20 s (that is, during the Acc mode), the core water head is almost the same between both tests because the Acc injection rate is almost the same between both tests. After the switch of the ECC injection mode from the Acc mode to the LPCI mode, the high LPCI flow rate test shows the higher core and downcomer water heads than those in the low LPCI flow rate test. This shows that the increase in the LPCI flow rate results in the increase of the water mass accumulated in the core and the downcomer.

Figure 4.2 shows the LPCI flow rate effect on the mass flow rate and the differential pressure through the primary loops. The mass flow rate was evaluated using the differential pressure through the pump orifice plates. In the evaluation, it was assumd that the flow resistance coefficients through the pump orifice plates of the intact and broken loops were 14.29 and 16.88, respectively. These values of the flow resistance coefficients were calculated from the pitot tube and differential pressure data in the CCTF test C1-5. Figure 4.2 shows that the mass flow rate and differential pressure through the intact loop are increased by the increase in the LPCI flow rate. On the other hand, for the broken loop, both the mass flow rate and the differential pressure are decreased by the increase in the LPCI flow rate. The results show that the LPCI flow rate affects the distribution of the mass flow rates through the primary loop.

Figures 4.3 and 4.4 show the comparisons of the flow resistance coefficients through the broken and intact loops, respectively. The flow resistance coefficient is defined by

$$K = \Delta P_L \; / \; (m_L^2 / 2\rho A_L^2) \;, \qquad (1)$$

where

ΔP_L: Differential pressure through a loop (Pa),
m_L: Mass flow rate through a loop (kg/s),
ρ : Saturated steam density in the upper plenum (kg/m^3),
A_L: Flow area of a loop (= 0.01892) (m^2) .

The mass flow rates shown in Fig.4.2 were used to calculate the flow resistance coefficients.

The flow resistance coefficient through the intact loop is about 15 during the Acc mode (at about 15 s). After the switch of the ECC injection mode from Acc to LPCI. the flow resistance coefficient increases with time and then it shows a nearly constant value by 440 s. At about 450 s, the flow resistance coefficients begin to increase. The time-averaged flow resistance coefficients between 100 and 300 s are 24.0 and 28.5 through the intact loop in the high and low LPCI flow rate tests, respectively. The flow resistance coefficient through the intact loop of the high LPCI flow rate test is 86 % of that in the low LPCI flow rate test. The increase in the LPCI flow rate resulted in the decrease of the loop flow resistance through the intact loop.

For the broken loop, the flow resistance coefficients are nearly constant during the tests as shown in Fig. 4.4. In these two tests, no ECC water was not injected into the broken loop. It seems that the ECC water injection rate has significant effect on the loop flow resistance coefficient through the primary loops.

Figure 4.5 shows the comparisons of the flow resistance coefficients along the intact loop between the high and low LPCI flow rate tests. The flow resistance coefficients were calculated with Eq.(1) for every section using the mass flow rate shown in Fig.4.2. From Fig.4.5, the following is found :

(1) The low flow resistance coefficient during the Acc mode is caused by the pressure recovery through the cold leg piping.

(2) The increase of the loop flow resistance at about 450 s is attributed to the increase of the flow resistance coefficient through the hot leg riser part.

(3) The decreased flow resistance coefficient with the LPCI flow rate shown in Fig. 4.3 results from the decrease in the flow resistance coefficient through the cold leg piping.

In order to explain the LPCI flow rate effect on the flow resistance coefficient through the intact loop, it is necessary to develop flow model for the differential pressure through the cold leg piping.

In the cold leg, the subcooled ECC water is mixed with the steam

flowing from the pump simulator. The water comes into direct contact with the steam and violent condensation takes place in the cold leg. One of the authors studied on the flow behavior with the scaled test facility and developed a correlation for the flow pattern transition in the cold leg,[6] given by

$$m_{gtr} = 0.84\ m_{cmax} \quad , \tag{2}$$

$$m_{BC} = 0.75\ m_{cmax} \quad , \tag{3}$$

$$m_{AB} = 0.0028\ m_{cmax}^2 + 0.47\ m_{cmax} \quad , \tag{4}$$

where

$$m_{cmax} = \frac{C_{p\ell}(T_{sat} - T_{\ell i})}{h_{fg}} \cdot m_{\ell i} \quad , \tag{5}$$

$m_{\ell i}$: ECC water injection rate (kg/m^2s),

m_{gtr} : Transition steam mass velocity between Type C and stable wavy flows (kg/m^2s),

m_{AB} : Transition steam mass velocity between Type A flow and Type B flows (kg/m^2s),

m_{BC} : Transition steam mass velocity between Type B flow and Type C flows (kg/m^2s),

m_{cmax} : Condensability of injectted water (kg/m^2s).

In the experiment, the flow pattern was characterized by the motion of the interface of the plugging water. Type A, B, C flows are characterized by the interface oscillation across the water injection nozzle, the interface oscillation downstream of the water injection nozzle, and the stationary interface downstream of the water injection nozzle, respectively.

Figure 4.6 shows the comparison of the steam mass flow rate m_I with the mass flow rates calculated by Eqs. (2) through (5) in the high LPCI flow rate test. Figure 4.6 shows that the steam mass flow rate is nearly equal to the flow boundary between Type B and C flows by about 530 s. The results predict that the cold leg is plugged with water and that the interface of the plugging water is rather stationary.

Figure 4.7 shows the fluid temperature along the cold leg in the high LPCI flow rate test. The fluid temperature labeled by TE12CW was measured upstream of the ECC water injection port and the fluid temperatures labeled by TE13CW and TE14CW were measured downstream of the ECC water injection port. The saturation temperature was about 400 K. Figure 4.7 shows that the fluid is saturated or superheated in the upstream of the ECC port and subcooled in the downstream of the ECC water injection port. The result suggests that the ECC water flow to the upstream of the ECC water injection port is not significant.

Figure 4.8 shows the measured fluid density in the high LPCI flow rate test with the spool piece installed at the downstream of the ECC water injection port. The fluid density is about 750 kg/m^3 during the test. The result demonstrates that the downstream of the ECC water injection port is plugged by the water. The result is consistent with the flow patterns predicted by Eqs.(2) through (5). Figure 4.9 shows the measured fluid density in the low LPCI flow rate test. The density is low between 100 and 800 s after the test initiation. The result indicates that the cold leg is not plugged by the water in the period.

Figure 4.10 shows the comparisons of the steam and water mass flow rates through the broken cold leg of the pressure vessel side. The steam mass flow rate was measured by the orifice plates installed at the connecting pipe between the containment tanks 1 and 2. The water mass flow rate is evaluated by the differentiation of the measued transient of the water level in the containment tank 1.

In the high LPCI flow rate test, the steam mass flow rate is nearly equal to zero. The result is consistent with the data shown in Figs. 4.6 through 4.8. It is considered that the low steam mass flow rate in the high LPCI flow rate test is attributed to the complete condensation of steam in the cold legs and the downcomer. In the low LPCI flow rate test, the steam mass flow rate is relatively high. As shown in Fig. 4.9, the steam was not condensed completely in the low LPCI flow rate test. The high steam mass flow rate is attributed to the incomplete condensation of steam in the cold legs and the downcomer.

4.2 LPCI flow rate effect on thermal hydraulic behavior in core

Figure 4.11 shows the comparisons of the clad surface temperature at the midplane of a peak power rod. The turnaround temperature and the quench time are 1109 K and 276.5 s in the high LPCI flow rate test, respectively. Those are 1100 K and 255.5 s in the low LPCI flow rate test, respectively. Test results show that the higher LPCI flow rate

resulted in the worse core cooling in these two tests. It is generally believed in the safety evaluation of a PWR that the higher LPCI flow rate results in the better core cooling,in other words, that the lower LPCI flow rate gives more conservatism of the core cooling. The CCTF results show that the lower LPCI flow rate is not necessarily a conservative assumption for the evaluation of the core cooling during the reflood phase of a PWR-LOCA.

Figure 4.12 shows the comparisons of the flow parameters at the core inlet, which is considered to affect the core cooling significantly. The effect of these flow parameters on the core cooling has been studied by many researchers.[7],[8] Previous tests showed that each of higher core inlet subcooling, higher core inlet mass flow and higher core inlet pressure results in the better core cooling. As shown in Fig. 4.12, none of these factor is the same between the high and low LPCI flow rate tests.

It is expected that the core cooling is enhanced through the effect of the increased core inlet subcooling and mass flow by the increase of the LPCI flow rate. On the other hand, it is expected that the core cooling is degraded through the effect of the decreased core inlet pressure by the increase of the LPCI flow rate. As shown in Fig. 4.11, the increase of the LPCI flow rate resulted in the worse core cooling. Thus, it is considered that the worse core cooling in the high LPCI flow rate is attributed to the effect of the lower core inlet pressure, which is predominant to the effect of the higher core inlet mass flow and subcooling.

The core inlet pressure P_{CR} is described by

$$P_{CR} = P_{CN} + \Delta P_{BCL} + \Delta P_{DC} \quad , \tag{6}$$

where

P_{CN} : Containment pressure (Pa) ,
ΔP_{BCL} : Differential pressure through the broken cold leg (Pa),
ΔP_{DC} : Downcomer water head (Pa).

Figure 4.13 shows the comparison of each term in the right-hand side of Eq.(6). Figure 4.13 confirms that the lower core inlet pressure in the high LPCI flow rate test is caused mainly by the lower pressure drop through the broken cold leg.

From these discussions, it is concluded that the worse core cooling in the high LPCI flow rate test is caused by the lower pressure drop

through the broken cold leg resulting in the lower core inlet pressure. In the current evaluation model (EM) code, the differential pressure through the broken cold leg is underpredicted. [4] Thus, it is expected that the current EM code is still conservative.

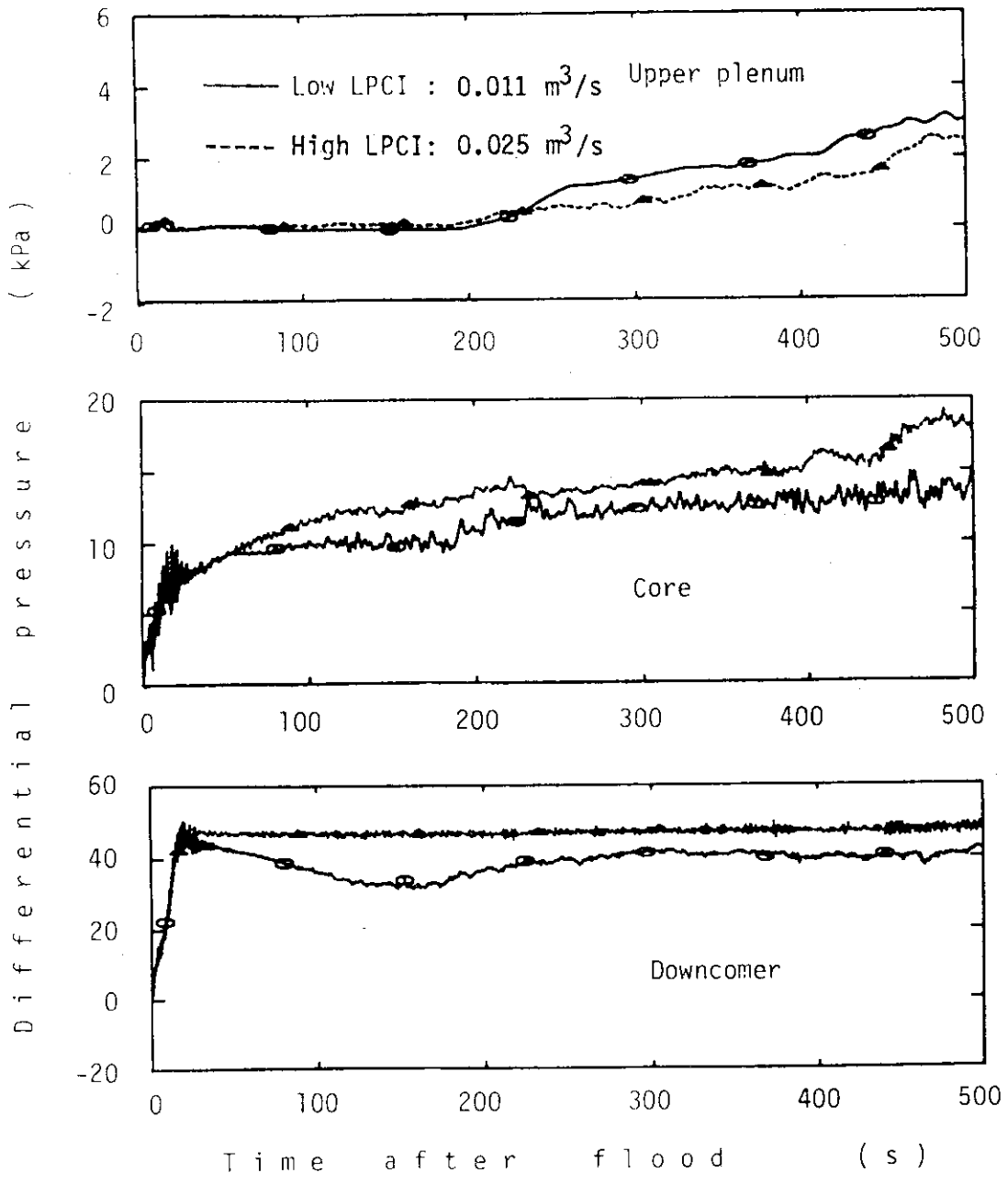

Fig. 4.1 LPCI flow rate effect on water head in upper plenum,core and downcomer

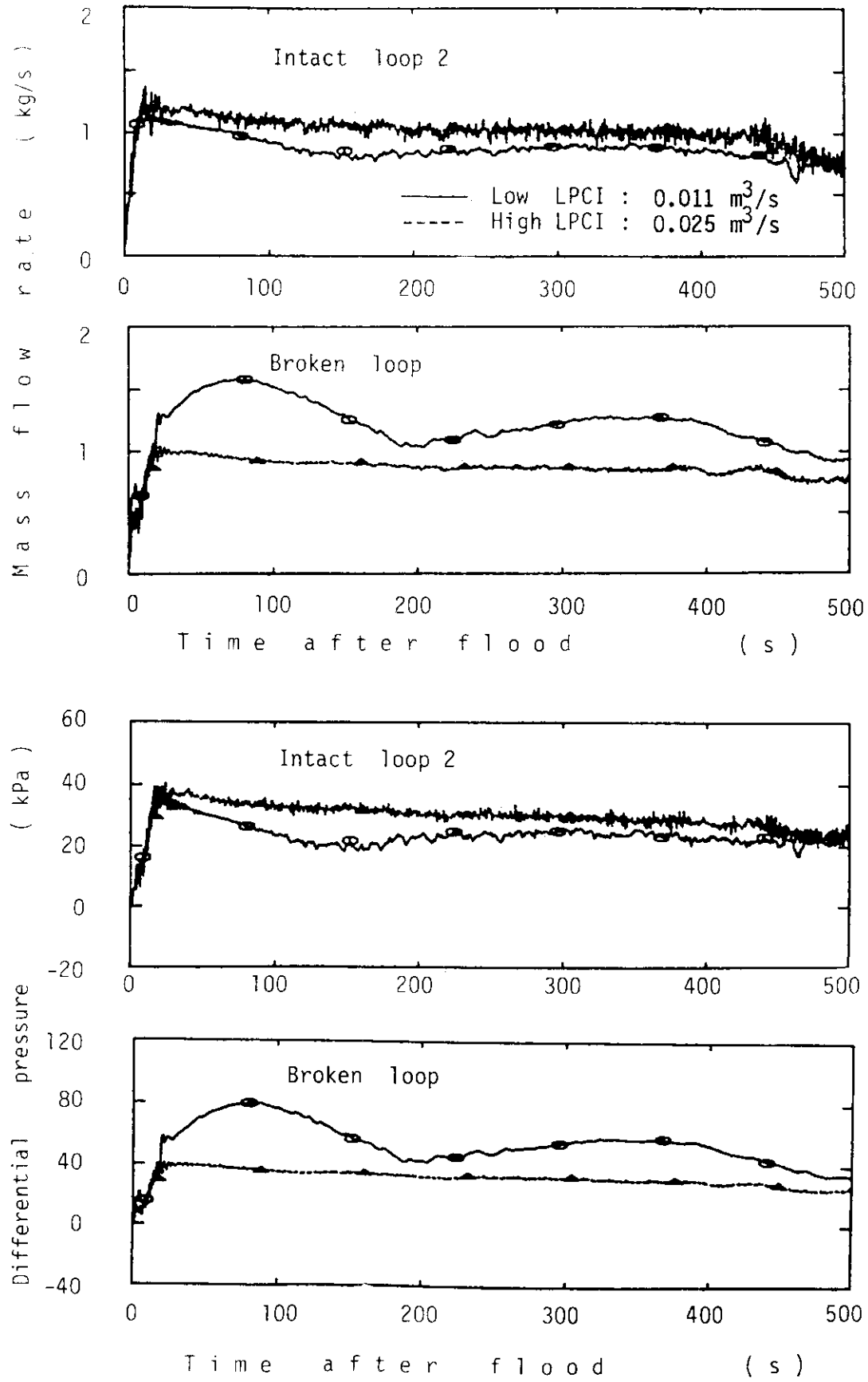

Fig. 4.2 LPCI flow rate effect on mass flow rate and differential pressure through primary loops in CCTF

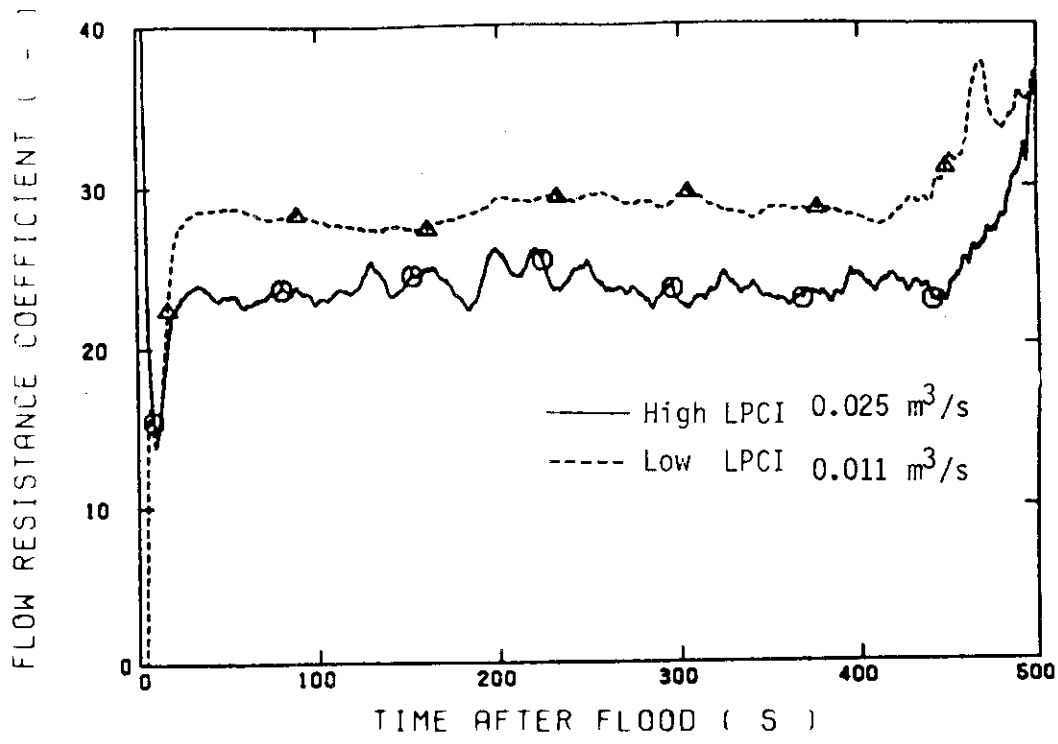

Fig. 4.3 Comparison of the flow resistance coefficient through the intact loop between the high and low LPCI flow rate tests

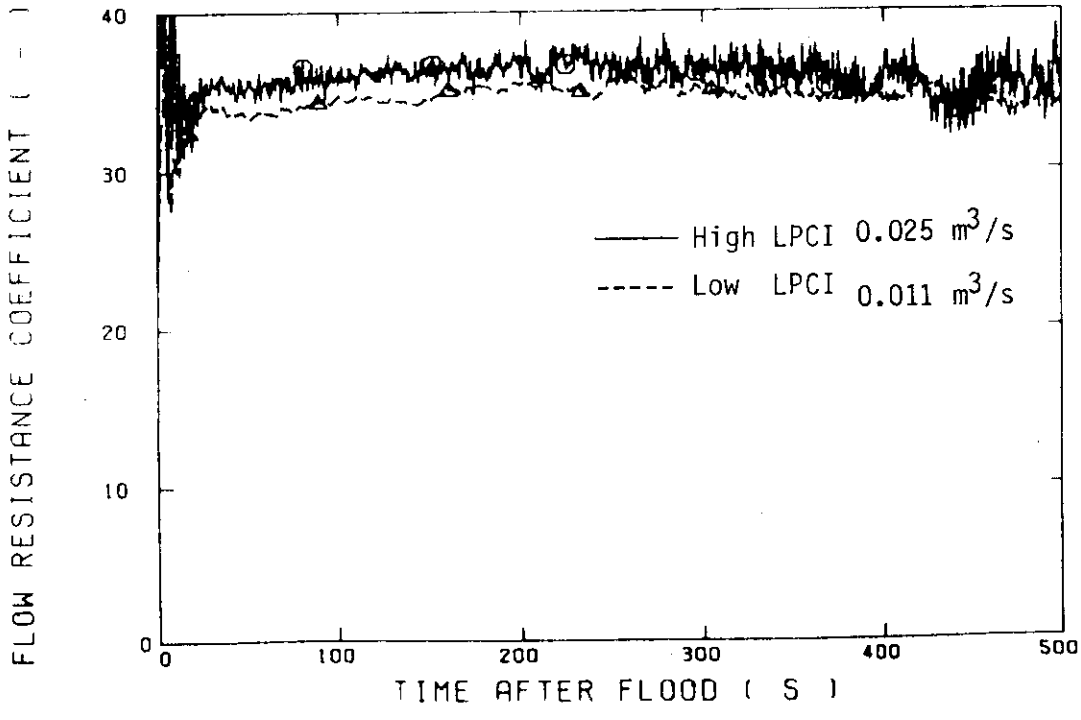

Fig. 4.4 Comparison of the flow resistance coefficient through the broken loop between the high and low LPCI flow rate tests

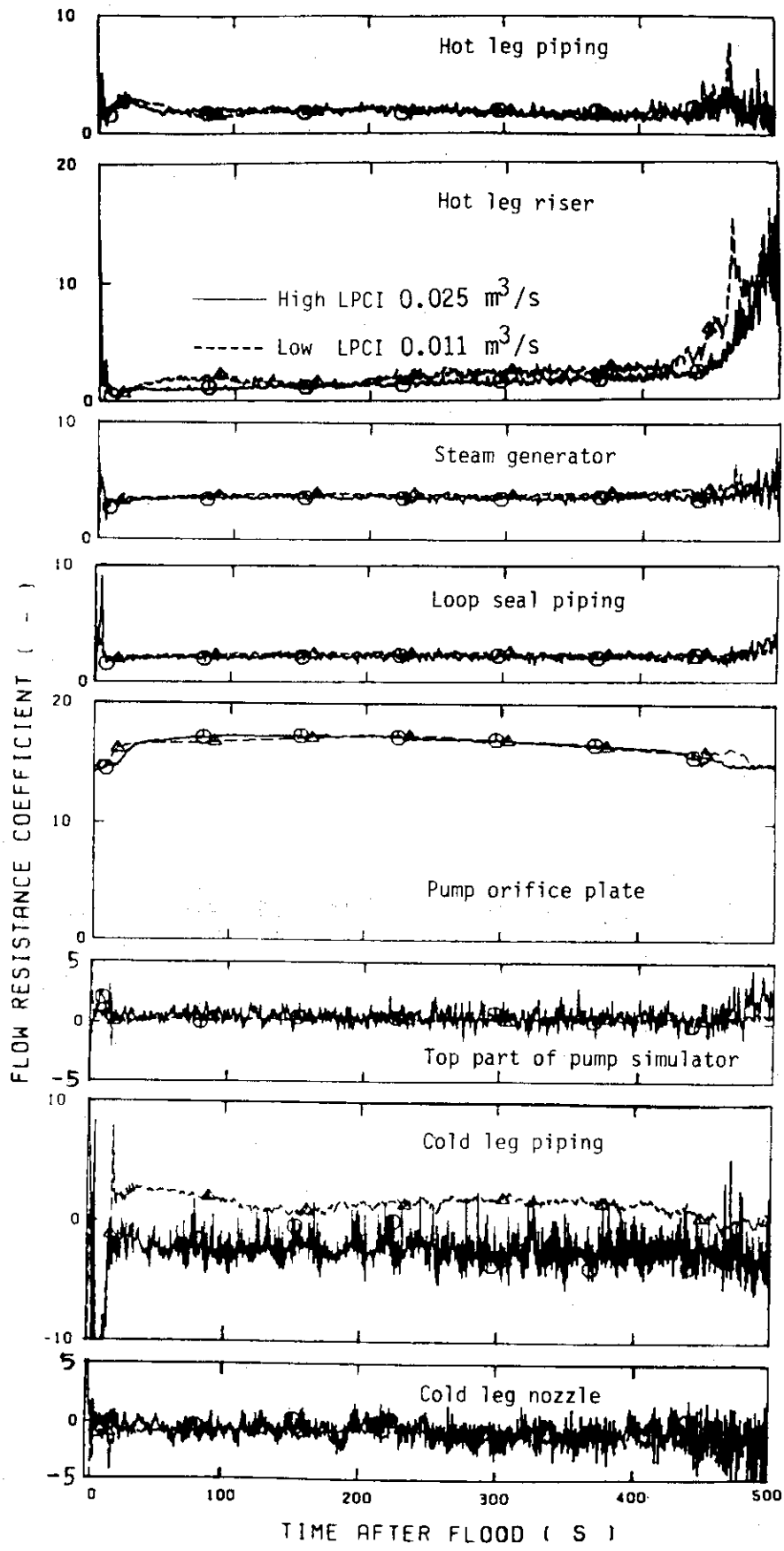

Fig. 4.5 Comparison of flow resistance coefficients along the intact loop between the high and low LPCI flow rate tests

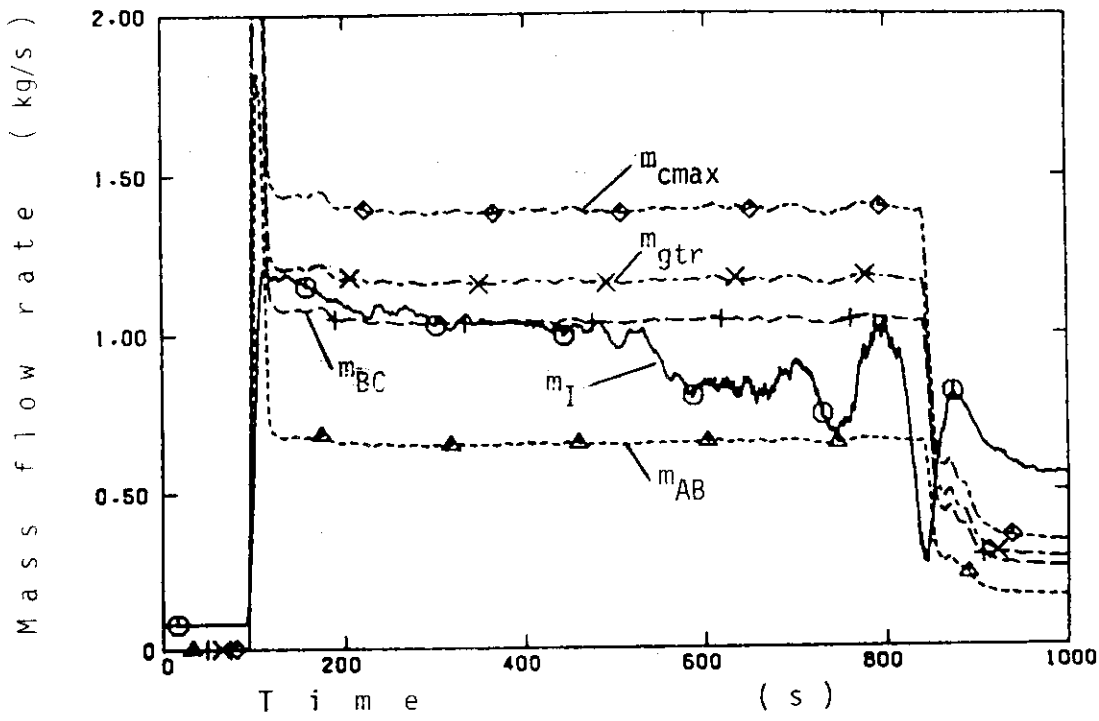

Fig. 4.6 Comparison of the steam mass flow rate with the condensability of the ECC water in the high LPCI flow rate test

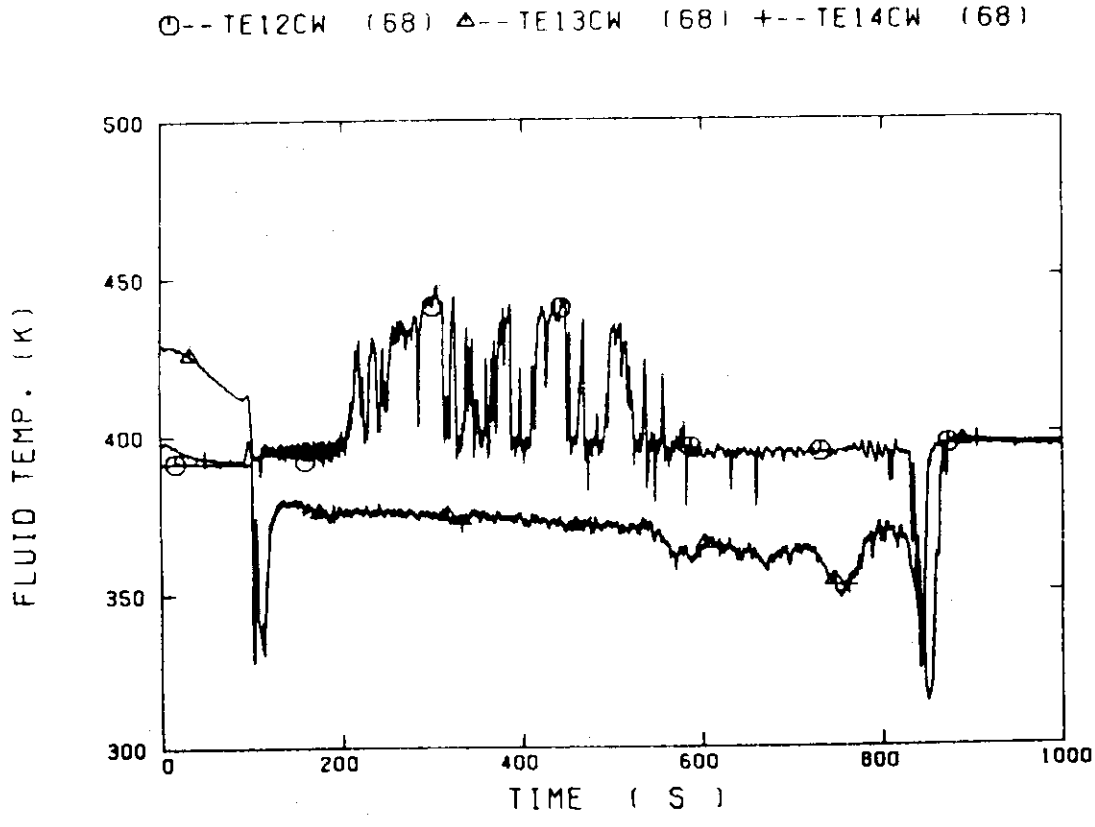

Fig. 4.7 Fluid temperature along the cold leg in the high LPCI flow rate test

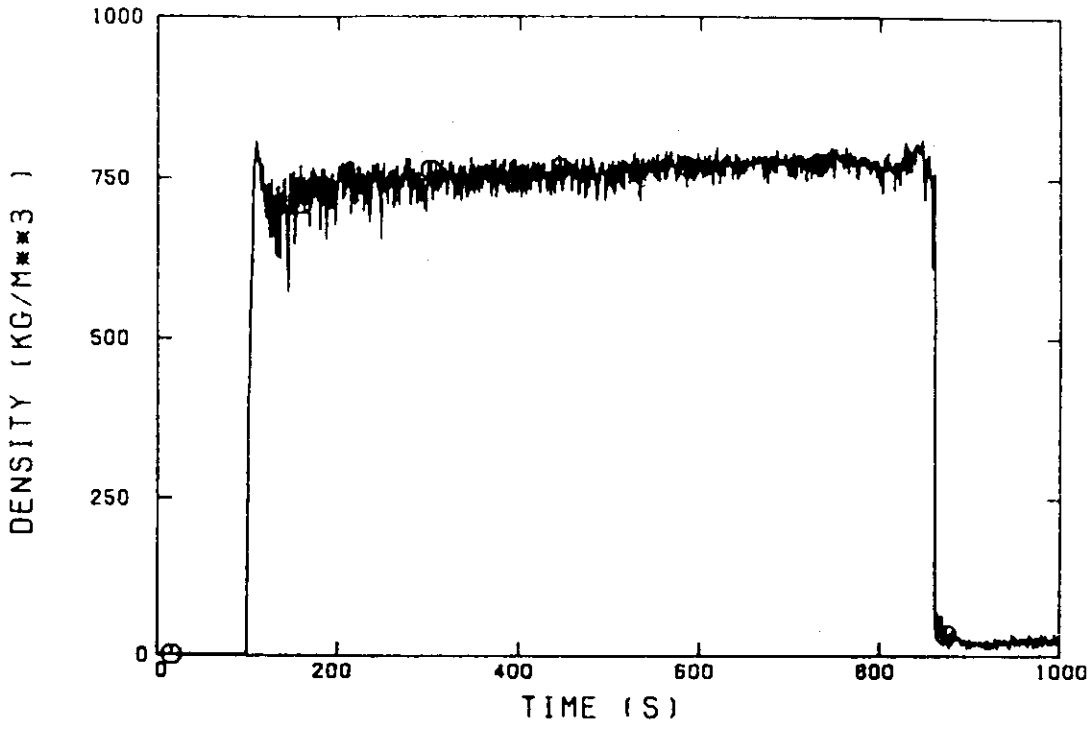

Fig. 4.8 Fluid density at the downstream of the ECC water injection port in the high LPCI flow rate test

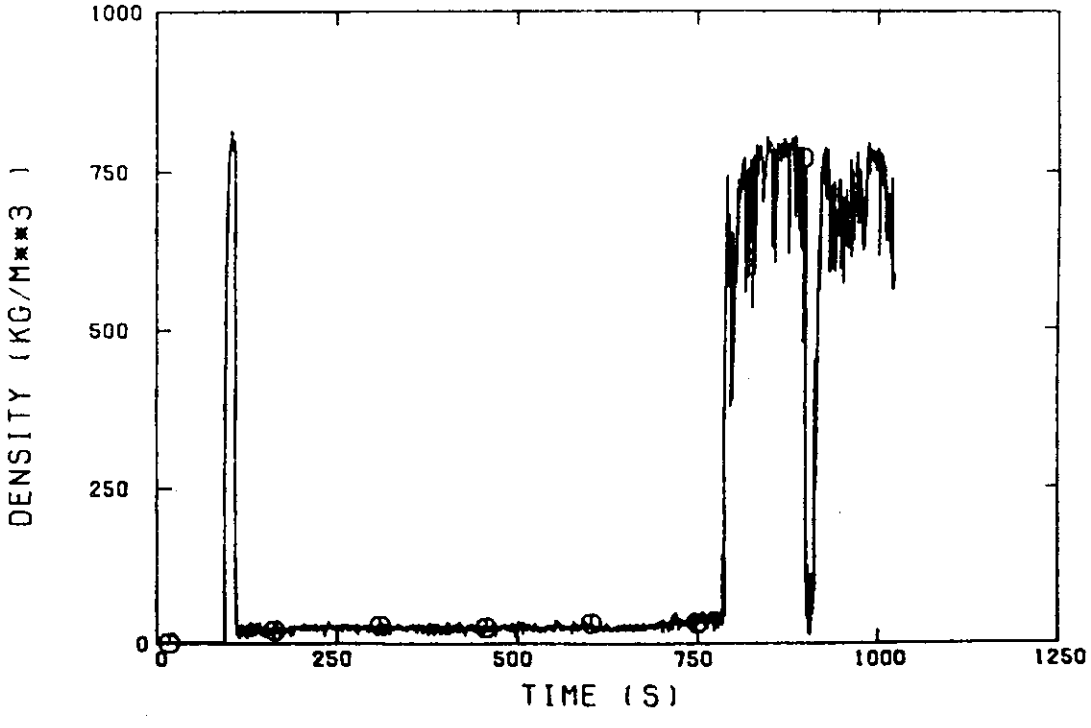

Fig. 4.9 Fluid density at the downstream of the ECC water injection port in the low LPCI flow rate test

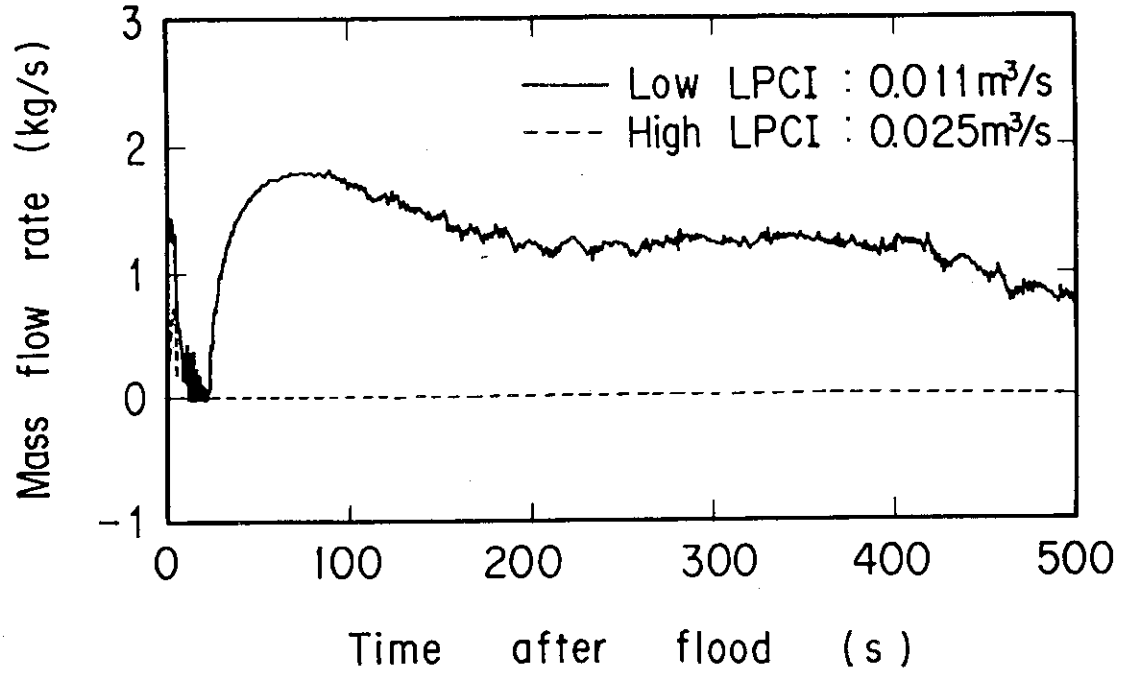

(a) Steam mass flow rate

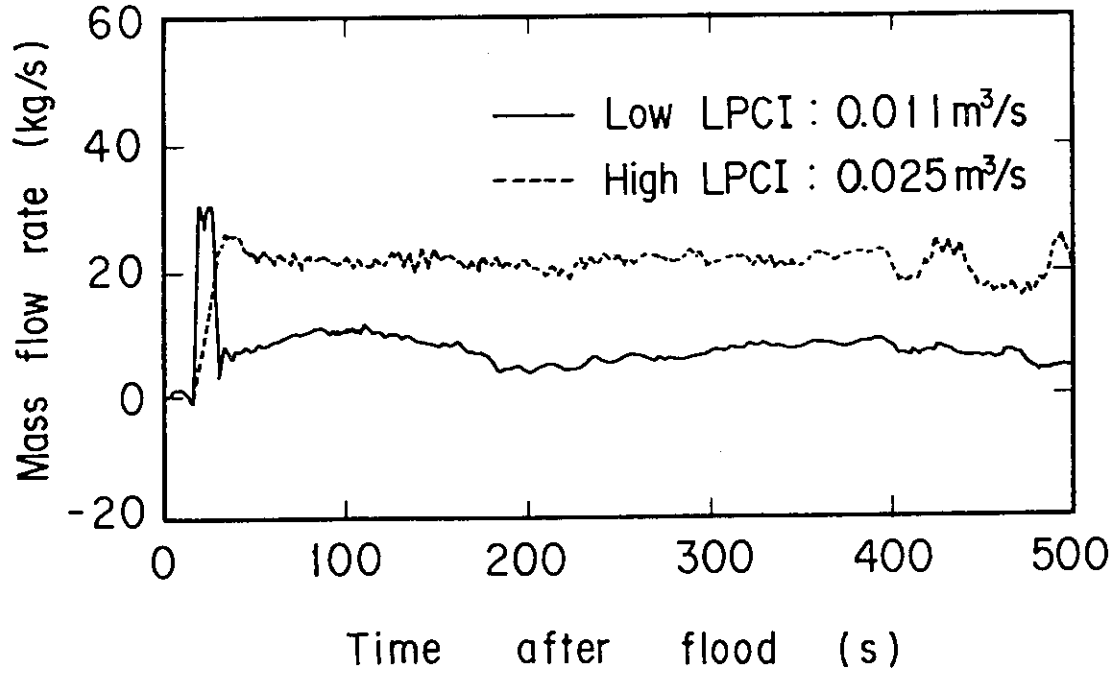

(b) Water mass flow rate

Fig. 4.10 LPCI flow rate effect on water and steam mass flow rate through the broken cold leg

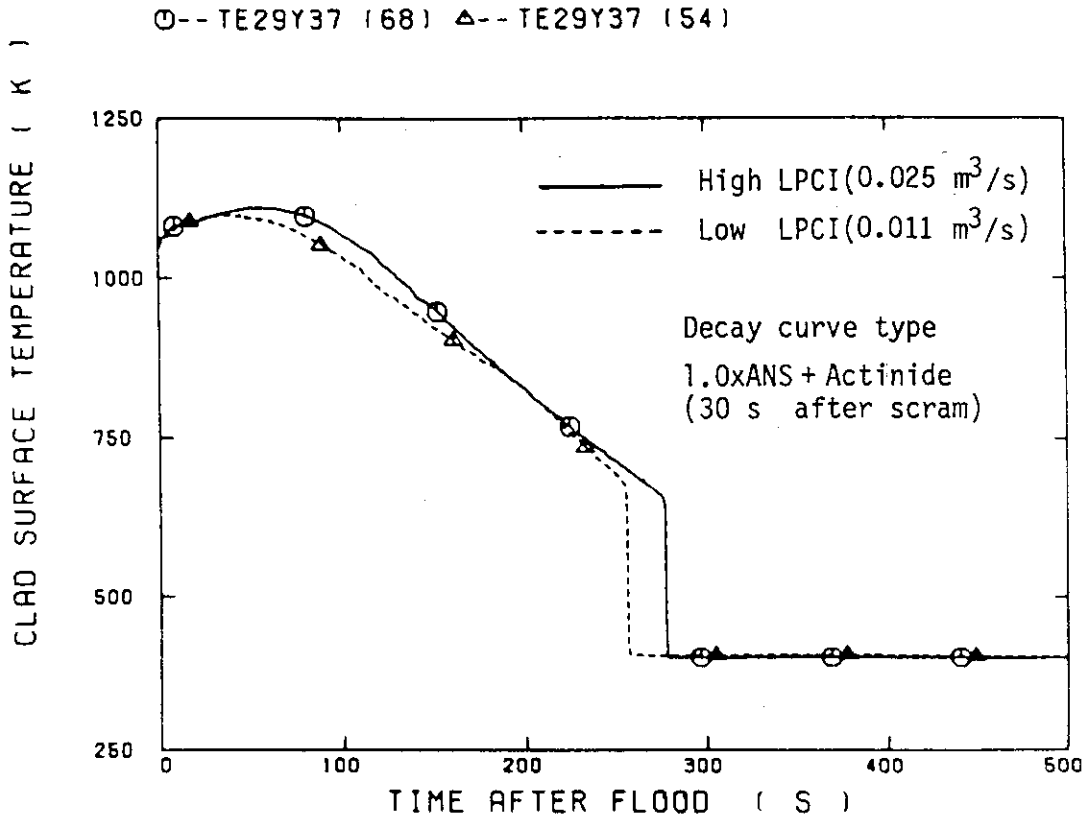

Fig. 4.11 LPCI flow rate effect on the clad surface temperature at the midplane of the peak power rod

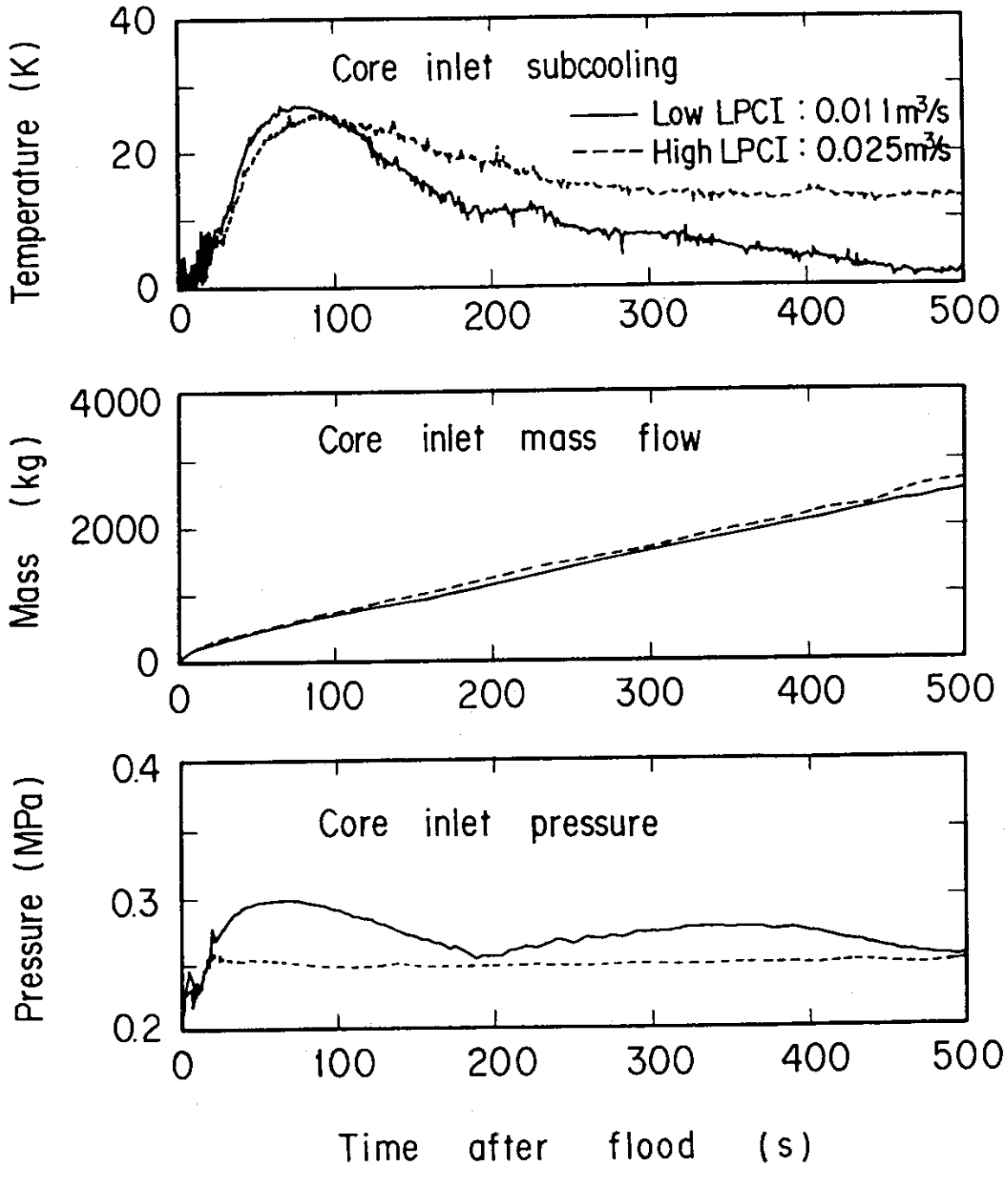

Fig. 4.12 LPCI flow rate effect on flow parameters at the core inlet

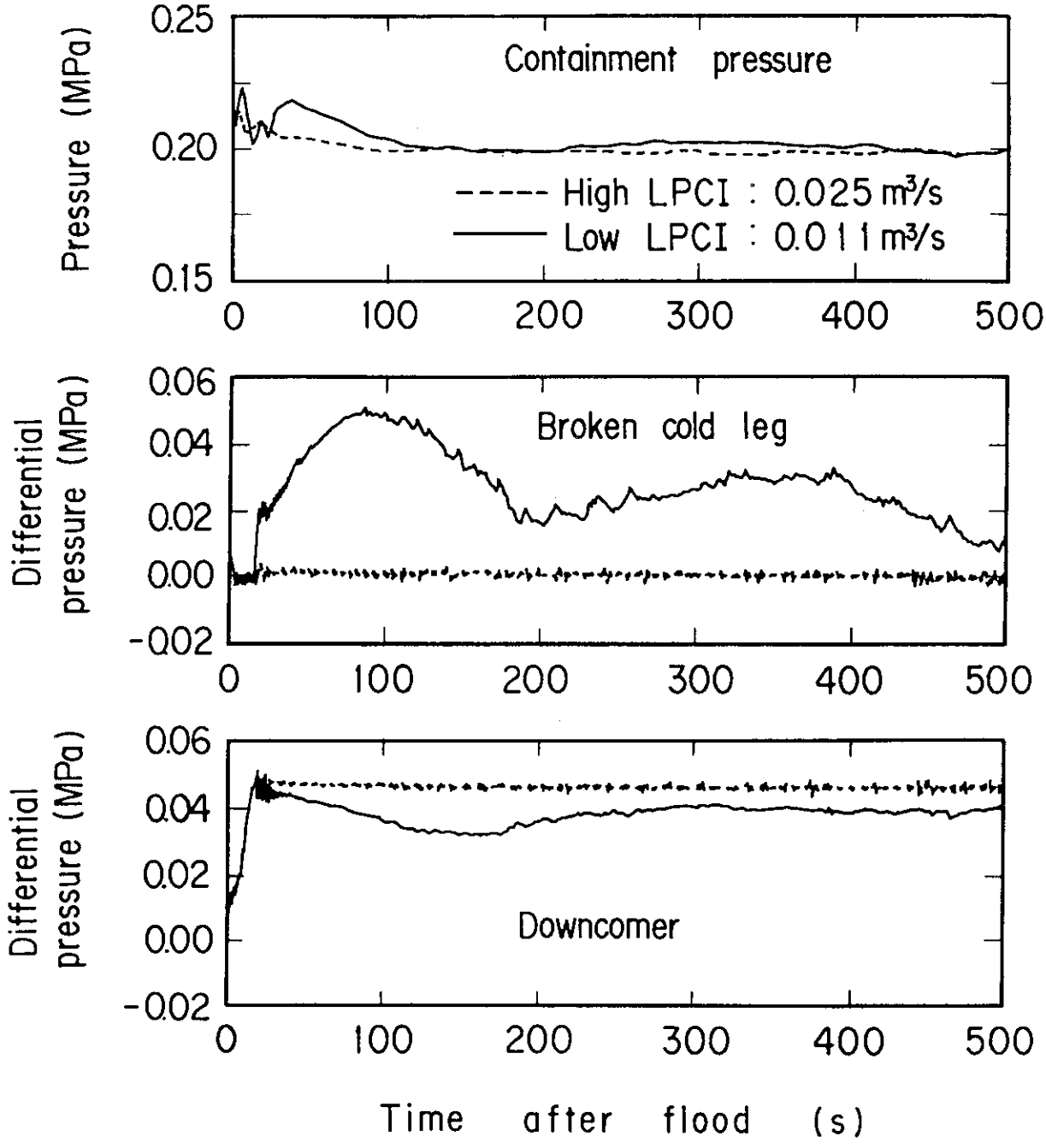

Fig. 4.13 Comparison of containment pressure, differential pressure through the broken cold leg and downcomer water head between the high and low LPCI flow rate tests

5. CONCLUSIONS

In order to study the LPCI flow rate effect on the core cooling and the system behavior, a test was performed with the LPCI flow rate of 0.025 m^3/s. The LPCI flow rate corresponds to the flow rate in case of no failure of the pump power unit in a PWR system. Through the comparisons of results with those from the test with the LPCI flow rate of 0.011 m^3/s, the following conclusions were obtained:

(1) The higher LPCI flow rate resulted in the slightly higher peak clad temperature and the slower quench propagation in these two tests. The test results show that the lower LPCI flow rate is not necessarily a conservative assumption for the evaluation of the core cooling during the reflood phase of a PWR LOCA.

(2) The worse core cooling in the high LPCI flow rate test is attributed to the lower core pressure than in the reference test. It is found that the lower core pressure results from the lower pressure drop through the broken cold leg arising from the complete condesation of steam due to direct contact with ECC water.

(3) It is expected that the current evaluation model(EM) code is still conservative because it usually predicts the low pressure drop through the broken cold leg.

(4) The flow oscillation in the cold leg was not significant even in the high LPCI flow rate test before the whole core quench.

Acknowledgements

The authors are much indebted to Drs. M. Nozawa, K. Hirano, K. Sato and T. Shimooke of Japan Atomic Energy Research Institute (JAERI) for their guidance and encouragement for this program.

The authors would like to express appreciation to the members of SCTF analysis group, especially Messrs. H. Adachi, M. Sobajima, T. Iwamura, A.Ohnuki and Y. Abe for valuable discussions. The authors are deeply indebted to Messrs. Y.Fukaya, I. Arase, T. Wakabayashi, T.Oyama, Y. Niitsuma, K. Nakajima, T. Chiba, J. Matsumoto, K. Komori and H. Sonobe for their contribution of the test conduction.

References

(1)Hirano,K. Murao,Y.: J.At. Energy Soc. Japan, (in Japanese), 22(10), 681 (1980).

(2)Murao,Y.,et al.: 12 th water reactor safety research information meeting. October (1984).

(3)Murao,Y.,et al.: J. Nucl. Sci. Technol.,19(9),705 (1982).

(4)Murao,Y.,et al.: JAERI-M 83-029, February (1983).

(5)Iguchi,T. et al.: JAERI-M 85-025, March (1985)

(6)Akimoto,H. et al.: J. Nucl. Sci. Technol.,22(4),269 (1985).

(7)Lilly,G.P., et al.: WCAP-8838, (1977).

(8)Waring,J.P. and Hochreiter,L.E.: WCAP-8583, (1975).

Acknowledgements

The authors are much indebted to Drs. M. Nozawa, K. Hirano, K. Sato and T. Shimooke of Japan Atomic Energy Research Institute (JAERI) for their guidance and encouragement for this program.

The authors would like to express appreciation to the members of SCTF analysis group, especially Messrs. H. Adachi, M. Sobajima, T. Iwamura, A.Ohnuki and Y. Abe for valuable discussions. The authors are deeply indebted to Messrs. Y.Fukaya, I. Arase, T. Wakabayashi, T.Oyama, Y. Niitsuma, K. Nakajima, T. Chiba, J. Matsumoto, K. Komori and H. Sonobe for their contribution of the test conduction.

References

(1)Hirano,K. Murao,Y.: J.At. Energy Soc. Japan, (in Japanese), 22(10), 681 (1980).

(2)Murao,Y.,et al.: 12 th water reactor safety research information meeting. October (1984).

(3)Murao,Y.,et al.: J. Nucl. Sci. Technol.,19(9),705 (1982).

(4)Murao,Y.,et al.: JAERI-M 83-029, February (1983).

(5)Iguchi,T. et al.: JAERI-M 85-025, March (1985)

(6)Akimoto,H. et al.: J. Nucl. Sci. Technol.,22(4),269 (1985).

(7)Lilly,G.P., et al.: WCAP-8838, (1977).

(8)Waring,J.P. and Hochreiter,L.E.: WCAP-8583, (1975).

Appendix A

Definition of Tag IDs for data in Appendix B

Figure List

Fig. A.1 Definition of power zones and bundle numbers

Fig. A.2 Definition of Tag. ID for void fraction (AG(EL.1) ∿ AG(EL.6))

Fig. A.3 Definition of Tag. ID for average linear power of heater and in each power unit zone (LP01A ∿ LP09A)

Fig. A.4 Definition of Tag. ID for differential pressure through downcomer, upper plenum, core, and lower plenum (DSD55, DT07RT5, LT08RM5, DSC75, DSC15)

Fig. A.5 Definition of Tag. ID for differential pressure through intact and broken loop and broken cold leg nozzle (DT23C, DT01B, DPBCN)

Fig. A.6 Definition of Tag. ID for fluid temperature iniinlet and outlet plenum and secondary of steam genrator (TE□2GW, TE□5GW, TE08G□H)

Fig. A.7 Definition of Tag. ID for ECC water injection rate, ECC water temperature and vented steam flow rate (MLEC1, MLEC2, MLEC3, MLECLP, MLECUP, MLECDC1, MLECDC2, TE11QW, TE21QW, TE01JW, TE01UW, TE02UW, TE03UW, MGVENT1)

Fig. A.8 Definition of initial temperature, turnaround temperature, quench temperature, temperature rise, turnaround time and quench time

1. Definition of Tag. ID for clad surface temperatures and heat fransfer coefficients

Notation : TEnnYlm (temperature)

HTEmmYlm (heat transfer coefficient)

nn : Bundle number (see Fig. A.1)

m : Elevation number

	Elevation (m)	Axial power factor
3	0.38	0.651
5	1.015	1.147
7	1.83	1.40
9	2.44	1.256
A	3.05	0.854

2. Definition of power zone and boundle number

See Fig. A.1

3. Definition of Tag. ID for void fraction

See Fig. A.2

4. Definition of Tag. ID for average linear power of heater rod in each power unit zone

See Fig. A.3

5. Definition of Tag. ID for differential pressure through downcomer, upper plenum, core and lower plenum

See Fig. A.4

6. Definition of Tag. ID for differential pressure through intact and broken loop and broken cold leg nozzle

See Fig. A.5

7. Definition of Tag. ID for fluid temperature in inlet and outlet plenum and secondary side of steam generator

See Fig. A.6

8. Definition of Tag. ID for ECC water injection rate, ECC water temperature and vented steam flow rate

See Fig. A.7

9. Definition of initial temperature, turnaround temperature quench temperature, temperature rise, turnaround time and quench time. (See Fig. A.8

T_i : Initial temperature (Clad surface temperature at reflood initiation)

T_t : Turnaround temperature (Maximum clad surface temperature in each temperature history)

ΔT_r : Temperature rise ($= T_t - T_i$)

T_q : Quench temperature (Clad surface temperature at quenching)

10. Definition of quenching

See Fig. A.8

Quench time t_t is determined as

$$t_t = i \times \Delta t - \text{(reflood initiation time)}$$

In above equation, i is determined by the following criteria.

(1) Clad surface temperature is high, compared with the saturation temperature.

$$T_i > T_{sat} + \Delta T_1$$

(2) Decreasing rate of clad surface temperature is large.

$$\frac{T_{i+1} - T_i}{\Delta t} < - C_{st}$$

(3) Clad surface temperature falls around the saturation temperature.

$$T_{i + k_1} \leq T_{sat} + \Delta T_1$$

(4) If the determined i is inadequate, the value i is manually re-determined.

Δt : Data sampling period (s)

T_i : Clad surface temperature (K)

T_{sat} : Saturation temperature at the pressure in upper plenum (K)

ΔT_1 : Temperature discrepancy (K)
Default value = 50.0

C_{st} : Decreasing rate of clad surface temperature (K/S)
Default value = 25.0

k_1 : Number of referred data (-)
Default value = 6

11. Definition of Tag. ID for core inlet mass flow rate, time-integral core inlet mass flow rate and carry-over rate fraction

(1) Core inlet mass flow rate : $\dot{m}_F$
Notation : MLCRI□ (□ = N, 1 or 11)

(2) Time-intefral core inlet mass flow rate : $\int \dot{m}_F dt$
Notation : IMLCRI□ (□ = N, 1 or 11)

(3) Carry-over rate fraction : $(\dot{m}_F - \dot{m}_{CR})/\dot{m}_F$
Natation : CRF□ (□ = N, 1 or 11)

where $\dot{m}_F$: Core inlet mass flow rate (See item 12)

$\dot{m}_{CR}$: Water accumulation rate in core

Suffix	$\dot{m}_F$ base on
N	Eq.(A.2)
1	Eq.(A.1) with K=15
11	Eq.(A.1) with K=20

12. Evaluation of core inlet mass flow rate

The reflood phenomena is a relatively slow transient and a steady state condition can be applied. In a steady state condition, based on the mass balance relations of the system, the core flooding mass flow rates $\dot{m}_F$s can be written as follows:

By using the data measured at the downstream of the core inlet, m_F is derived as,

$$\dot{m}_F = \dot{m}_C + \dot{m}_U + \dot{m}_B + \Sigma \dot{m}_I \quad , \qquad (A.1)$$

where $\dot{m}_C$ and $\dot{m}_U$ are the mass accumulation rates in the core and the upper plenum respectively. The $\dot{m}_B$ and $\dot{m}_I$ are the mass flow rates in the broken loop and the intact loop, respectively.

By using the data measured at the upstream of the core inlet, $\dot{m}_F$ is derived as,

$$\dot{m}_F = \Sigma \dot{m}_{DL} - \dot{m}_D - \dot{m}_O + \dot{m}_{ECC/LP} \quad , \tag{A.2}$$

where $\dot{m}_{DL}$ and $\dot{m}_O$ are the mass flow rates of the water flowing into and overflowing from the downcomer, $\dot{m}_{ECC/LP}$ and $\dot{m}_D$ are the mass flow rate of the ECC water injected into the lower plenum and the water accumulation rate in the dowmcomer respectively.

The $\dot{m}_I$s and $\dot{m}_B$ can be obtained from the pressure drops at the pump simulators with orifices by assuming the K-factor of the orifice is constant. The values of $\dot{m}_C$, $\dot{m}_D$ and $\dot{m}_U$ can be evaluated with the differential pressure ΔP_C, ΔP_D and ΔP_U, respectively, as follows:

$$\dot{m}_n = d(\Delta P_n S_n/g)/dt \quad (n : C, D, U) \quad , \tag{A.3}$$

where g is the gravitational acceleration and S_n is the cross sectional area. The value of $\dot{m}_O$ can be obtained from the liquid level X in the Containment tank 1 as,

$$\dot{m}_O = d(X\rho_\ell S_o)/dt \quad , \tag{A.4}$$

where ρ_ℓ is the liquid density and S_o is the cross sectional area of the containment tank 1.

The value of $\dot{m}_{DL}$, $\dot{m}_{DV}$ and h, which are liquid flow rate, steam flow rate and enthalpy of two phase mixture downstream each ECC port respectively, are obtained from the following mass and energy balance relations at each ECC port under the assumption of thermal equilibrium:

$$\dot{m}_{DV} + \dot{m}_{DL} = \dot{m}_{ECC} + \dot{m}_I \quad , \tag{A.5}$$

$$(\dot{m}_{DV} + \dot{m}_{DL})i = \dot{m}_{ECC} h_{ECC} + \dot{m}_I h_f \quad , \tag{A.6}$$

$$\text{if} \quad h_g \geq h \geq h_f \ , \ (\dot{m}_{DV} + \dot{m}_{DL})h = \dot{m}_{DV} h_g + \dot{m}_{DL} h_\ell$$

$$\text{if} \quad h \geq h_g \quad , \ \dot{m}_{DL} = 0 \quad , \tag{A.7}$$

$$\text{if} \quad h \geq h_\ell \quad , \ \dot{m}_{DV} = 0$$

where h is enthalpy of fluid and h_ℓ and h_g are enthalpies of liquid and steam at the saturation temperature, respectively.

The fluid temperatures can be measured with thermocouples immersed in the fluid and the enthalpies h_I and h_{ECC} can be estimated.

Mass balance calculations were performed with Eqs. (A.1) and (A.2). The K-factor of the orifice in the pump simulator was evaluated in the following two ways.

The K-factor of 20 was obtained with the steam and water single phase calibration tests using the flow meter and spool piece data. The K-factor of 15 was obtained with the Pitot tube measurement in a typical reflood condition assuming the flat velocity profile in the pipings. In the differentiation, higher frequency components of the data tends to be amplified more. Therefore, in the differentiation of the differential pressure data, the smoothing procedure was used to suppress the high frequency components of the data.

In the Acc injection period, the calculated $\dot{m}_F$s with Eqs. (A.1) and (A.2) are significantly different from each other. This discrepancy may be caused by inaccuracy of the mass flow rate injected into the system and by the unaccounting of the storage of water in the cold leg pipe. The former might be introduced from the slow time response of the flow meter (time constant 1 second) and the change of the gas volume in the injection line. In this period, especially before the steam generation from the core becomes noticeable, the mass flow rate, $\dot{m}_F$, calculated with Eq. (A.1) is probably reasonable, since the calculation uses the increasing rates of the masses in the core and the upper plenum and their accuracy is good enough for our estimation.

In the LPCI injection period, the calculated $\dot{m}_F$s are slightly different from each other. Judging from the time-integral values of both $\dot{m}_F$s, their average values are nearly proportional. The discrepancy was inferred to be caused by the disregard of the bypass of steam and liquid from the upper plenum without going through the hot legs in the calculation with Eq. (A.1). And additionally the discrepancy was caused by the disregard of the steam generation in the downcomer due to the hot wall of the pressure vessel in the calculation with Eq. (A.2). It was estimated that the disregard of the downcomer steam generation causes the error of 0.25 kg/s on predicted $\dot{m}_F$. The estimation was made by comparing the results of the tests with hot and cold downcomer conditions.

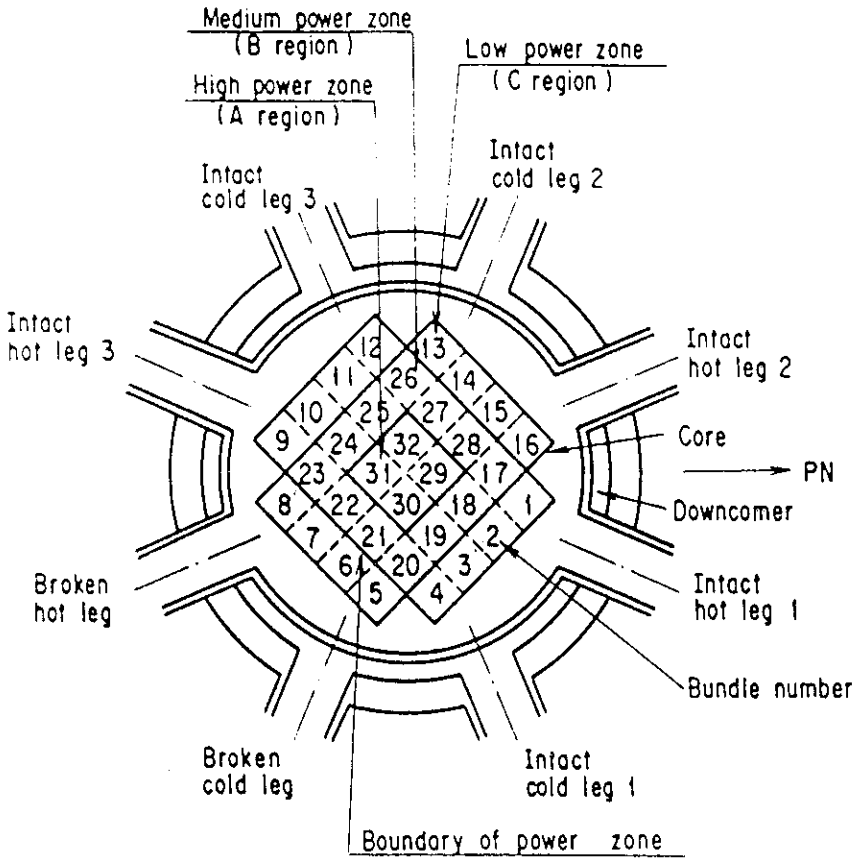

Fig. A. 1 Definition of power zones and bundle numbers

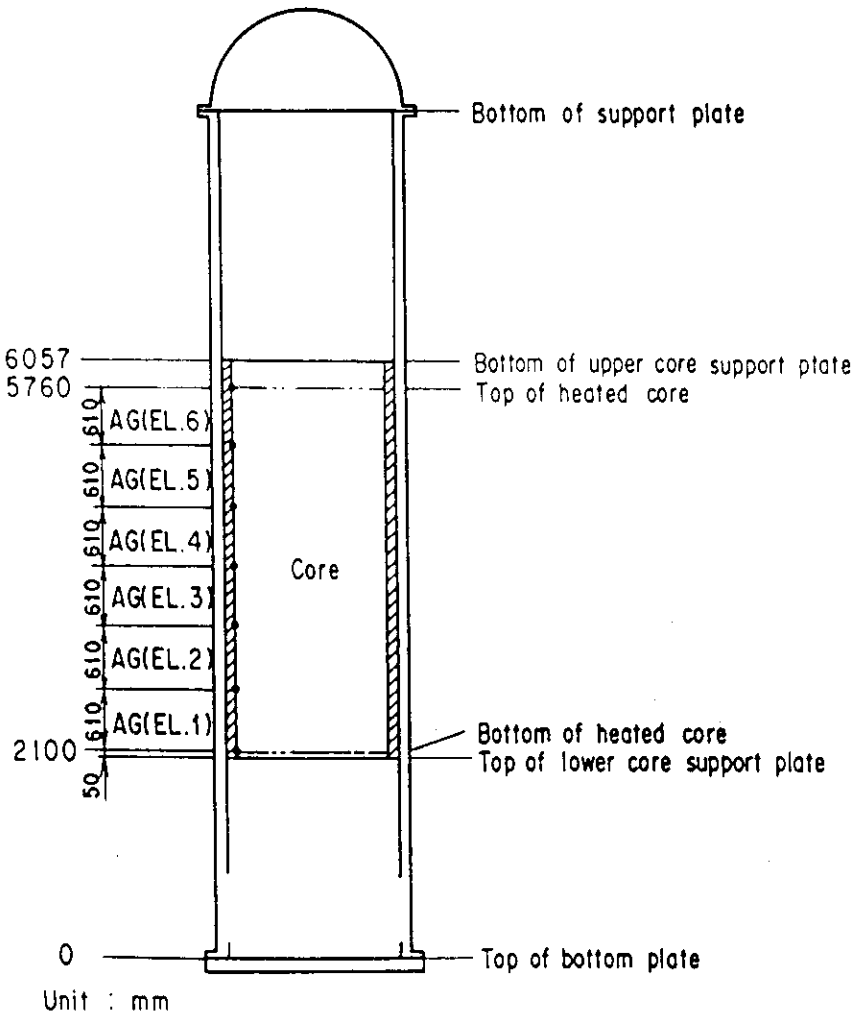

Fig. A. 2 Definition of Tag ID for void fraction (AG(EL. 1)~ AG(EL. 6))

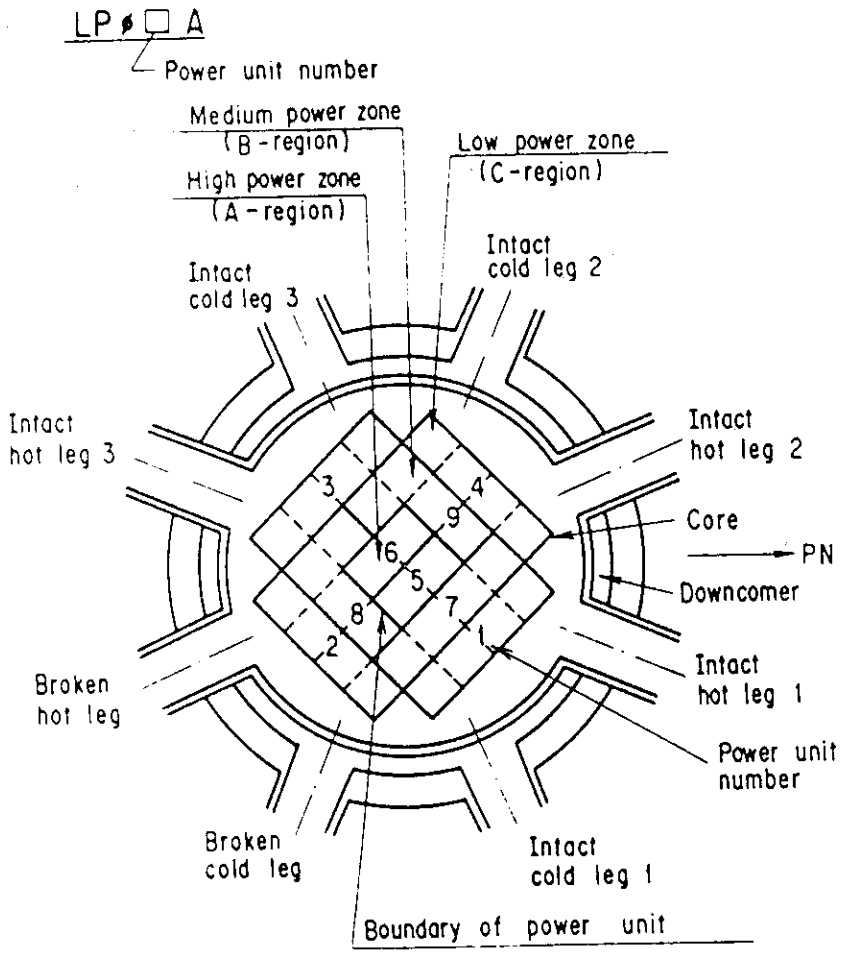

Fig. A. 3 Definition of Tag. ID for average linear power of heater rod in each power unit zone
(LP01A ~ LP09A)

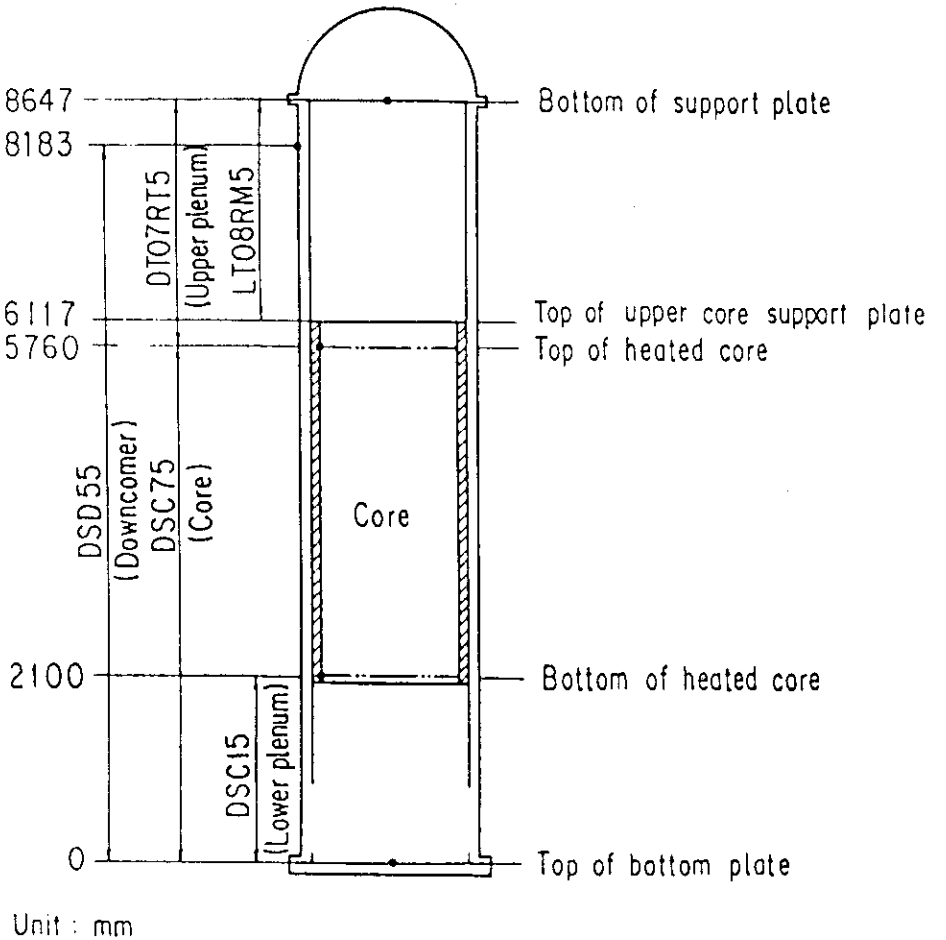

Fig. A. 4 Definition of Tag. ID for differential pressure through downcomer, upper plenum, core, and lower plenum
(DSD55, DTO7RT5, LTO8RM5, DSC75, DSC15)

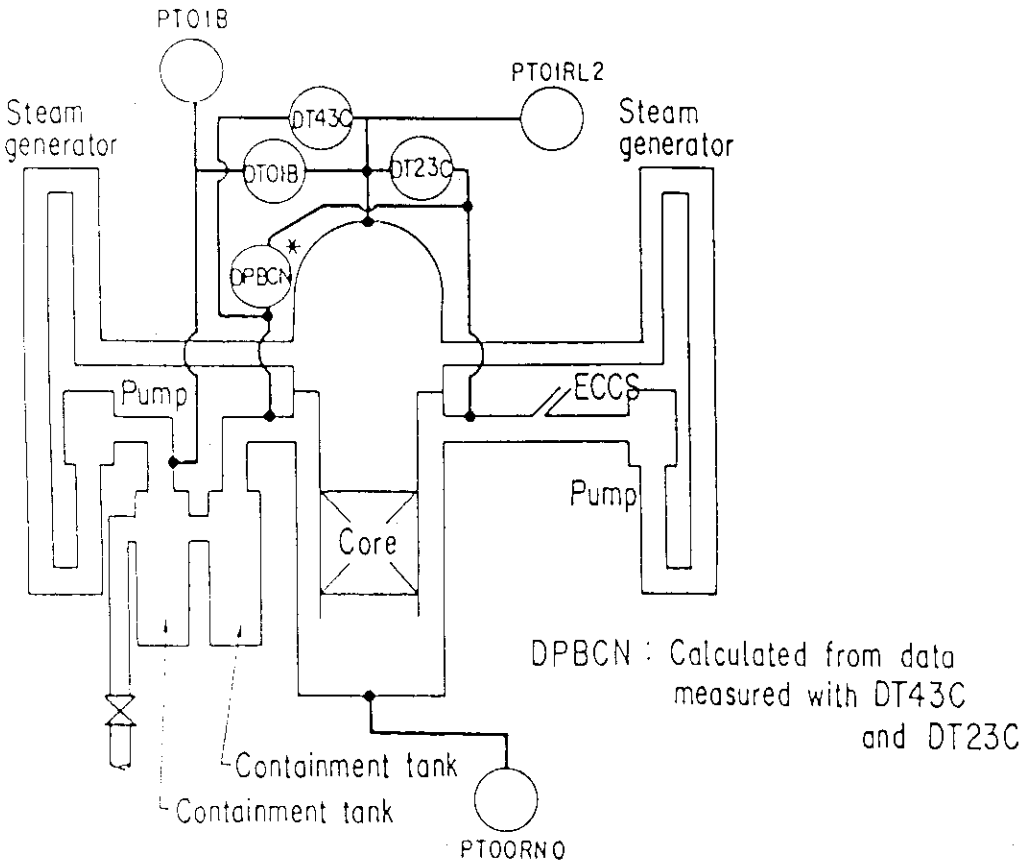

Fig. A. 5 Definition of Tag. ID for pressures in upper and lower plena and containment tank 2 (PT01RL2, PT00RN0, PT01B) and for differential pressure through intact and broken loop and broken cold leg nozzle (DT23C, DT01B, DPBCN)

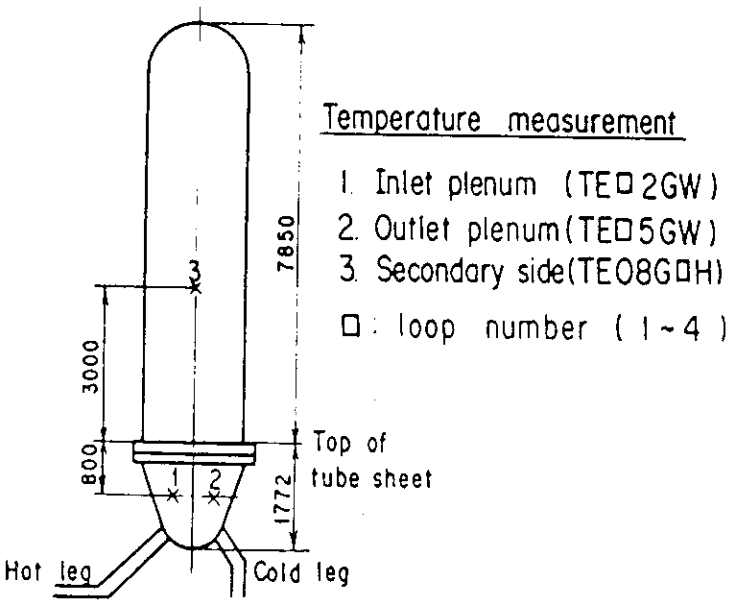

Fig. A. 6 Definition of Tag. ID for fluid temperature in inlet and outlet plenum and secondary of steam generator (TE□2GW, TE□5GW, TE08G□H)

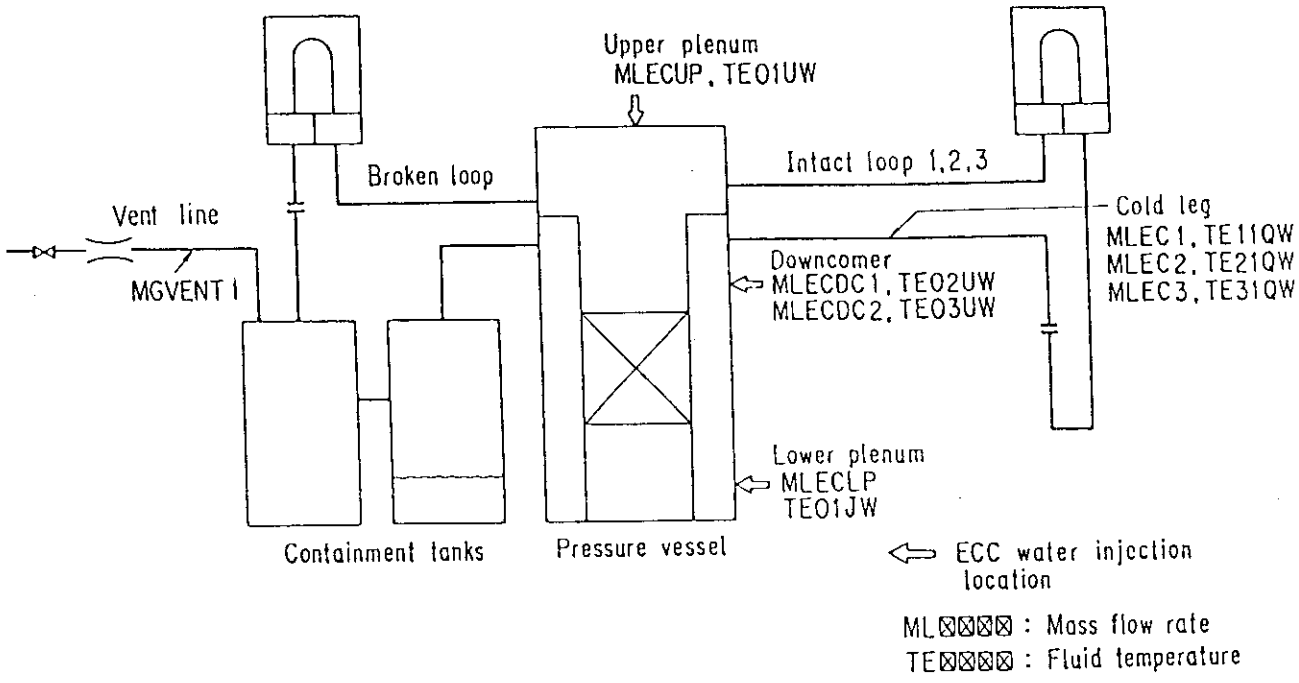

Fig. A. 7 Definition of Tag. ID for ECC water injection rate, ECC water temperature and vented steam flow rate

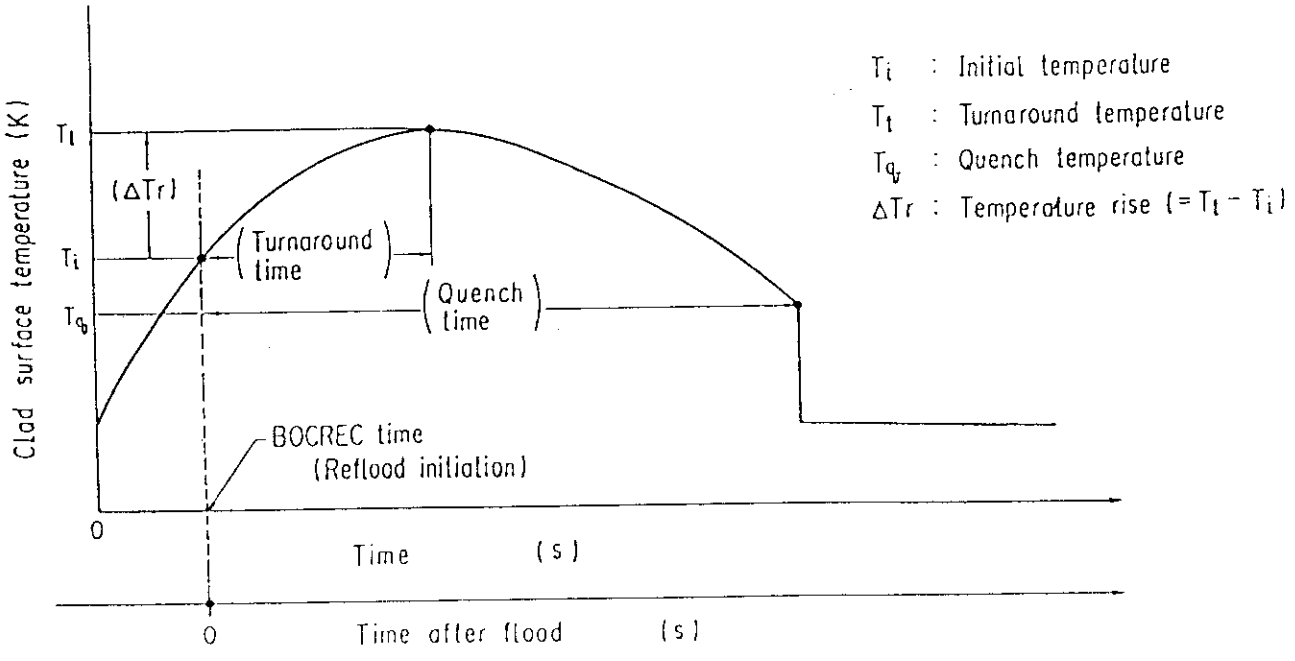

Fig. A. 8 Definition of initial temperature, turnaround temperature, quench temperature, temperature rise, turnaround time and quench time

Appendix B

Selected data of CCTF Test C2-9 (Run 68)

Figure List

Fig. B.1 ECC water injection rates into the primary system.
Fig. B.2 ECC water temperature.
Fig. B.3 Average linear power of heater rod in each power unit zone.
Fig. B.4 Pressure history in containment tank 2, upper plenum and lower plenum.
Fig. B.5 Clad surface temperature at various elevations along a heater rod in high power region (A region).
Fig. B.6 Clad surface temperature at various elevations along a heater rod in medium power region (B region).
Fig. B.7 Clad surface temperature at various elevations along a heater rod in low power region (C region).
Fig. B.8 Heat transfer coefficient at various elevations along a heater rod in high power region (A region).
Fig. B.9 Heat transfer coefficient at various elevations along a heater rod in medium power region (B region).
Fig. B.10 Heat transfer coefficient at various elevations along a heater rod in low power region (C region).
Fig. B.11 Initial clad surface temperature.
Fig. B.12 Temperature rise.
Fig. B.13 Turnaround temperature.
Fig. B.14 Turnaround time.
Fig. B.15 Quench temperature.
Fig. B.16 Quench time.
Fig. B.17 Void fraction in core.
Fig. B.18 Differential pressure through upper plenum.
Fig. B.19 Differential pressure through downcomer, core, and lower plenum.
Fig. B.20 Differential pressure through intact and broken loops.
Fig. B.21 Differential pressure through broken cold leg nozzle.
Fig. B.22 Fluid temperature in inlet plenum, outlet plenum, and secondary of steam generator 1.
Fig. B.23 Fluid temperature in inlet plenum, outlet plenum, and secondary of steam generator 2.
Fig. B.24 Core flooding mass flow rates evaluated with Eqs. (A.1) and (A.2)

Fig. B.25 Time-integral mass flooded into core evaluated with Eqs. (A.1) and (A.2).

Fig. B.26 Carry-over rate fraction.

Fig. B.27 Core inlet subcooling.

Fig. B.28 Exhausted mass flow rate from containment tank 2.

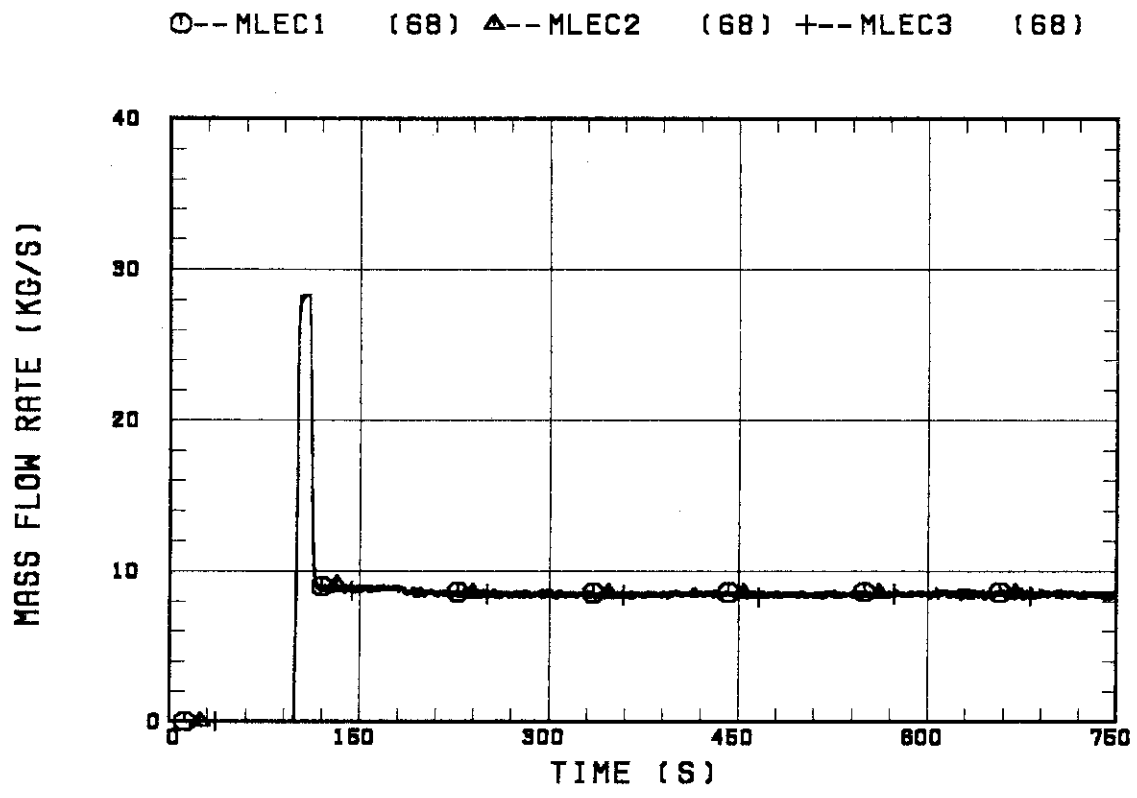

Fig.B.1 ECC water injection rates into the primary system.

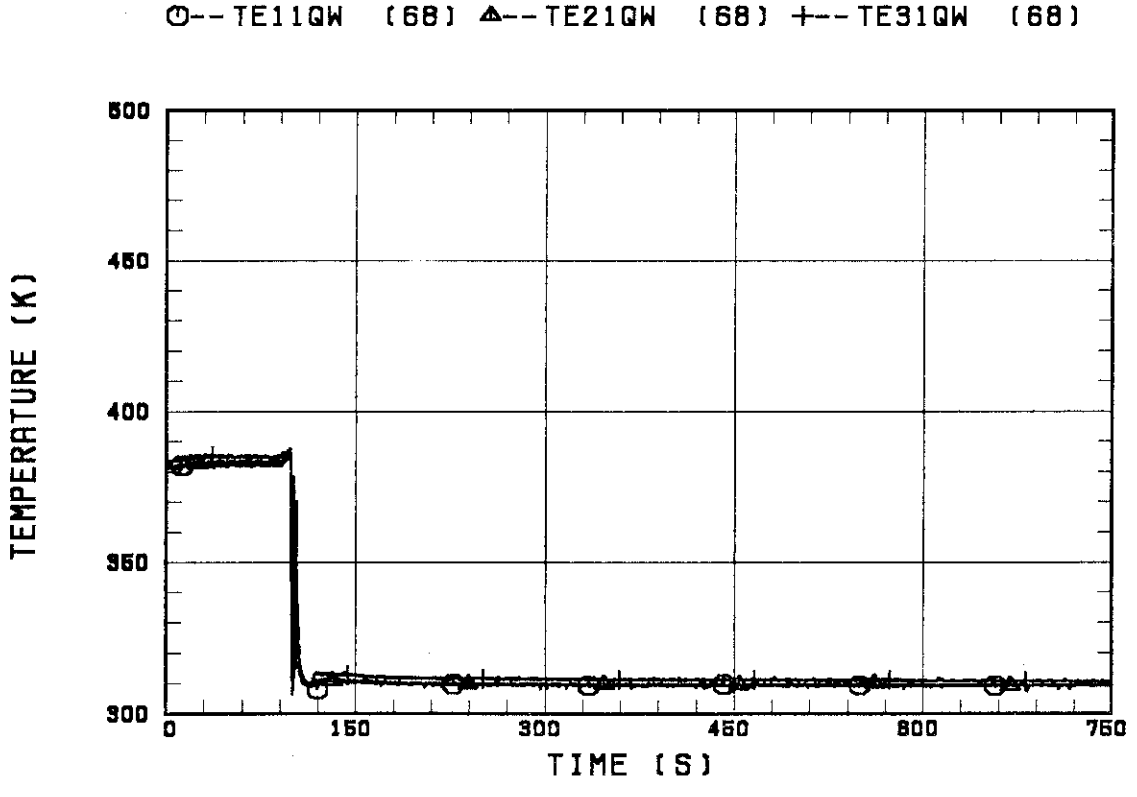

Fig.B.2 ECC water temperature.

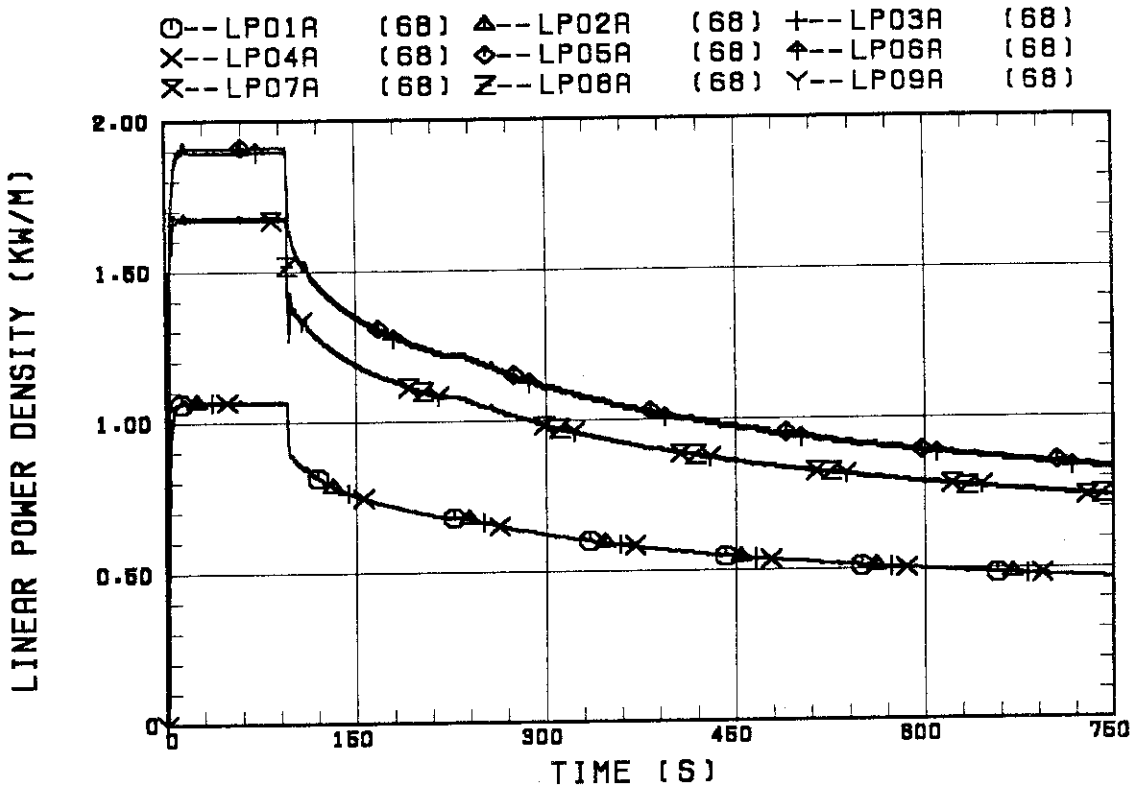

Fig.B.3 Average linear power of heater rod in each power unit zone.

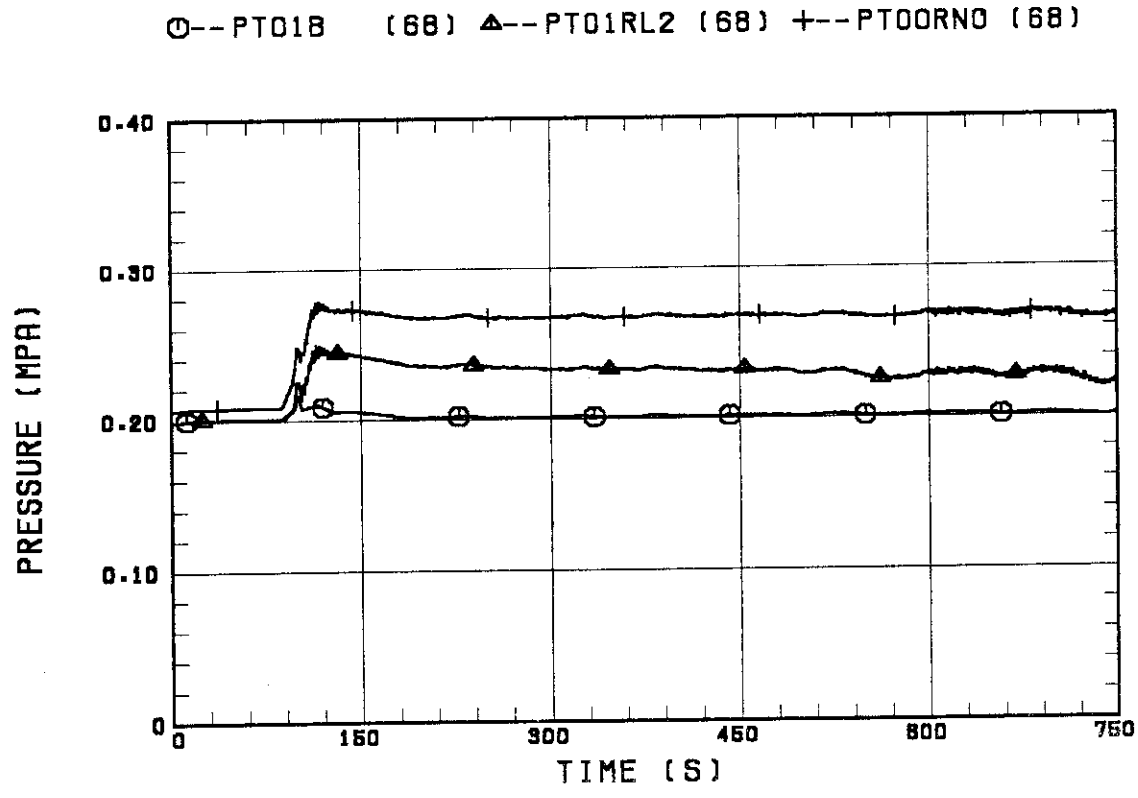

Fig.B.4 Pressure history in containment tank 2, upper plenum and lower plenum.

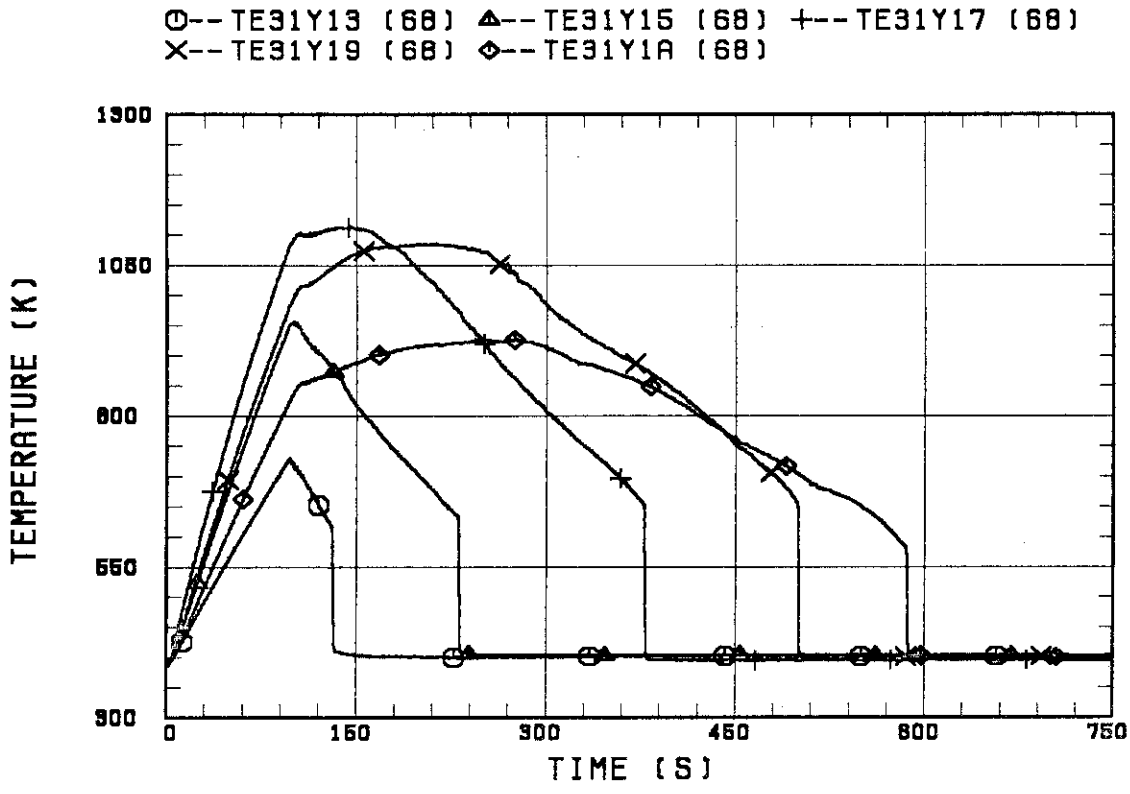

Fig.B.5 Clad surface temperature at various elevations along a heater rod in high power region (A region).

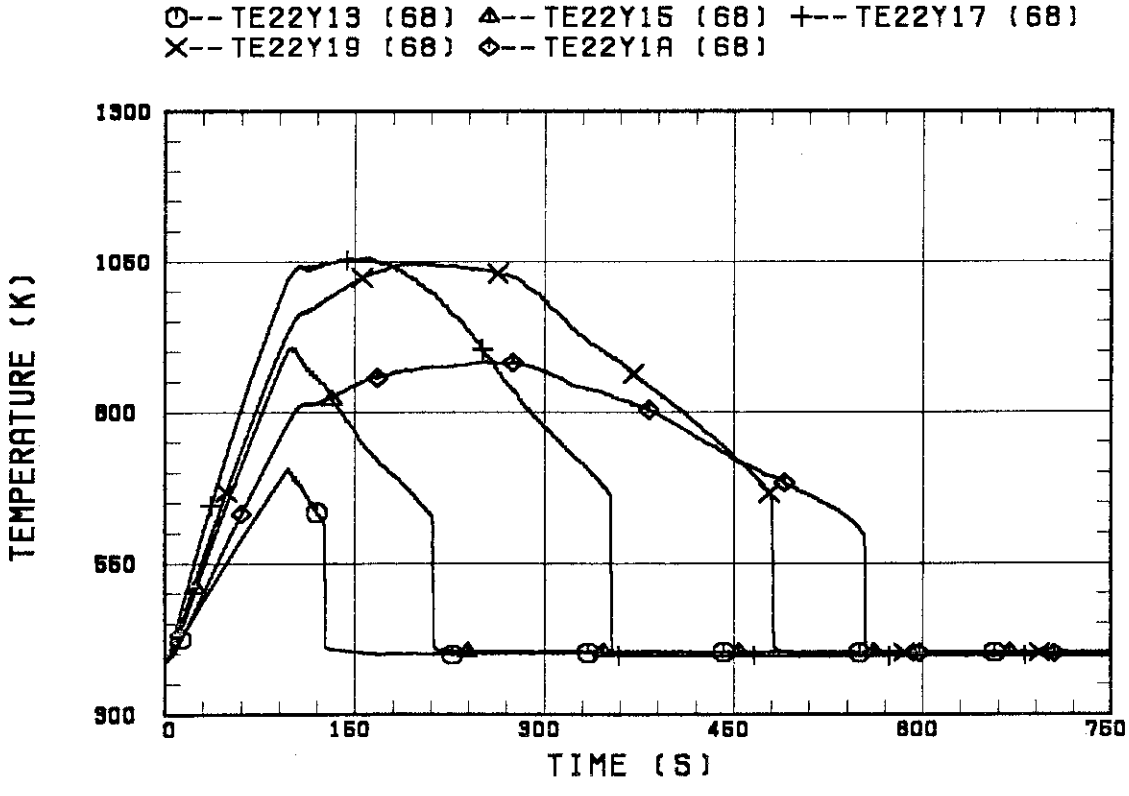

Fig.B.6 Clad surface temperature at various elevations along a heater rod in medium power region (B region).

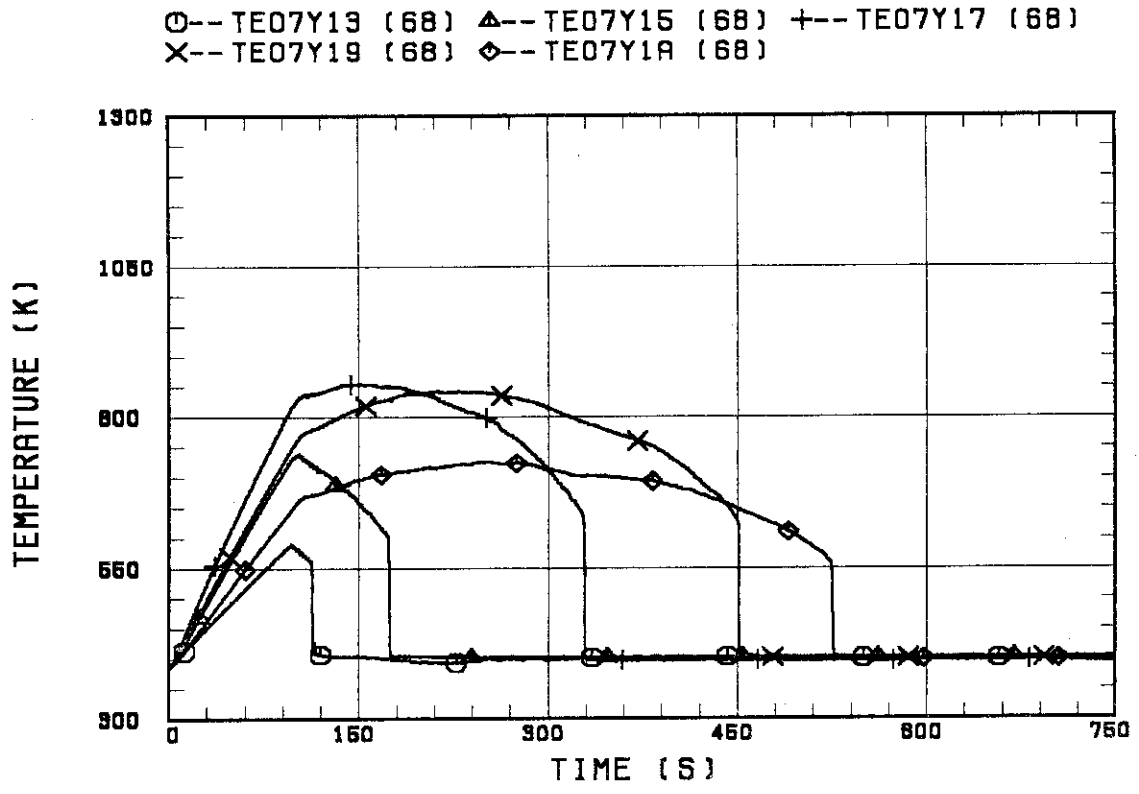

Fig.B.7 Clad surface temperature at various elevations along a heater rod in low power region (C region).

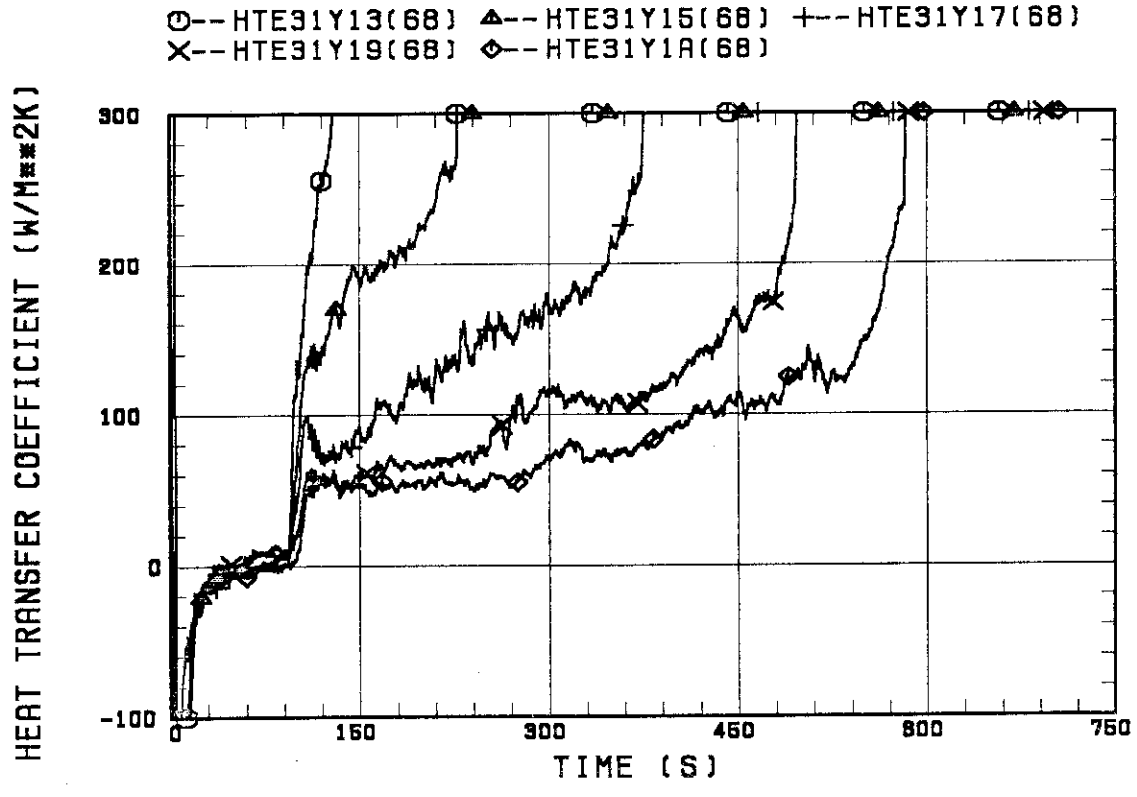

Fig.B.8 Heat transfer coefficient at various elevations along a heater rod in high power region (A region).

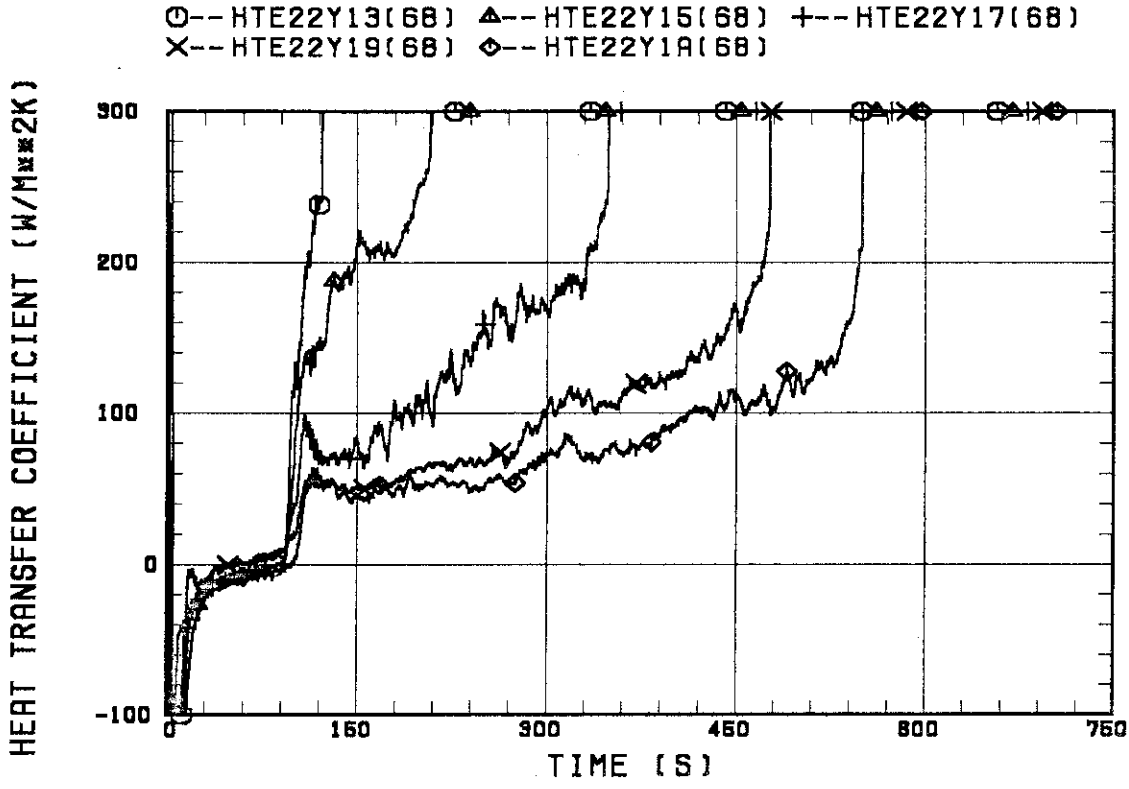

Fig.B.9 Heat transfer coefficient at various elevations along a heater rod in medium power region (B region).

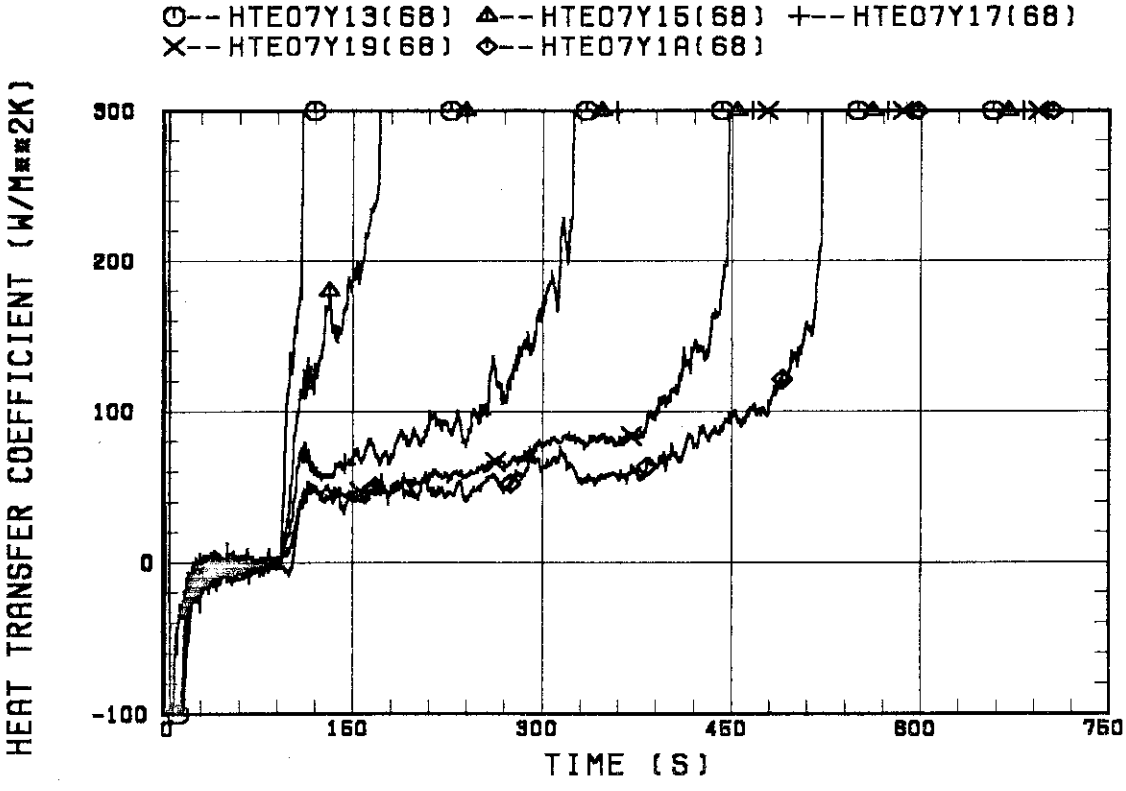

Fig.B.10 Heat transfer coefficient at various elevations along a heater rod in low power region (C region).

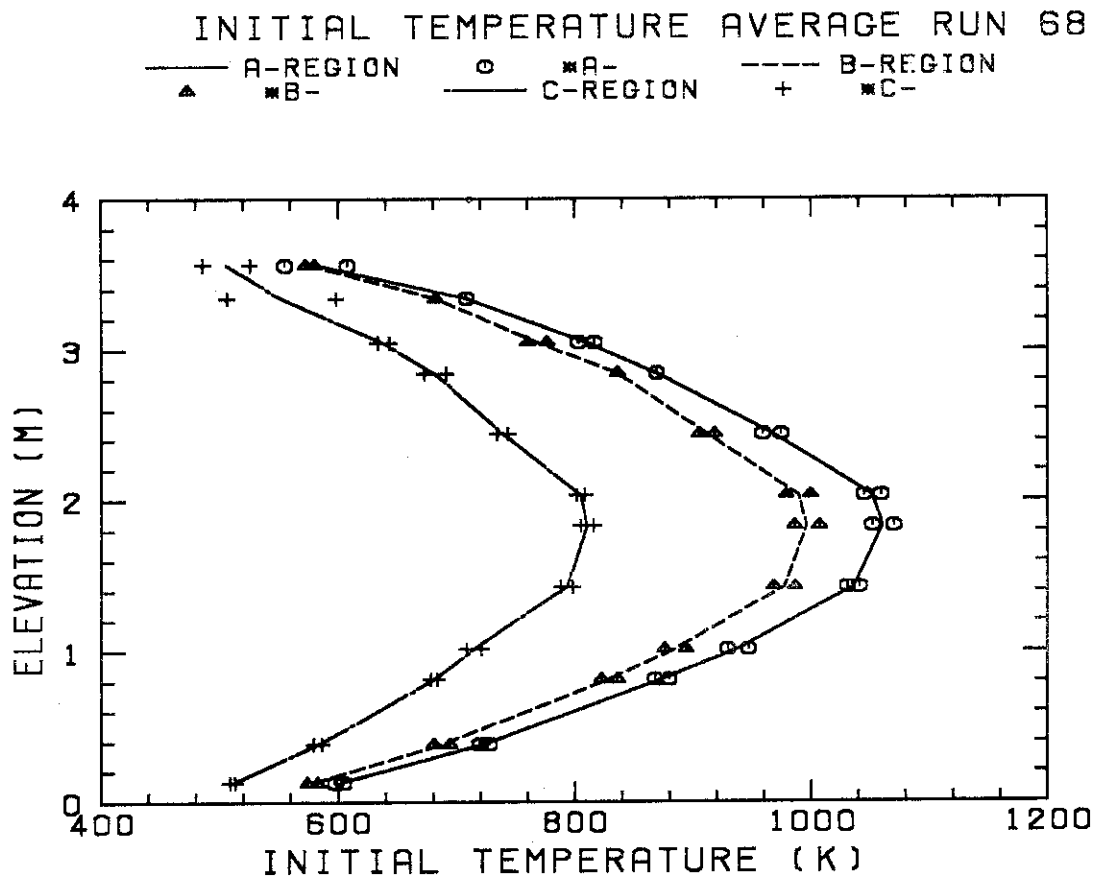

Fig.B.11 Initial clad surface temperature.

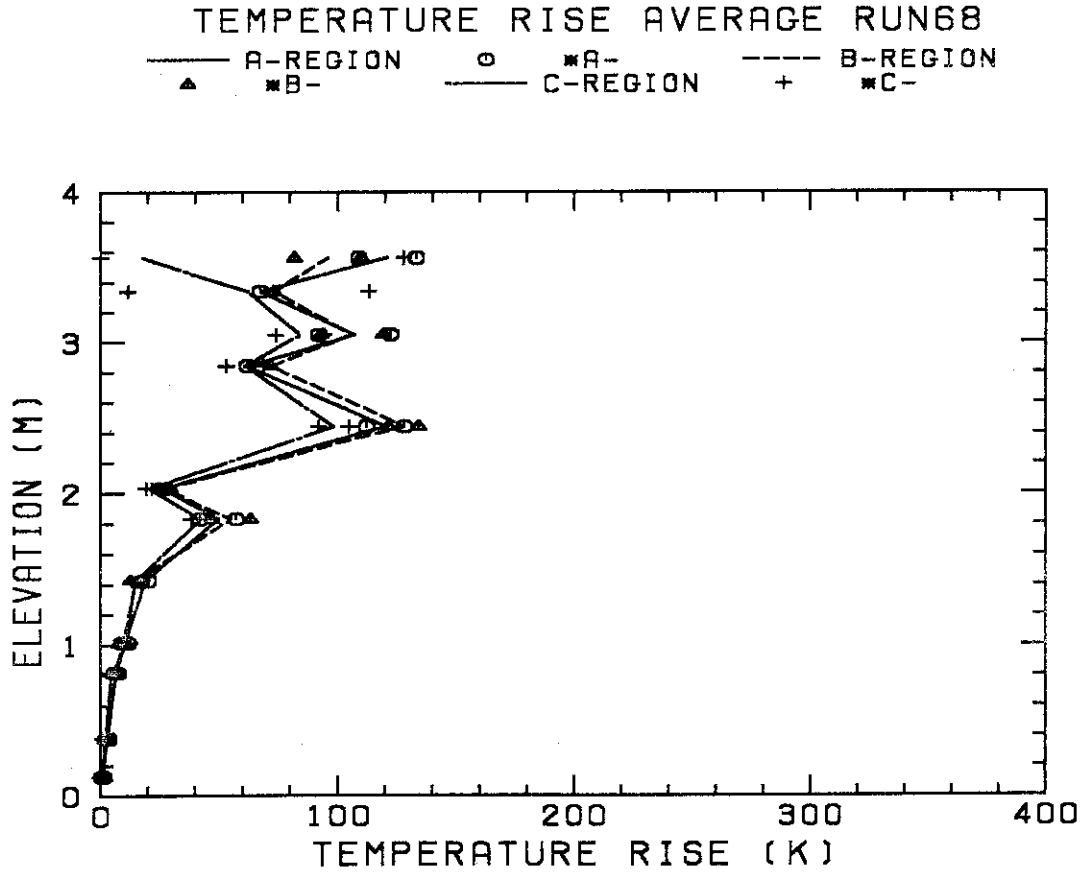

Fig.B.12 Temperature rise.

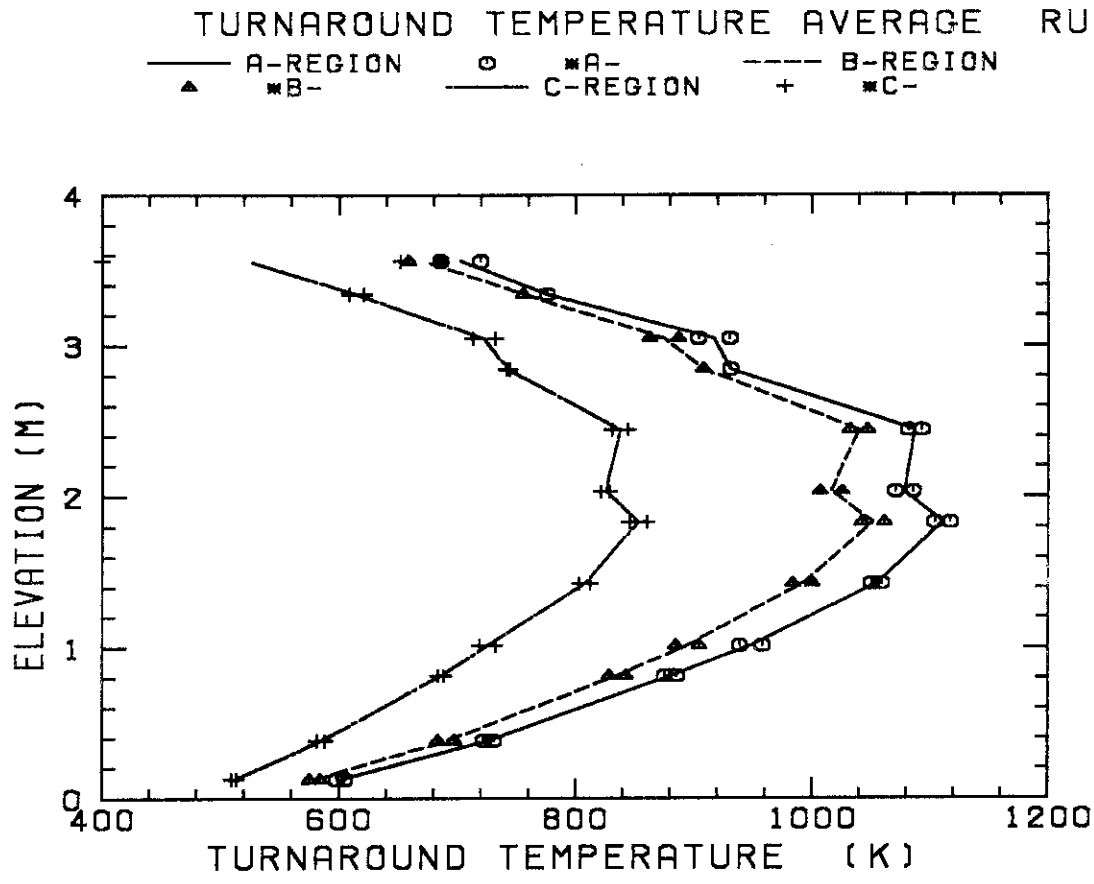

Fig.B.13 Turnaround temperature.

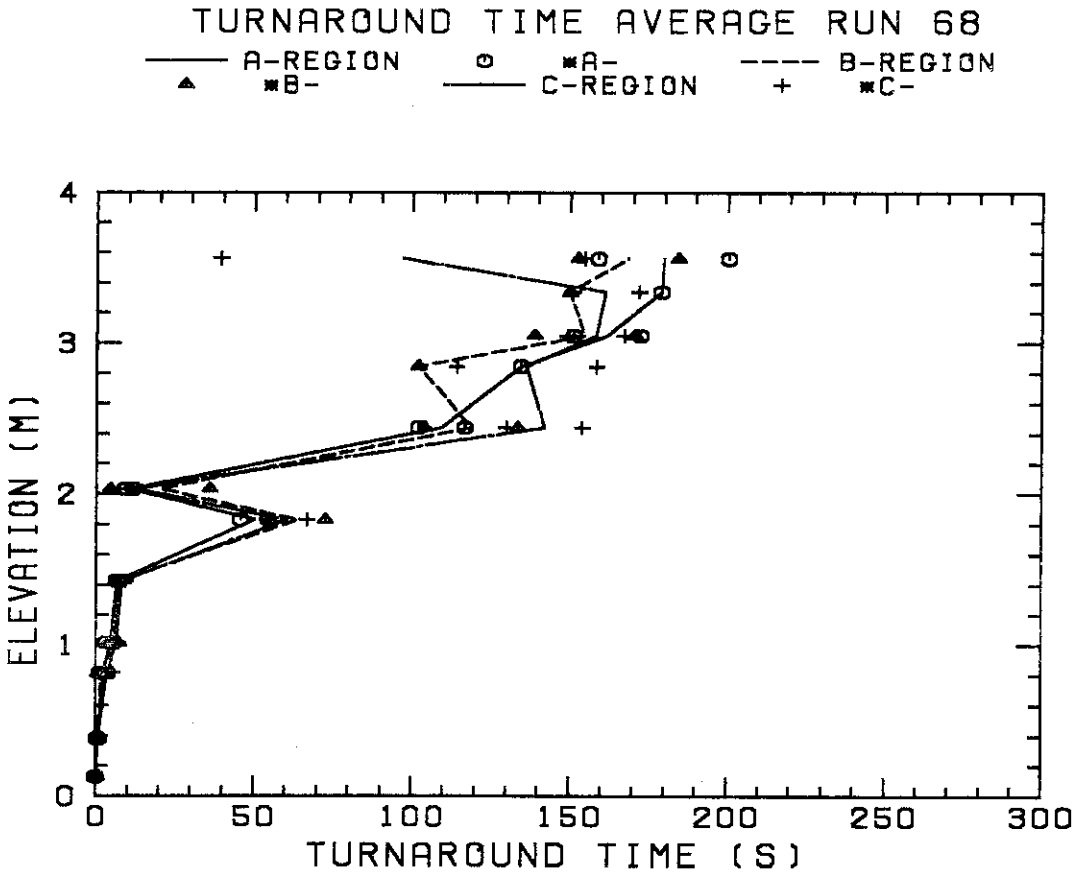

Fig.B.14 Turnaround time.

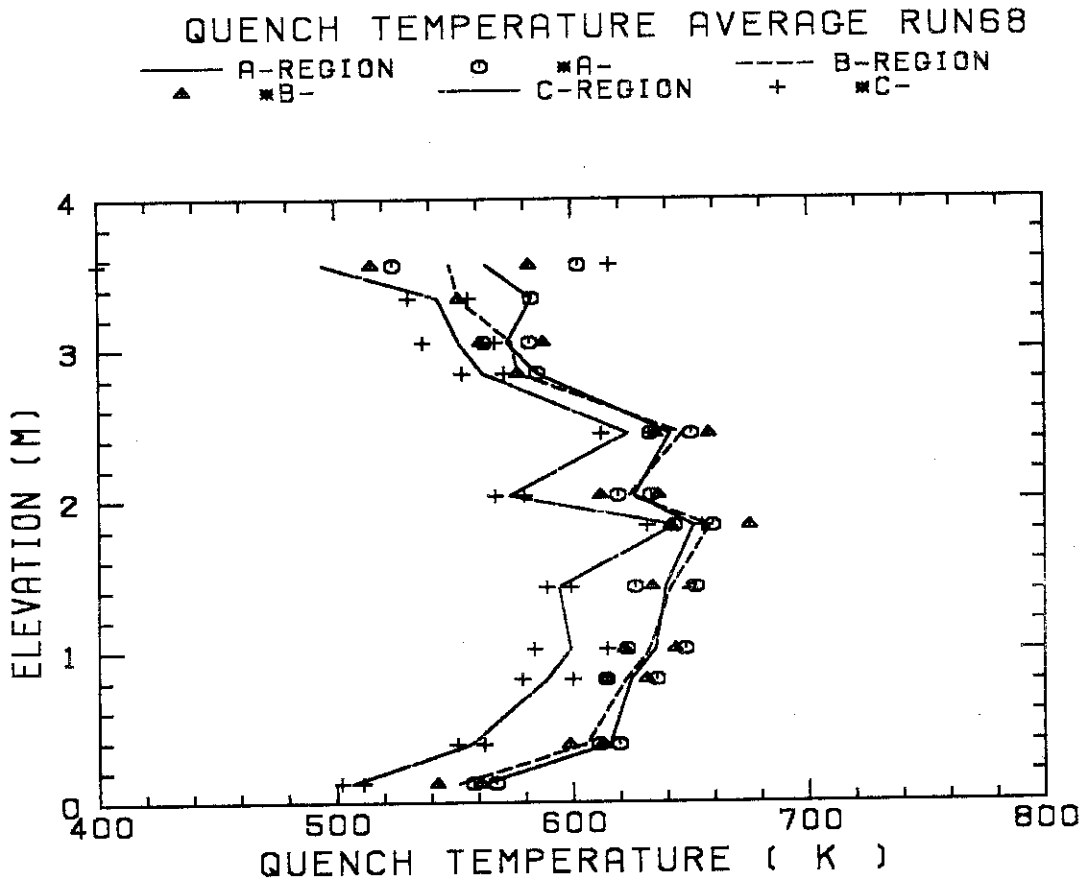

Fig.B.15 Quench temperature.

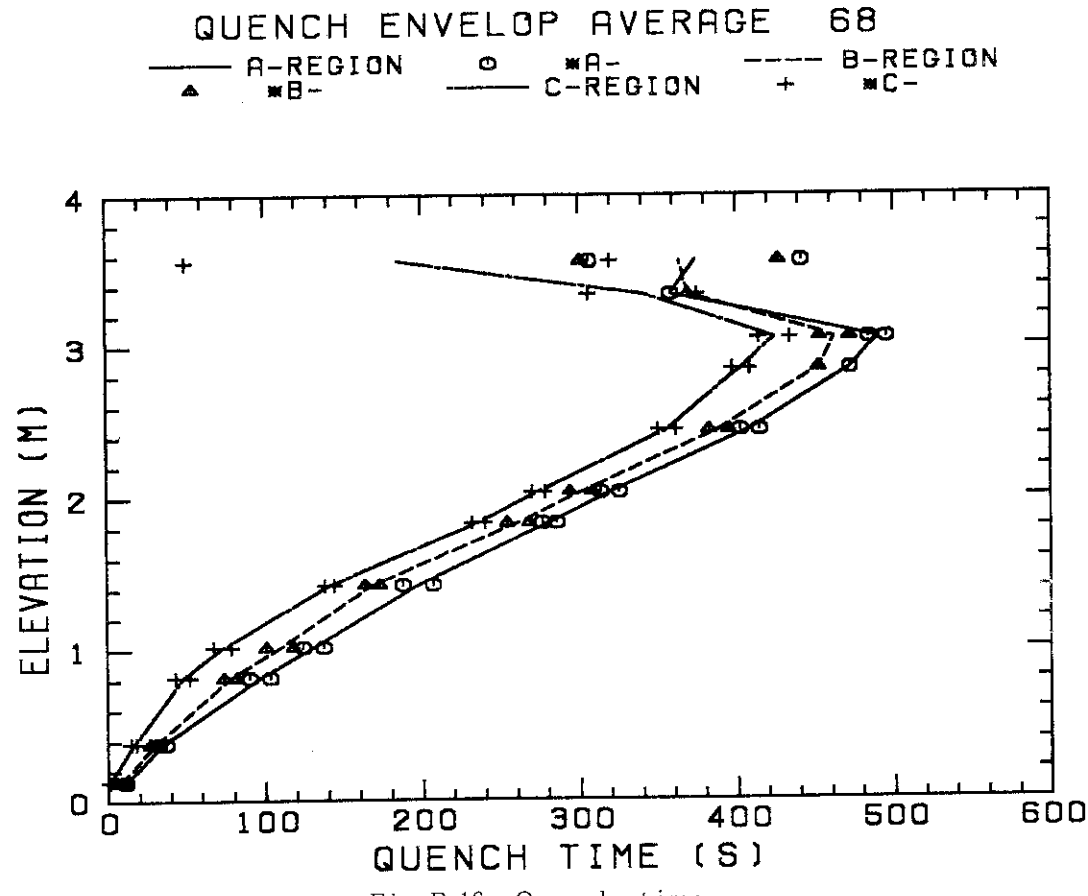

Fig.B.16 Quench time.

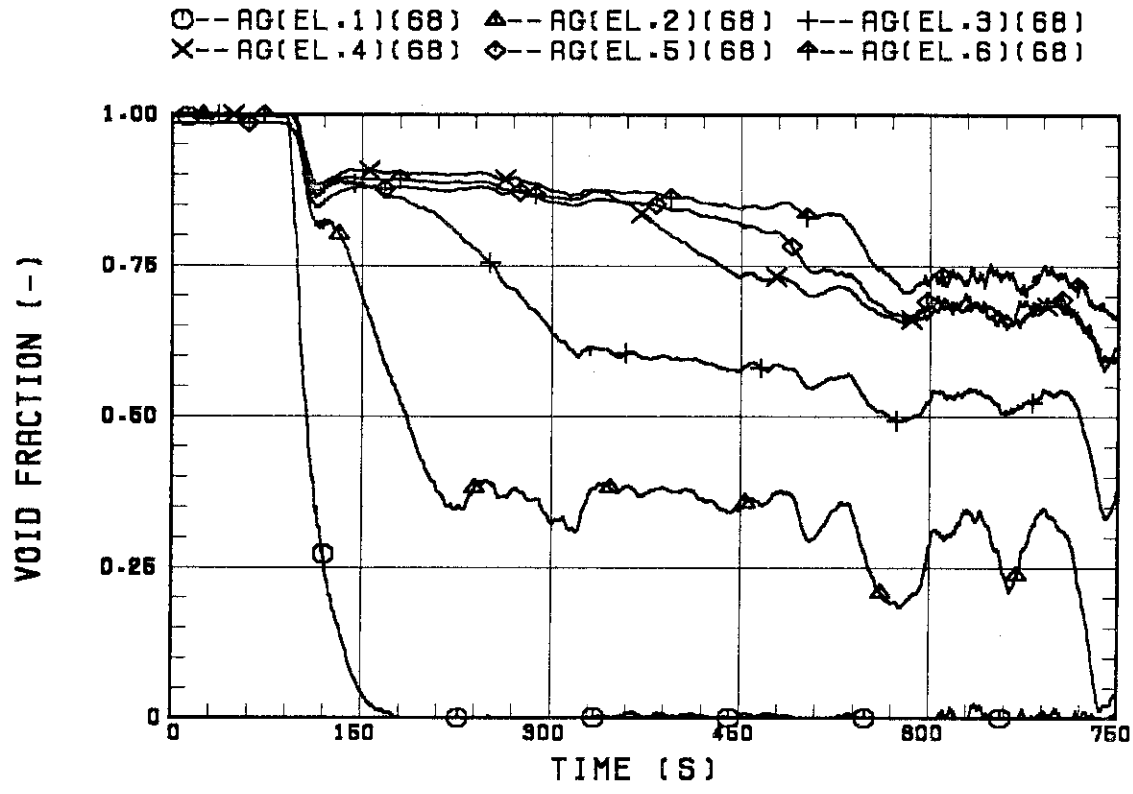

Fig.B.17 Void fraction in core.

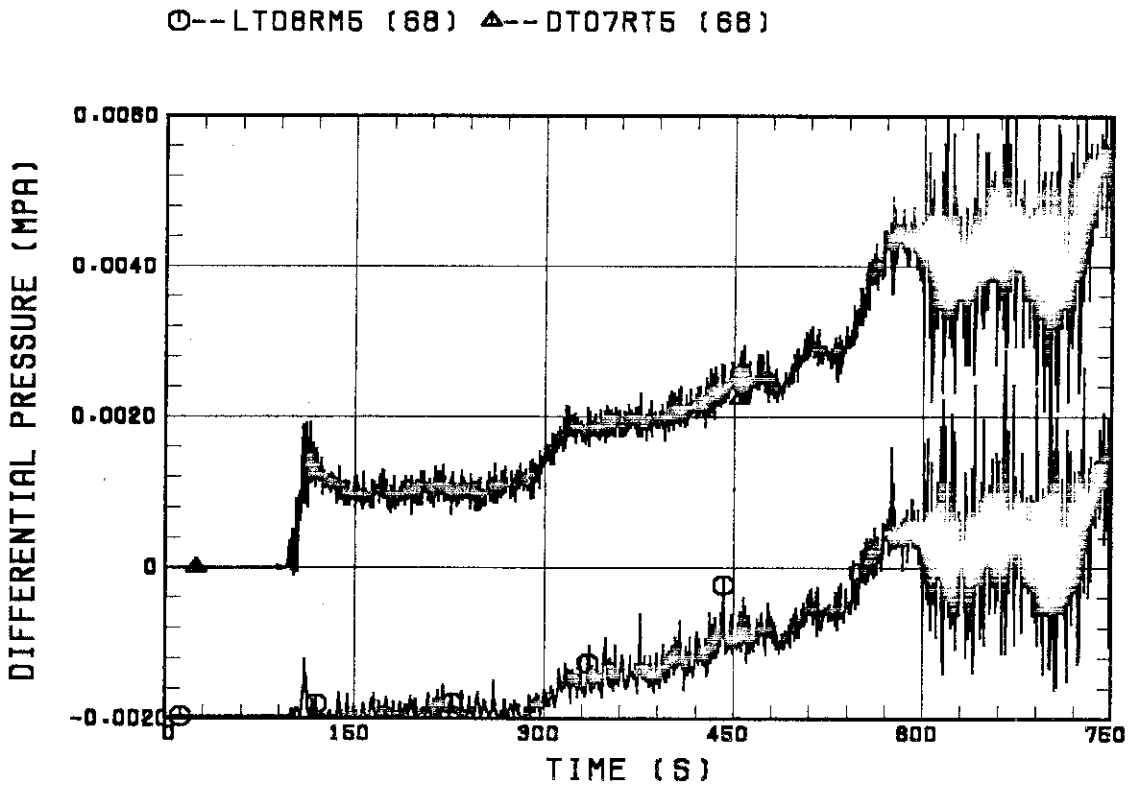

Fig.B.18 Differential pressure through upper plenum.

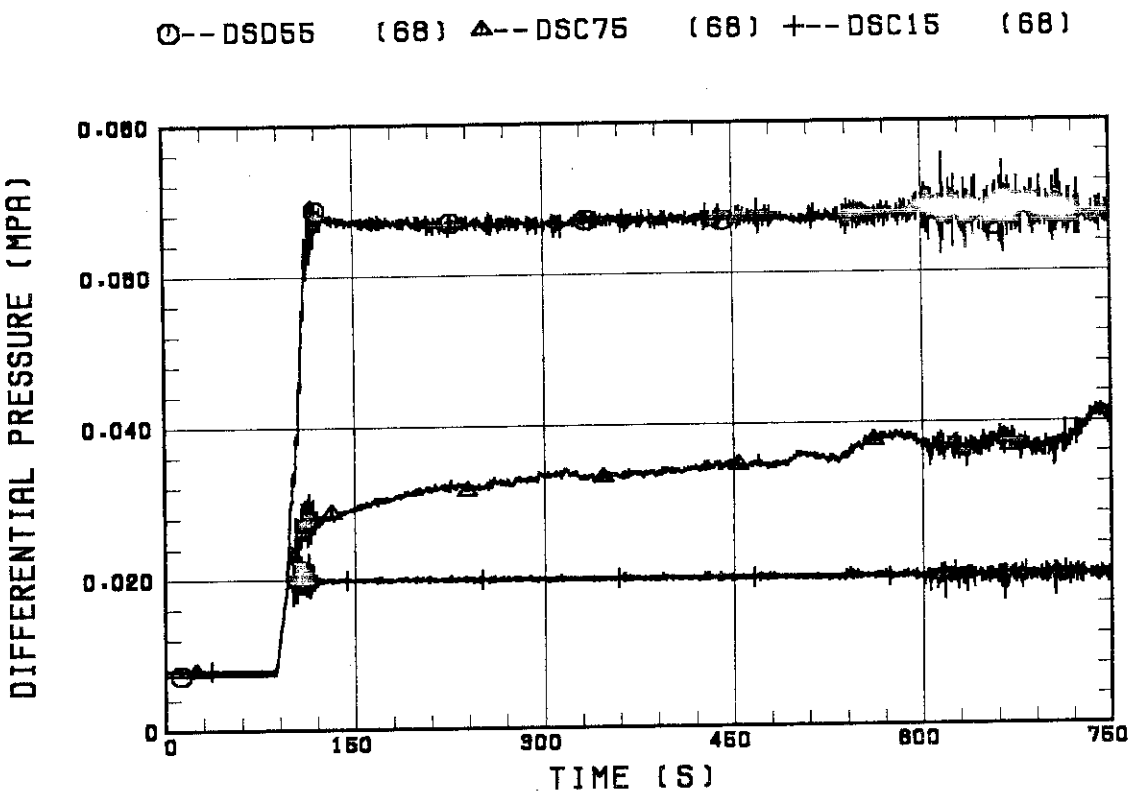

Fig.B.19 Differential pressure through downcomer, core, and lower plenum.

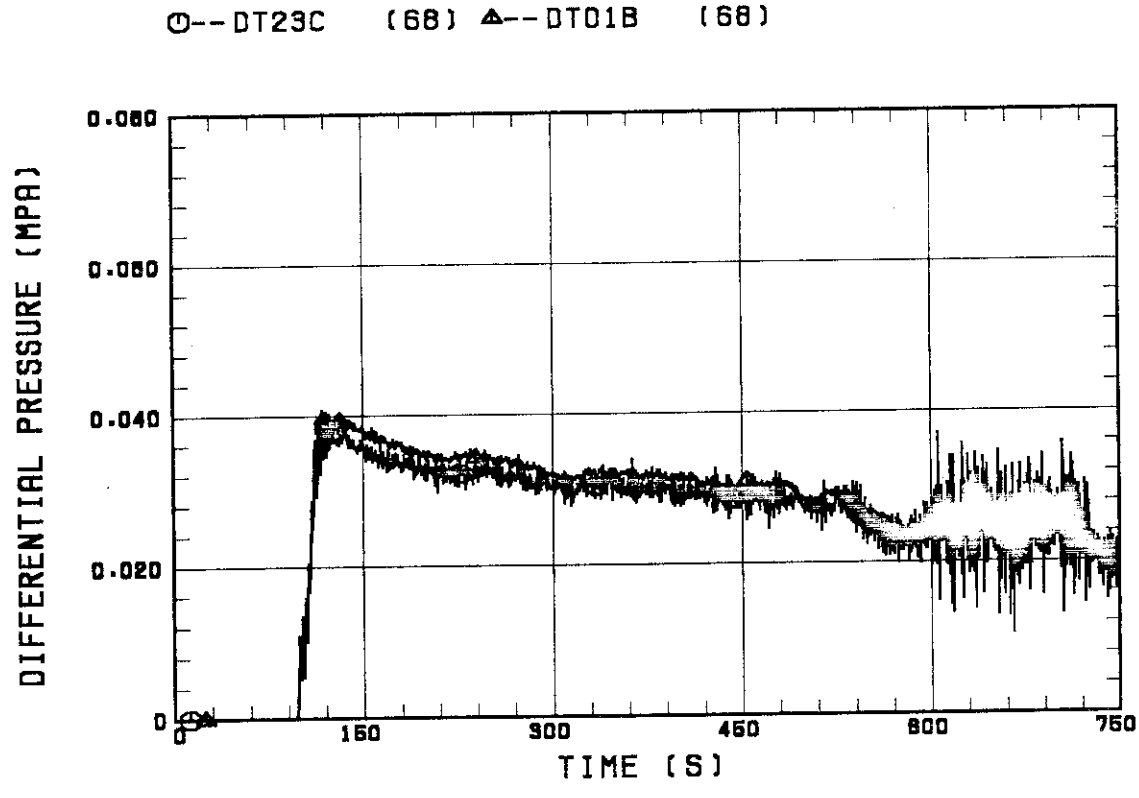

Fig.B.20 Bifferential pressure through intact and broken loops.

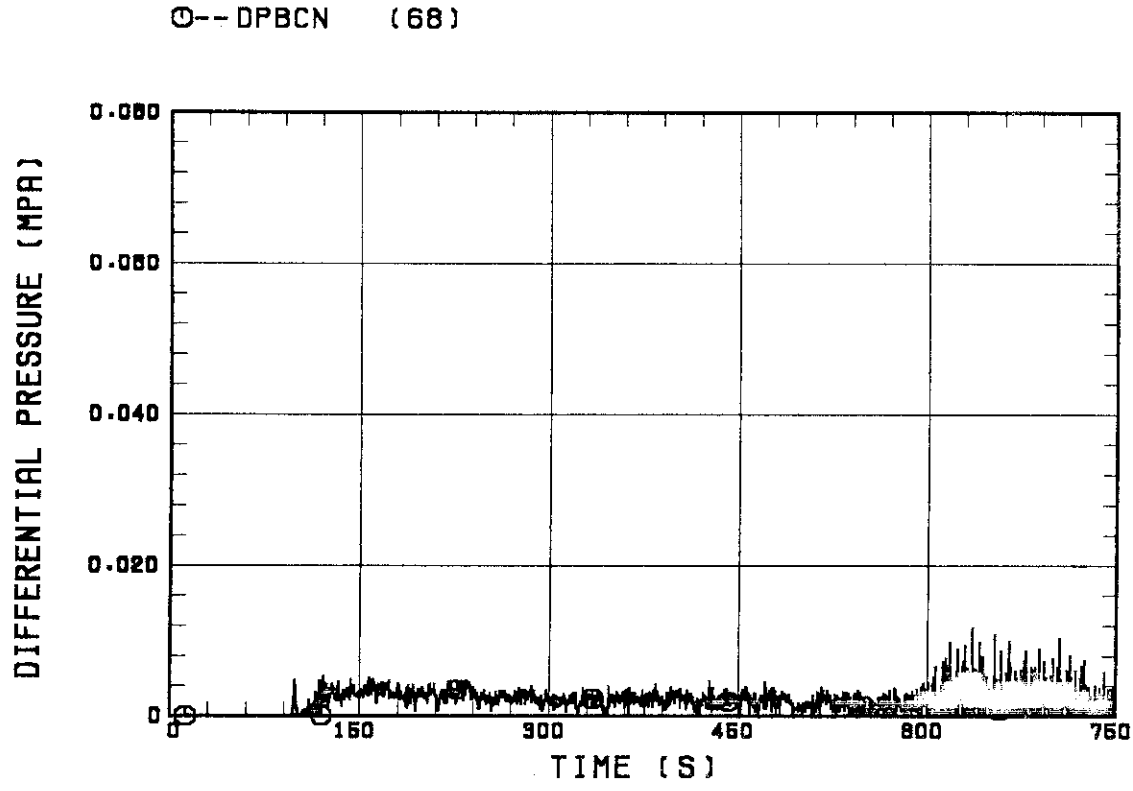

Fig.B.21 Differential pressure through broken cold leg nozzle.

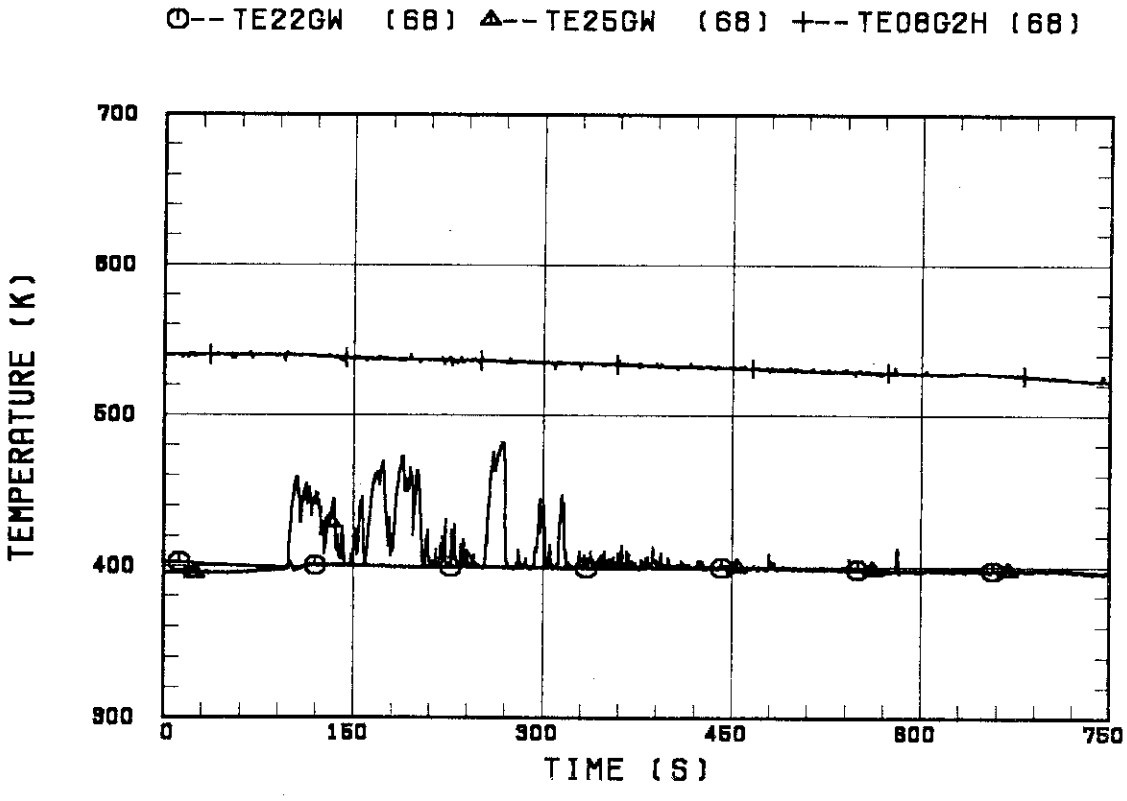

Fig.B.22 Fluid temperature in inlet plenum, outlet plenum, and secondary of steam generator 1.

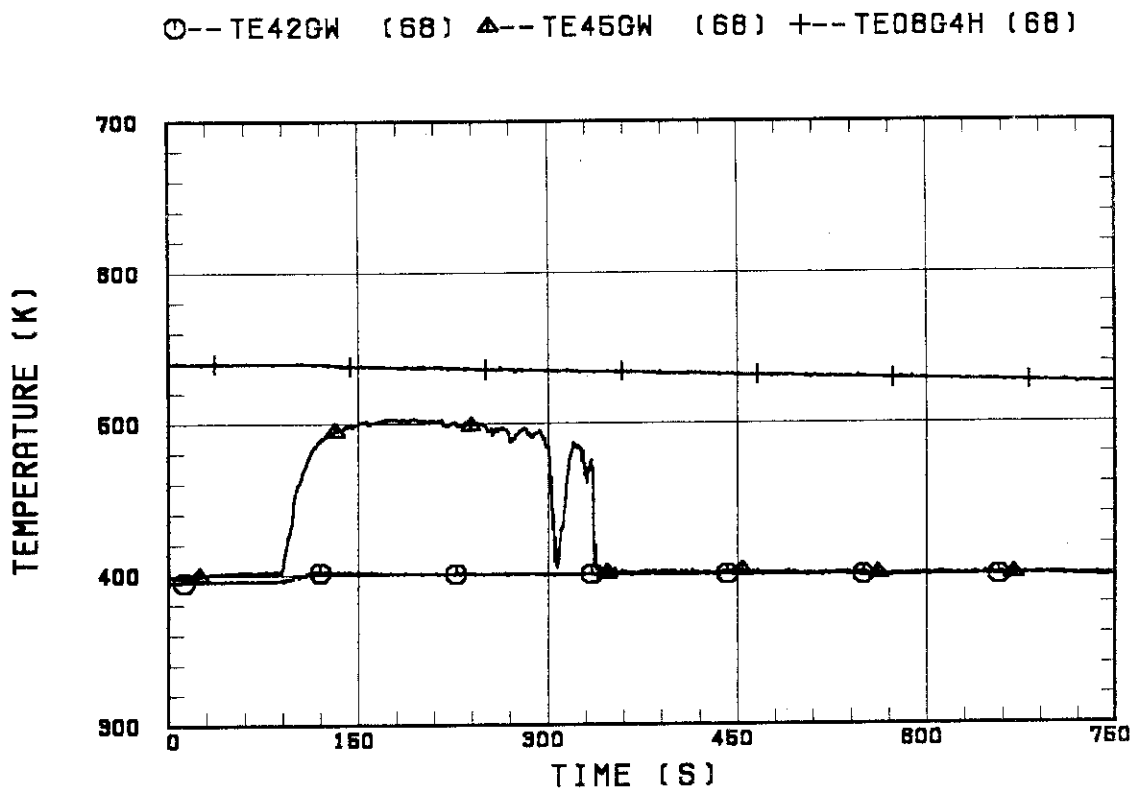

Fig.B.23 Fluid temperature in inlet plenum, outlet plenum, and secondary of steam generator 2.

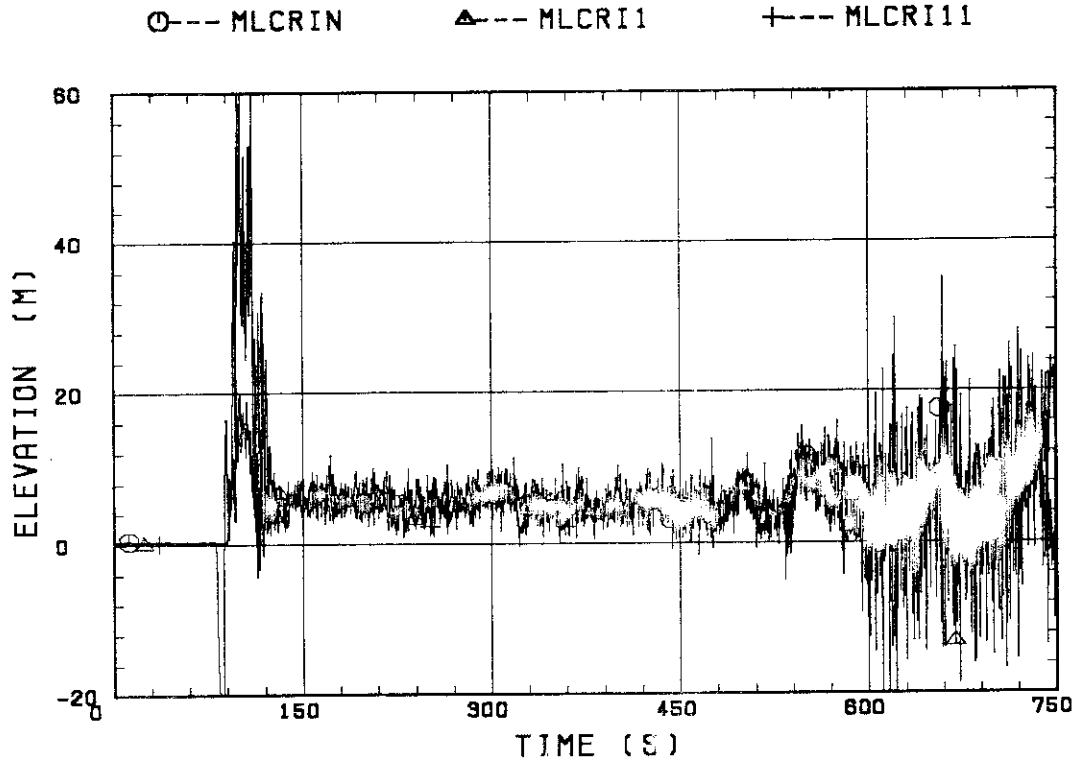

Fig.B.24 Core flooding mass flow rates evaluated with Eqs. (A.1) and (A.2)

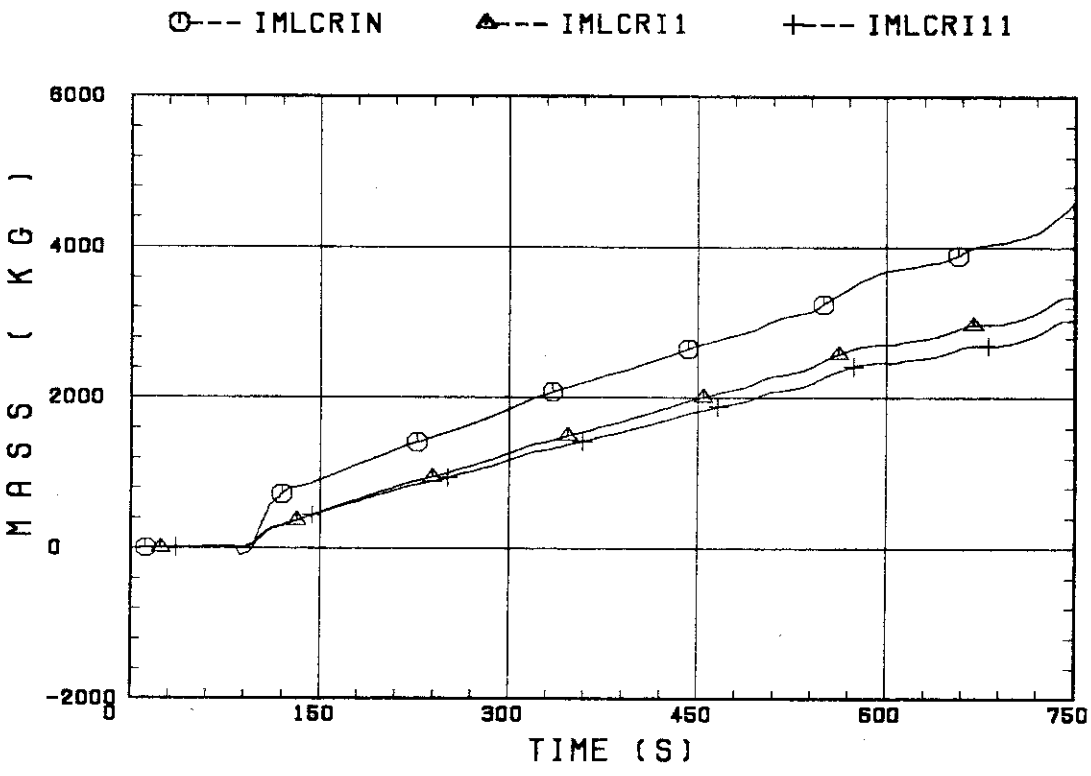

Fig.B.25 Time-integral mass flooded into core evaluated with Eqs. (A.1) and (A.2)

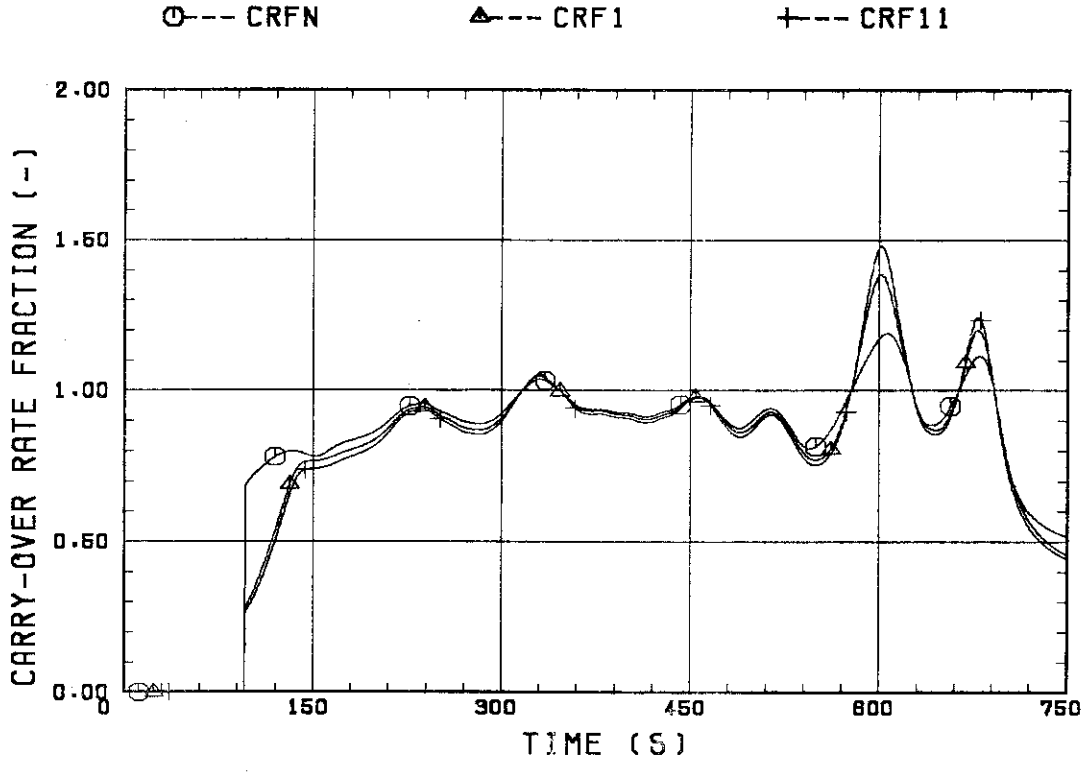

Fig.B.26 Carry-over rate fraction.

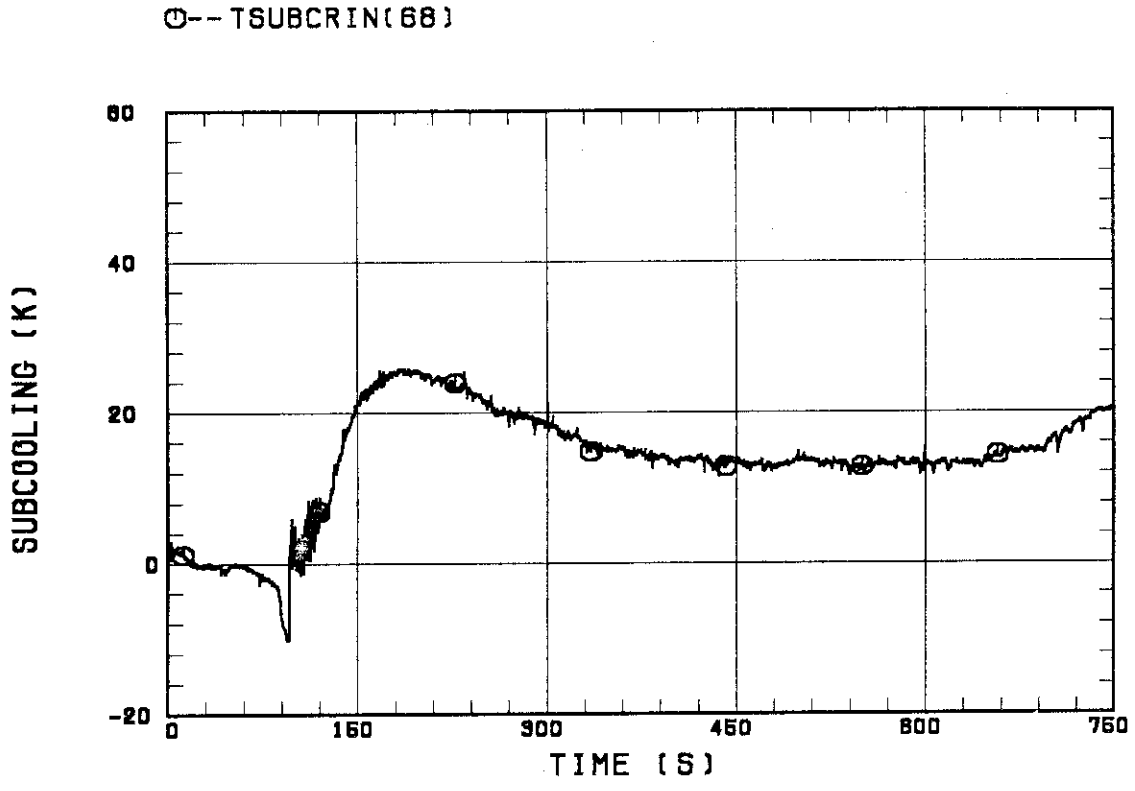

Fig.B.27 Core inlet subcooling.

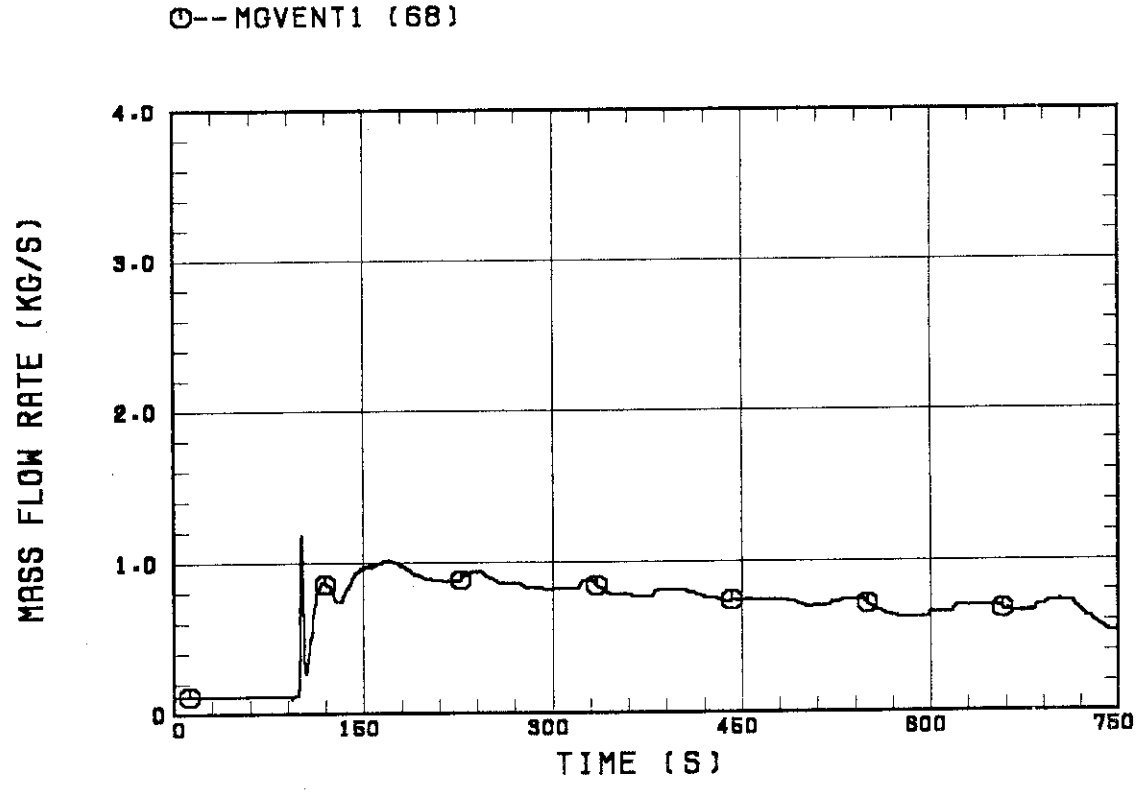

Fig.B.28 Exhausted mass flow rate from containment tank 2.